DERIVATION OF FIRST-ORDER DECAY HEAT GENERATION FUNCTION AND PREDICTION OF THERMAL ENERGY POTENTIAL FOR A MUNICIPAL SOLID WASTE LANDFILL

A Thesis Submitted to the College of Graduate and Postdoctoral Studies

In Partial Fulfillment of the Requirements for the Degree of Master of Science

In the Department of Civil, Geological, and Environmental Engineering

University of Saskatchewan, Saskatoon Canada

By

BRODY GLEN HUCL

PERMISSION TO USE

In presenting this thesis in partial fulfilment of the requirements for a Postgraduate degree from the University of Saskatchewan, I agree that the Libraries of this University may make it freely available for inspection. I further agree that permission for copying of this thesis in any manner, in whole or in part, for scholarly purposes may be granted by the professor or professors who supervised my thesis work or, in their absence, by the Head of the Department or the Dean of the College in which my thesis work was done. It is understood that any copying or publication or use of this thesis or parts thereof for financial gain shall not be allowed without my written permission. It is also understood that due recognition shall be given to me and to the University of Saskatchewan in any scholarly use which may be made of any material in my thesis.

DISCLAIMER

Reference in this thesis/dissertation to any specific commercial products, process, or service by trade name, trademark, manufacturer, or otherwise, does not constitute or imply its endorsement, recommendation, or favoring by the University of Saskatchewan. The views and opinions of the author expressed herein do not state or reflect those of the University of Saskatchewan, and shall not be used for advertising or product endorsement purposes.

Requests for permission to copy or to make other use of the material in this thesis in whole or part should be addressed to:

Head of the Department of Civil, Geological, and Environmental Engineering
3B48 Engineering Building, 57 Campus Drive
University of Saskatchewan
Saskatoon, SK S7N5A9

OR

Dean of the College of Graduate and Postdoctoral Studies
116 Thorvaldson Building, 110 Science Place
Saskatoon, SK S7N 5C9

ABSTRACT

As the consequences of green house gas production at landfills become more apparent to both the public and private sector, work has been performed at many landfills over the last two decades to explore the mechanisms controlling gas and heat generation within buried solid waste. Mechanisms and numerical models of the physical, chemical, and biological processes have been studied in order to better predict the conditions within the waste fill and the rates of gas and heat production. These models are useful tools for operators and designers to develop plans for mitigating some negative environmental impacts of landfilling, by collecting and using the recoverable natural gas or thermal energy to supplement conventional energy sources.

The Northern Landfill near Saskatoon, SK is a private landfill where the methane and thermal energy potential of the site is of interest. The landfill has been in operation since 1987 and contains approximately 2.5 megatonnes of waste. Vertical temperature distribution within the buried waste was measured using thermistors installed in boreholes, which were advanced using a sonic drill rig. Transient temperature data was collected from four locations across the top of the landfill, with two of the locations providing daily average temperatures with depth over a period of 800 days (2.2 yr). A 1D heat transport model was developed to compare calculated outputs to in-situ site temperature data over a 1-year period. The model was also used to simulate cell construction, waste placement, and heat generation over the life of the landfill.

The background and theory describing anaerobic landfill gas generation available in the literature was reviewed. Research completed to date in the literature predicting or estimating heat generation and transport within landfills was also reviewed. In the literature, heat generation is stated to be related to gas generation through anaerobic digestion, though no exact conversion factor was agreed upon. Empirically derived equations that define transient heat generation were reviewed however it was found that the variables and methodology did not relate heat generation to gas generation or degradable organic matter of the waste. Climatic factors of annual precipitation and average annual temperature were two of the variables governing the empirical heat generation function, however the climate experienced by the Northern Landfill did not produce a useable curve. Therefore, a first-order decay function was derived to represent the transient heat generation rate associated with the anaerobic digestion of organic matter in the landfill environment. This offers a mechanistic approach to defining heat generation in landfills, as opposed to empirical

definitions which are available in the literature. The two variables defining the function are biochemical heat potential (BHP_{ULT}), comparable to biochemical methane potential (BMP or L_0) in the gas generation literature, and a decay rate *k*.

The results of the 1D heat transport model which used a first-order decay function for heat generation suggest that a single *k* value representing the average decay rate poorly defined the dependency of heat generation to microbial populations and environmental conditions within the landfill. As a result, heat generation rates predicted by the derived function over the 2018 to 2019 monitoring period were significantly higher than those estimated through model calibration. Nonetheless, the model was able to simulate waste placement and the accumulation of thermal energy at the Northern Landfill, reaching temperatures at depth equivalent to those measured in the field in the year 2019. Two locations were modelled within the core of the landfill. BHP_{ULT} was predicted to be between 115 and 240 MJ per cubic metre of waste (MSW). BMP and equivalent cellulose content (C_{eq}) of the MSW was calculated from BHP_{ULT}, resulting in ranges of 19 to 120 L_{CH4}/kg_{MSW} and 4 to 27 % weight respectively. Peak heat generation rates from the first-order decay function were between 0.13 and 0.28 W/m^3. The lower limits of the ranges results from the location within older average MSW age (16.2 y) and the higher limits from the younger location (6.6 y). Calibrated present-day heat generation rates were between 0.020 and 0.148 W/m^3 at the older location and 0.009 and 0.205 W/m^3 at the younger location.

It is recommended that an improvement to the first-order decay function be implemented which incorporates a stepwise function governing the value of *k*, dependent on the temperature of the surrounding waste. The *k* value should be limited by a maximum potential decay rate of 0.12 y^{-1} (3.3×10^{-4} d^{-1}) at temperature values reported in the literature optimal for mesophilic microbial activity (20 to 45 °C). The *k* value should decrease until a threshold temperature reported in the literature at which no methanogenesis takes place (a *k* value of zero). A dependency of the decay rate to moisture availability should also be included, as well as the inclusion of updated modelling parameters or waste layer geometries as they are investigated further.

ACKNOWLEDGMENTS

I would like to thank my supervisor, Dr. Ian Fleming for his help and support during my time on this research project. His expertise in geo-environmental engineering and knowledge regarding the field investigation and report writing was invaluable. I am appreciative of my Advisory Committee members for making recommendations to improve the technical components and writing within this document. I have many thanks for Tyler Casavant and Logan Morhart who were involved in this project and made long, cold days in the field an overall fun experience. I want to also thank Adam Hammerlindl for his time and expertise around the laboratory and to all the other Geotech nerds who were always available to chat or offer advice. Lastly, I'd like to thank NSERC and Loraas Disposal Ltd. for their financial support of this research, and the staff at the Northern Landfill for accommodating and assisting my research at their site.

DEDICATION

This thesis is dedicated to my wife Madeleine, who encouraged me to pursue my graduate degree and who also planned and attended our wedding in the midst of this project. I would like to also dedicate this to my friend Andrew, who I wish more than anything I could celebrate this milestone with.

TABLE OF CONTENTS

LIST OF TABLES

LIST OF FIGURES

TABLE OF ABBREVIATIONS

Acronym/Abbreviation	Full Wording
MSW	Municipal solid waste
C/D	Construction/Demolition
ICI	Institutional/Commercial/Industrial
SRB	Sulfate-reducing bacteria
BMP	Biochemical methane potential
BHP	Biochemical heat potential
HR	Heat rate
NTP	Normal temperature and pressure conditions
VWC	Volumetric water content
HC	Heat capacity
AAAT	Average annual air temperature
MAET	Mean annual earth temperature
FEA	Finite element analysis
FEM	Finite element modelling
PVC	Polyvinyl chloride
TGA	Thermo-graphic analysis
LOI	Loss on ignition
ASL	Above sea level
LFG	Landfill gas
NDS	No dry season

TABLE OF VARIABLES

Variable	Definition	Description
CH_4	Methane	Chemical short form for methane (gas)
CO_2	Carbon dioxide	Chemical short form for carbon dioxide (gas)
$C_6H_{10}O_5$	Cellulose	Chemical short form for cellulose (solid)
ΔH	Enthalpy of reaction	Change in energy according to a chemical equation
BMP_{ULT}	Ultimate biochemical methane potential	Maximum volume of methane that can be produced from a mass of MSW
k	Decay rate	Coefficient of exponential decay
t_{lag}	Lag time	Time period prior to initiation of methane production in BMP experiments
K_T	Thermal conductivity (bulk)	Material property dictating the rate at which heat passes through it when experiencing a thermal gradient
HC	Bulk volumetric heat capacity	Material property dictating the energy required to change the temperature of a volume by 1 °C
α	Thermal diffusivity	Quotient of thermal conductivity and heat capacity
θ	Volumetric fraction	A value between 0 and 1 representing the fractional volume of a phase within a volume of soil
BHP_f	Biochemical heat potential (factor)	Conversion factor for calculating heat potential from methane potential
BHP_{ULT}	Biochemical heat potential (ultimate)	Maximum magnitude of energy released from a volume of MSW from anaerobic digestion of cellulose
ρ	Dry density	Mass of solids within a specified volume of soil
M	Molar mass	Mass of a material per mole of its elemental constituents

1.0 Introduction

1.1 Research Justification

Across Canada, there are hundreds of engineered landfills that exist for the purpose of storing municipal solid waste (MSW) and limiting its negative environmental impacts as it degrades in place. Landfills in the operating and closure phase are potential sources of energy which could reduce demand from conventional energy sources, and in some cases, contribute energy to nearby structures. The most common form of energy extraction from landfills is gas collection and its subsequent combustion and conversion to electrical energy. Another source, which is not yet common at landfill sites, is geothermal heat extraction from the above-ambient temperatures that are present in the core of MSW landfills. Temperatures above 30 °C were measured year-round at the mid-depth region of the Northern Landfill by instruments installed on site. An understanding of the in-situ thermal properties of mixed MSW is important for the prediction of how landfills will respond to different heat extraction designs and predicting the viability and lifespan of the process. As well, modelling the spatial temperature distribution is important because of the influence MSW temperature has on other processes taking place such as biodegradation, settlement, gas generation, leachate percolation, and liner degradation.

MSW produces heat as a by-product after placement, primarily via the biochemical breakdown of organic matter present in the waste, and secondarily from inorganic chemical reactions taking place over time (Hanson et al., 2010; Yeşiller et al., 2016a; Hao et al., 2017). Similar to landfill gas, this heat will be generated over decades and slowly be released to the surrounding environment if not extracted for practical use on site or in the surrounding community. It is of growing interest to landfill operators whether geothermal energy recovery can be economically included in facility construction or closure designs. In addition to heating structures, heat extraction is also useful for managing high temperatures (>80°C) encountered in some landfills, which increases the risk of underground fires. Heat extraction has also been explored as a means of maintaining a low temperature along an HDPE liner to increase its service life (Reinhart et al., 2017; Rowe et al., 2010; Yeşiller et al., 2016b).

1.2 Project Overview and Objectives

1.2.1 Site Location and Background

The Northern Landfill is located 10 km north of Saskatoon, Saskatchewan as shown in Figure 1.1. The landfill is located on a quarter-section of land divided into sixteen square cells, 170 m in width. Cell construction and waste placement began in 1987 in the northeast corner of the site. In 2018, the existing waste fill was approximately 25 m in thickness at the center of the northern eight cells and approximately 2.5 megatonnes of MSW had been landfilled to date. The MSW received by the landfill is mainly categorized as construction/demolition (C/D) and institutional/commercial/ industrial (ICI) sources. In recent years, a growing proportion of the waste received at the site has included independent resident drop-offs and mixed MSW collected from growing communities outside the city. The location of the landfill makes it an excellent candidate for energy recovery research at the University of Saskatchewan, both in the form of landfill gas generation and low-grade geothermal energy. The geothermal energy is to be evaluated as a potential source of heat for buildings on site, the nearby community of Martensville, and as a means of de-icing scales and roadways on site during winter operations.

The Northern Landfill was designed as a hydraulic trap (hydrodynamic containment) as outlined in the initial site investigation, landfill design, and liner study published by Haug et al. (1989) and Yanful et al. (1990). Due to the high local water table reported from the site investigation, cell liner elevations were designed to be 5 m below ground surface so as to fully excavate the hydraulically conductive surficial deposits while also inducing an upwards hydraulic gradient across the liner. Sump pumps are present in locations across the liner to limit leachate levels in the lower-most layer of MSW. The cell liners are constructed of 0.3 m thick unoxidized Floral till reworked and compacted for low hydraulic conductivity ($1x10^{-9}$ to $1x10^{-10}$ m/s). A modified area method of landfill operation was recommended to excavate sufficient cover material and minimize the final height of the landfill (Haug et al., 1989; Yanful et al., 1990).

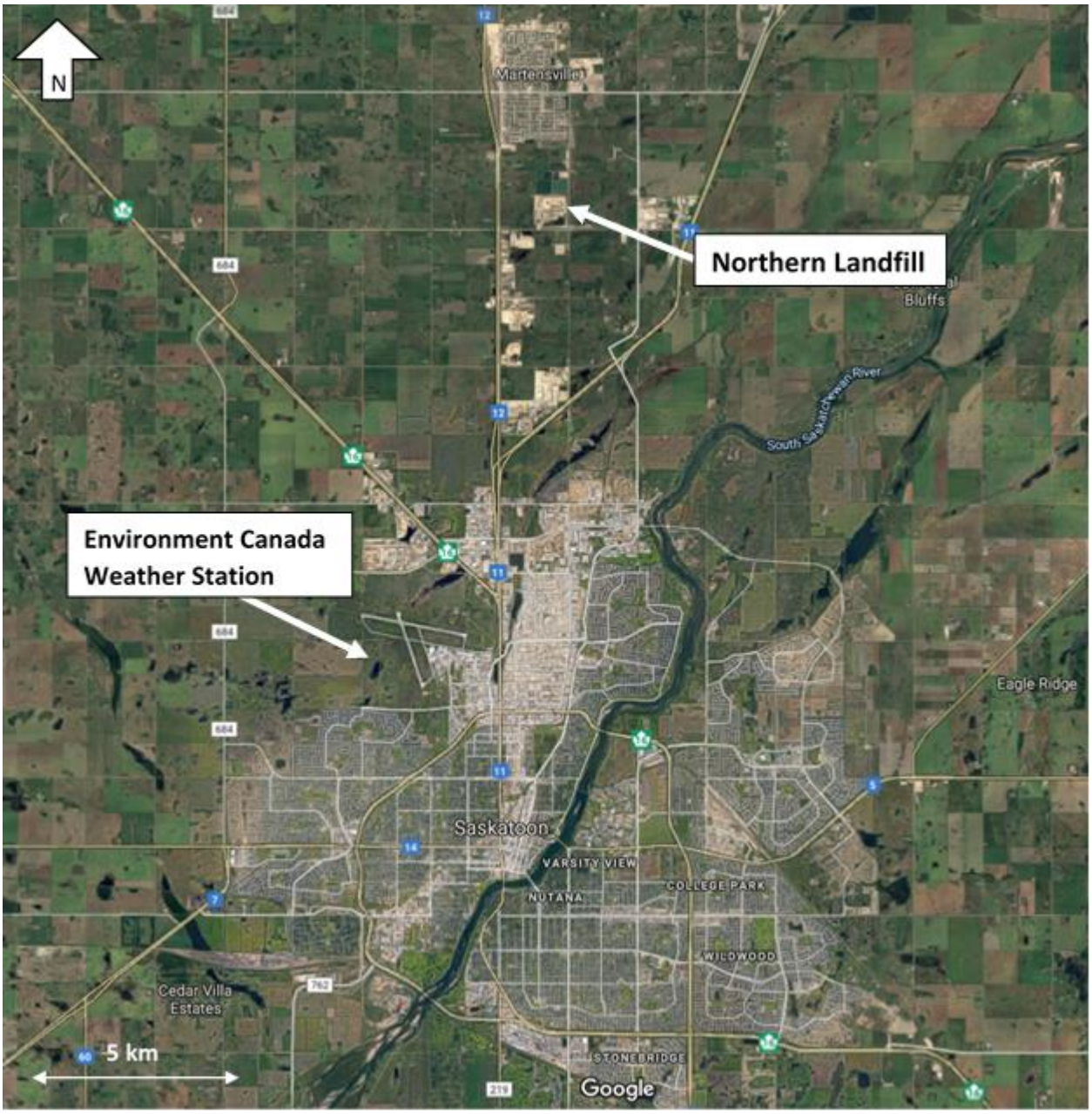

Figure 1.1: Landfill location plan view map with weather station providing climate data for this research included

1.2.2 Research Objectives

Prior to evaluating geothermal energy extraction from a practical and economical perspective, the energy potential of the MSW should be estimated and a numerical model developed to represent the accumulation of thermal energy over time. My thesis objectives are to derive and evaluate a first-order decay heat generation function and predict thermal energy potential of waste at the Northern Landfill through comparison of heat transport model outputs to temperatures measured

from instrumentation installed at the landfill. The heat generation function is mechanistic, being derived from theory defining methanogenesis in the anaerobic landfill environment. The function differs from empirical formulations presented in the literature. My research can be divided into three main objectives:

- Determine the spatial and temporal temperature distribution within the core of the completed waste cells at the Northern Landfill.
- Define a transient heat generation rate function for waste at the Northern Landfill dependent on energy potential and based on existing theory of methanogenesis. The function should be applicable to different waste layers, locations, and landfill geometries.
- Determine upper and lower limits of anaerobic heat (energy) potential for waste at the Northern Landfill via numerical modelling and calculate upper and lower bound degradable cellulose contents and biochemical methane potentials for the waste.

Key tasks required to complete the objectives were:

- Estimate the age of waste immediately surrounding the instrumented borehole locations based on known operational conditions, cell construction schedule, and dated objects recovered from MSW core samples.
- Determine bounding minimum and maximum volumetric heat capacity and bulk thermal conductivity properties of the waste at the Northern Landfill within limits published in the literature.
- Perform a sensitivity analysis on the numerical model developed to evaluate the affect unknown parameters and assumed values have on the results as it relates to the main objectives

1.2.3 Scope of Research

The landfill environment is a complex, time-dependent system subject to coupled physical, chemical, and biological processes. The scope of this research had to be defined to efficiently plan and implement a field instrumentation and data collection program and for successfully developing a numerical model to address the research objectives. The scope of this research is:

- Measure temperatures in the core of the landfill in locations where instrumentation will not interfere with site operations and only to the depth of the landfill liner
    - Instrumentation will measure atmospheric temperature at the surface of the landfill, but no other weather data is to be collected
- The focus of the literature reviewed is to be on heat generation and transport. Gas generation, migration, and hydraulic conditions in landfills is out of scope
- With limited or no information available regarding the initial MSW conditions, properties, or composition and no record of the landfill geometry as the site developed, a physical model of the landfill incorporating settlement, consolidation, and density change is not to be developed
- The MSW material model considers MSW on a bulk basis independent of time and converts MSW properties to units per cubic metre of MSW, which combines the volumetric fractions of solids, water, and gasses
- The priority is to develop a conduction-only heat transport model and modelling convective or advective processes of heat transport is out of scope

1.3 Significance of Research

The results of my research will establish a range of MSW heat potentials and define transient heat rate curves derived from gas generation theory. These parameters, as well as the installation of temperature measuring instrumentation are the initial tasks required for evaluating the geothermal energy potential of MSW landfills, such as the Northern Landfill. This work will aid in the design and operation of landfills where operators are considering geothermal energy exploitation. Methods will be outlined for attaining MSW temperature data and calibrated heat generation rates in the field. With the numerical model developed, engineers at the Northern Landfill or elsewhere can explore the impact that different construction or operating techniques would have on the thermal regime of future or existing waste cells. A few examples of applications for the results of my research include comparing the maximum waste temperature and rate of heating/cooling at depth as influenced by different liner or cover materials (such as tire-derived aggregate or various final cover soils), increasing the landfill height through additional waste layers, or variation of the organic content in placed MSW (due to recyclables diversion, composting, and inclusion/exclusion of household wastes). By exploring different material and geometry alternatives, geothermal

energy exploitation can be designed according to the landfill's response to extraction. Additionally, more comprehensive hydro-thermo-mechanical models in 2D or 3D can be constructed using the proposed heat rate functions and thermal properties as baseline inputs.

Loraas Disposal is directly invested in the research being undertaken as it will provide technical information to aid engineers in their decision making regarding operational techniques and the potential for geothermal energy extraction at their site. The work is compelling because of the number of existing and future landfills that will exist across the Canadian prairies and other regions. The potential to source thermal energy from these sites before the waste heat is exhausted to the atmosphere is a new field of geo-environmental engineering. Tapping into this low-grade geothermal energy source will help reduce the demand for other conventional sources of energy and is a step towards sustainability and circular economies.

2.0 Literature Review

Landfill temperatures have been measured and published from sites spanning several continents including North America, Europe, and Asia (Yeşiller et al., 2015a). Numerical models have been developed and used over the last three decades to predict gas, leachate, and heat generation and transport in landfills (El-Fadel et al., 1996c; Nastev et al., 2001; Rowe et al., 2010; Hanson et al., 2013; Kutsyi 2015a; Megalla et al., 2016; Khire et al., 2020).

The complex physical, chemical, and biological processes related to heat generation in a landfill environment were reviewed and are summarized in Section 2.1. This provided background information on enthalpy of methanogenesis reactions and environmental factors (temperature and moisture content) within buried waste that could impact heat generation rates. Findings in the literature regarding heat generation and energy potential at other landfill sites are also summarized for reference and to understand the theory behind existing heat generation functions applicable to landfills. Section 2.2 summarizes the material properties of MSW as it relates to heat transport and numerical models in the literature. This provided reference values for properties such as density, heat capacity, and thermal conductivity which were key parameters for defining a heat transport model. Section 2.3 summarizes the results and methods of various studies measuring temperature distribution and variation across landfills. These studies provided examples of expected temperatures, temperature trends, and the theory behind temperature accumulation and dissipation at landfills of varying ages and geometries. Section 2.4 summarizes the methodology and results of various landfill heat transport models published in the literature, identifying frameworks and methods applicable to the Northern Landfill and what heat generation functions have been used in past research. At the end of the chapter, knowledge gaps in the reviewed literature are identified and discussed. A review of the geology at the location of the Northern Landfill and published documents regarding the design of the landfill is included in Section 2.6.

2.1 Heat Generation in MSW

Heat is primarily produced in landfill conditions as a result of exothermic decomposition processes (Grillo, 2014). Because of the variable composition of MSW, numerous chemical and biological pathways can be initiated when the physical conditions exist to accommodate a given reaction (pH, temperature, availability of reactants). A waste layer at a landfill typically experiences an aerobic,

transitional, and anaerobic environment from placement to burial. The three phases are delineated by changes in gas compositions within the void spaces of the waste material (Yeşiller et al., 2005). The mechanisms of landfill gas generation via methanogenesis are well-documented because of the established methods for capturing and converting landfill gas into useable energy. It can be inferred that heat generation is a direct result of the four steps involved in landfill gas generation based on the conservation of carbonic mass and enthalpy of known reactions (El-Fadel et al., 1996b). It therefore became critical to quantify the amount of heat (energy) produced per unit of gas generated.

The aerobic phase begins at waste placement (pore-gas at atmospheric concentrations of O_2 and N_2) and persists until oxygen concentrations are reduced to zero or trace amounts. The anaerobic phase is marked by stable concentrations of methane (CH_4) and carbon dioxide (CO_2) at 60% and 40% by volume, respectively (landfill gas). The transition phase is a period between those previously described, where depleted oxygen concentrations and sharply increasing CO_2 concentrations can be observed, with unstable CH_4 concentrations of less than 60%. The aerobic phase lasts between a few weeks to three months and the transition phase typically ends no later than five months after waste placement (Yeşiller et al., 2005). Although greater rates of heat generation have been reported for the aerobic phase when compared to the anaerobic, the peak heat generation rate has been reported to occur at the onset of the anaerobic phase (Lanini et al., 2001; Hanson et al., 2008). Because of the disparity in timeframes that heat is generated when comparing the aerobic (weeks to months) and anaerobic (decades) phases, total heat generated and temperature increase is greater in the anaerobic phase due to the much longer time frame (Yeşiller et al., 2005; Coccia, 2013). As a result, the anaerobic phase and associated generation rates has been the focus of most field studies and numerical models evaluating gas and heat potential of MSW landfills.

2.1.1 Biochemical Processes and Population Kinetics

Landfill gas generation takes place over a long period of time, often for several decades because of relatively abundant organic matter and an environment which remains undisturbed indefinitely (Grillo, 2014). Microorganisms, which are present in fresh MSW, facilitate or directly convert organic matter into other molecular forms which then feed subsequent microbial populations. The biochemical pathway leading to methanogenesis is depicted in Figure 2.1 (after Grillo, 2014).

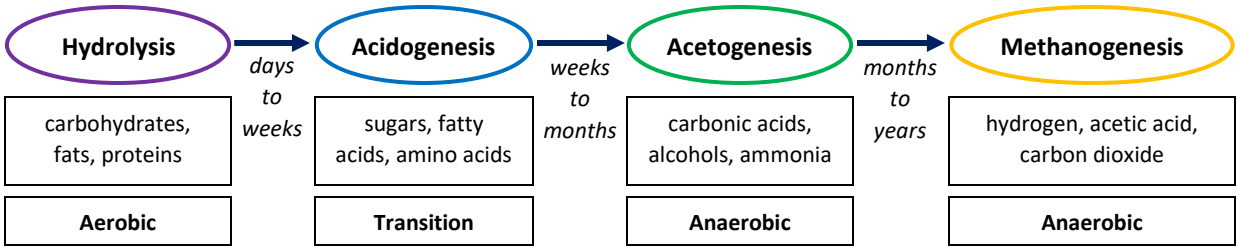

Figure 2.1: Steps in the dominant methanogenesis pathway with oxygen environment required for each step

Different microorganism species are required in order to carry out the degradation process in its entirety (until the production of landfill gas). Hydrolysis is performed extracellularly by glucose-consuming microbes and is both the initial and rate-limiting step in the entire process. Factors that affect the hydrolysis rate in a landfill environment includes lignin content of cellulosic material, pH, temperature, nutrient availability, and moisture content. As well, the resistance to movement of the microbes in the void spaces influences the rate but is difficult to quantify (El-Fadel et al., 1996a). The by-products of hydrolysis are consumed by acidogens, whose by-products are in turn converted by acetogens. Acidogens produce organic acids (butyric and propionic acid) and acetogens produce acetic acid in an anaerobic environment. Acetic acid (or acetate) is considered the most representative and prevalent reactant in the final step of methanogenesis which is performed anaerobically by microorganisms termed methanogens. The largest microorganism populations in the landfill environment are typically acidogens and methanogens. Mesophilic species of microorganisms thrive between 20 and 45 °C and thermophiles between 50 to 65 °C (El-Fadel et al., 1996a).

The rate of gas and resulting heat generation is proportional to the population of methanogens, which is influenced by many factors, similarly to the rate of hydrolysis. Temperature effects on biokinetics have been studied by El-Fadel et al. (1996a; 1996b; 1996c) as it relates to biodegradation of MSW. Temperature was reported to marginally influence hydrolysis rates and initial rates of subsequent steps (higher rates at higher temperatures). Temperature reportedly had little effect on long-term rates for the anaerobic processes as more stable waste temperatures tend to exist and the rates are more sensitive to the consumption of available reactants than temperature. Hydrolysis rates were reported to be more sensitive to the water content, lignin content, and structure of the cellulosic matter than to temperature (El-Fadel et al., 1996a; 1996b; 1996c). It has been noted from field measurements that gas generation is reduced substantially when temperatures are less than approximately 20 °C (Yeşiller et al., 2005; 2015a; Hanson et al., 2008;

2010; 2013) which correlates to the lower bound of the range of optimal temperatures for mesophilic microorganisms.

Other factors that may reduce methanogenesis rates during the anaerobic phase include ammonia content, oxygen ingress, and sulfate-reducing bacteria (SRB). SRB are present in landfills with large quantities of sulfate (such as from gypsum drywall in C/D waste streams) and compete with methanogens over volatile fatty acids and carbohydrates while consuming hydrogen (Krause et al., 2016).

The peak gas generation rate and exponential decay rate of MSW has been measured in the laboratory as well as estimated on a field scale (Nastev et al., 2001; De La Cruz & Barlaz, 2010). Experimentally measured biochemical methane potential (BMP) of MSW has also been reported (Ivanova et al., 2008; Mathison, 2015, Krause et al., 2016). The chemical equations of the previously described biochemical processes and the resulting energy released is reviewed in the Section 2.1.2.

2.1.2 Carbon Lifecycle and Enthalpy of Reactions

Carbonic mass is conserved throughout the various processes outlined in Figure 2.1 and can be traced from organic solids in the waste to CH_4 and CO_2 in landfill gas. Apart from its original solid state and final gaseous state, carbon can be expected to exist in the following forms: aqueous organic, acidogenic biomass, acetate, and methanogenic biomass (El-Fadel et al., 1996a). For the purpose of defining the most relevant chemical equations for the lifecycle of organic matter to landfill gas, cellulose ($C_6H_{10}O_5$) was reported as the most abundant and overall representative molecule capable of undergoing hydrolysis in the solid organic carbon fraction of MSW (El-Fadel et al., 1996a; 1996b; 1996c; Yeşiller et al., 2005; Shi et al., 2020). As a result, understanding the amount of energy released by the degradation of cellulose was an objective of the literature review.

A series of chemical equations can be defined for each step in Figure 2.1. The individual equations and enthalpies of reaction (ΔH) are listed in Table 2.1 (after El-Fadel et al., 1996b). Aside from methanogens consuming acetic acid, CH_4 can also be produced directly through CO_2 reduction with hydrogen. This process was stated to be limited by hydrogen availability in the landfill environment and is overshadowed by the biological acetic acid pathway (El-Fadel et al., 1996a).

The condensed anaerobic reactions and an estimate of overall ΔH per mole of cellulose is shown in Equation 2.1 and the aerobic reaction is Equation 2.2 from Shi et al. (2020).

$C_6H_{10}O_5 + H_2O \Rightarrow 3CH_4 + 3CO_2 + 271\ kJ/mol$……Equation 2.1

$C_6H_{10}O_5 + 6O_2 \Rightarrow 6CO_2 + 5H_2O + 2812\ kJ/mol$……...……...……...Equation 2.2

Table 2.1: Enthalpies of reaction for each step in anaerobic methanogenesis of cellulose (after El-Fadel et al., 1996b)

Process	**Step**	**Chemical Equation**	**ΔH(1) (kJ/mol)**
Hydrolysis	Cellulose chains to Glucose(2):	$C_6H_{10}O_5 + H_2O \Rightarrow C_6H_{12}O_6$	-
Acidogenesis	Formation of Butyric Acid:	$C_6H_{12}O_6 \Rightarrow CH_3(CH_2)_2COOH + 2H_2 + 2CO_2$	+198
	Formation of Propionic Acid:	$C_6H_{12}O_6 + 2H_2 \Rightarrow 2CH_3CH_2COOH + 2H_2O$	+216
	Formation of Acetic Acid:	$C_6H_{12}O_6 + 2H_2O \Rightarrow 2CH_3COOH + 4H_2 + 2CO_2$	+164
Acetogenesis	Conversion of Butyric to Acetic Acid:	$CH_3(CH_2)_2COOH + 2H_2O \Rightarrow 2CH_3COOH + 2H_2$	-34
	Conversion of Propionic to Acetic Acid:	$CH_3CH_2COOH + 2H_2O \Rightarrow CH_3COOH + 3H_2 + CO_2$	-26
Methanogenesis	Consumption of Acetic Acid:	$CH_3COOH \Rightarrow CH_4 + CO_2$	+16
	Carbon Dioxide reduction:	$4H_2 + CO_2 \Rightarrow CH_4 + 2H_2O$	+31

(1) Note that a positive value is exothermic, and negative is endothermic
(2) Note that $C_6H_{12}O_6$ is a glucose molecule

It is apparent from Table 2.1 that the most exothermic of the reactions are the formations of carboxylic acids, which would occur primarily during the transition phase leading up to methanogenesis. Due to the large source of solid material present in most landfills, and the existence of more degradation-resistant organic matter, it is likely that reduced or residual rates of acidogenesis and acetogenesis continue well into the anaerobic phase. The various energy values of methanogenesis reported in the literature per mole of cellulose or glucose are summarized in Table 2.2 (after Yeşiller et al., 2005).

Table 2.2: Summary of reported total enthalpies of methanogenesis (after Yeşiller et al., 2005)

Decomposition Conditions	Heat Generation Reported	Source
Aerobic digestion of glucose	1,146 kJ/mol$C_6H_{12}O_6$	Pirt (1978)
Anaerobic conversion of organic fraction (glucose) to CO_2 and CH_4	0.068 kJ/mol$C_6H_{12}O_6$	
Aerobic and anaerobic enthalpy of reactants	1,023 kJ/mol$C_6H_{10}O_5$	El-Fadel et al. (1996b)
Anaerobic enthalpy of stepwise biochemical reactions	436 kJ/mol$C_6H_{10}O_5$	
Anaerobic biodegradation of glucose	121 kJ/mol$C_6H_{12}O_6$	Nastev et al. (2001)
Anaerobic biological decomposition (equivalent glucose)	14.5 kJ/mol$C_6H_{12}O_6$	Yoshida & Rowe (2003)
Aerobic transformation of organic matter (equivalent glucose)	2,815 kJ/mol$C_6H_{12}O_6$	Jafari et al. (2017)
Anaerobic transformation of organic matter (equivalent glucose)	145 kJ/mol$C_6H_{12}O_6$	
Aerobic enthalpy of reactions	2,812 kJ/mol$C_6H_{10}O_5$	Shi et al. (2020)
Anaerobic enthalpy of reactions	271 kJ/mol$C_6H_{10}O_5$	

From Table 2.2 it is apparent that there is significant variance in reported values for heat generation per mole of cellulose or glucose, even among those based on anaerobic enthalpy of reactions only. Values range over four orders of magnitude for the anaerobic estimates (0.068 to 436 kJ/mol). Consistently however, the aerobic enthalpy (1,146 to 2,815 kJ/mol) is greater when compared to the anaerobic. A relatively brief aerobic phase can generate considerable heat assuming optimal conditions for aerobic microbial activity exist and it is evident that a direct relation between landfill gas and heat generation exists during the long anaerobic phase (Yeşiller et al., 2015a; Megalla et al., 2016). A review of BMP and gas generation potential of MSW is included in the next section.

2.1.3 Biochemical Methane Potential and Decay Rates

The theory linking BMP and gas generation rate to biochemical heat potential (BHP) and heat rate (HR) via enthalpy of reactions has been introduced in Section 2.1.1 and 2.1.2. BMP is a laboratory test that is performed on shredded samples of MSW to measure the volume of CH_4 produced per

unit mass of MSW. Testing methods vary among researchers but are designed to anaerobically digest MSW by inoculating samples with anaerobic microorganisms in sealed jars (Owen et al., 1979). One problem with many reported BMP values, aside from the variation in test apparatus and procedure, is the absence of an associated age with the MSW sample tested. This dictates that the results are a measure of the CH_4 potential of the organic matter that remains after an unknown length of time. Thus, an unknown amount of degradation has already occurred to the samples in the landfill environment. For the purpose of predicting BHP, values of BMP performed on fresh MSW samples are most desirable. BMP tests track the cumulative methane produced versus time and plot in a first-order decay relationship after a short lag phase (Gunaseelan, 2004; Gregory & Browell, 2011; Raposo et al. 2011). The gas production rate starts high (e.g. 2.07 L/kg/d) and decreases exponentially with time until the cumulative gas generated approaches an asymptotic value (for example 0.055 L/kg/d) (Mathison 2015). An equation fit to the experimental BMP curves was presented by Mathison (2015) and is,

$$BMP(t) = BMP_{ULT} * \left(1 - e^{-k(t-t_{lag})}\right) \quad \text{.....Equation 2.3}$$

BMP is cumulative CH_4 produced (L_{CH4}/kg dry MSW) at time t (d), BMP_{ULT} is the asymptotic maximum (ultimate) value (L_{CH4}/kg of dry MSW), k is the decay rate (d^{-1}), and t_{lag} is the lag phase duration (d).

Ivanova et al. (2008) provided data of fresh MSW composition, organic content (as cellulose, hemicellulose, and lignin), resulting gas volumes generated, and the mass of organic content consumed after 919 days of anaerobic digestion in a laboratory environment (conventional BMP tests using 100 g of dry MSW). The authors reported that, with an initial combined cellulose and hemicellulose content of 31.6% by weight, 167.4 L_{CH4}/kg was produced at normal temperature and pressure (NTP) conditions. It was determined after the tests that 79% of the combined cellulose and hemicellulose was digested, which according to Equation 2.1 would produce 110.5 L_{CH4}/kg at NTP. It was concluded that the difference between theoretical and actual CH_4 generation (57 L/kg) was attributed to CH_4 generation from other organic molecules such as proteins and fats (Ivanova et al., 2008). The analysis assumed lignin (9.7% by weight) was not degradable and did not contribute to BMP. CH_4 could also have been produced by reduction of CO_2 with H_2 (El-Fadel et al., 1996a).

The decay rate of CH_4 generation (*k* value in Equation 2.3) was estimated by Nastev et al. (2001) from landfill gas recovery across four separate cells in a landfill near Montreal, Quebec. Based on the cells' average age, the gas recovery rate demonstrated an exponential decay with respect to time and a fitted decay rate of 0.055 y^{-1} (1.5 x 10^{-4} d^{-1}) was reported. Although a lot of error exists when estimating decay on such a large scale, it provides an average value applying to a large mass (36 Mt) of heterogenous MSW (Nastev et al., 2001). As well, it is a result of field conditions as opposed to laboratory or controlled conditions and was an initial reference point for modelling the heat generation functions for the Northern Landfill, however Montreal experiences a wetter and warmer average annual climate compared to Saskatoon. De La Cruz & Barlaz (2010) published a method of correcting laboratory MSW decay rate estimates to a landfill scale by analyzing the decay rates of specific waste components. Although decay rate was stated to be dependent on more variables than just waste composition (also moisture content and waste temperature) the authors stated that field decay rates should fall between 0.02 y^{-1} (5.5 x 10^{-5} d^{-1}) as a lower limit representative of arid regions and 0.12 y^{-1} (3.3 x 10^{-4} d^{-1}) as an upper limit representing bioreactor conditions (De La Cruz & Barlaz, 2010).

2.2 Material Properties of MSW

This section summarizes ranges of thermal properties of MSW reviewed. The focus of the review was on properties which are relevant to conduction-only numerical modelling and includes volumetric heat capacity and thermal conductivity. A portion of the properties presented in this section result from numerical models formulated by researchers over the last several decades. The methodology behind these models are reviewed in Section 2.4. The other properties included are the result of field-scale or laboratory experiments on MSW samples.

2.2.1 Physical Properties

MSW properties are typically studied and modelled as an extension of soil mechanics considering it is a porous media composed of a solid matrix with liquid and gas-phase pore fluid. The solid matrix can be composed of any household, industrial, or commercial waste material but is typically categorized into dominant categories (by % total mass) such as paper, plastic, glass, soil, metal, wood, and food/garden/yard waste. The fluid phase may begin as relatively fresh water but, due to leaching of soluble solid matter or other liquids, becomes contaminated with many different ions and metals such as high concentrations of chloride, sulphate, and nitrate (Yanful et al., 1990). The

gas phase begins as atmospheric but transitions to a mixture of CH_4 and CO_2 as landfill gas is generated. The heterogeneous composition of MSW, as dictated by the sources of waste collected for a site, results in a wide range of potential values for any given property.

Literature was reviewed to understand the influence of void ratio on thermal properties in landfills. The oedometer testing of MSW by Stoltz et al. (2010a) and unit weight analysis of landfill field data by Zekkos et al. (2007) analyzed the heterogeneity of MSW physical properties caused by overburden stress. Dry density and volumetric water content (VWC) of MSW samples tested in the laboratory increased with effective stress due to primary consolidation (Stoltz et al. 2010a). This is a typical property of conventional soils. A hyperbolic relationship was fit to unit weight field data and large-scale laboratory tests, with unit weight increasing with depth (Zekkos et al. 2007). The overall gas and heat potential on a volumetric basis is expected to increase with depth into the landfill proportional to the dry density increase, attributed to increased mass of organic matter per unit volume. As a result of void space reduction due to consolidation, bulk thermal conductivity and heat capacity likely increase with depth at MSW landfills proportional to the reduced volumetric component of the gas phase in the void space. This is demonstrated mathematically in the next section.

2.2.2 Thermal Properties

The key thermal properties to define heat transport within MSW are thermal conductivity (K_T in W/m·°C) and heat capacity (HC as either specific; in kJ/kg·°C or volumetric; in MJ/m^3/°C). Thermal conductivity quantifies the rate of heat flow through a material along a thermal gradient and heat capacity quantifies the energy required to change the temperature of a material. Thermal diffusivity (α in m^2/s) is defined as K_T divided by HC and a high α value indicates that a material will increase in temperature faster than a material with a lower α value when energy is introduced (Hanson et al., 2000). Both thermal properties for MSW are a function of the properties and volumetric fraction of the three-phase components (leachate, solid matrix, and landfill gas).

The thermal properties of MSW, similar to physical properties, can vary from one sample to another due to the heterogenous composition of the solid matrix.

Potential thermal properties of MSW had to be determined as material properties for the numerical model. It was found that thermal properties of MSW reported were either determined by physical

experimentation of MSW in the laboratory or field or else calibrated using numerical modelling methods. A combination of field-scale and laboratory needle probe tests were performed by Hanson et al. (2000) to estimate thermal conductivity of high water content materials including MSW, peat, and bentonite slurries. Faitli et al. (2015) constructed a 1.8 x 1.8 x 0.8 m square box capable of compacting excavated or fresh MSW to different densities. The upper surface was heated and the temperature response at the bottom of the box was measured. These methods provided experimental estimates of bulk thermal properties which were then compared to analytical calculations of bulk thermal properties based on MSW composition and component-specific thermal properties. Proposed equations for calculating the bulk properties from phase-specific properties and volumetric fractions by the above-mentioned studies both conclude that the system behaves in parallel as opposed to a serial summation (Faitli et al., 2015). The method of calculation using parallel conductance is shown in Equation 2.4 as developed by Faitli et al., (2015),

$$K_T = (K_{Tsol} * \theta_{sol}) + (K_{Tliq} * \theta_{liq}) + (K_{Tgas} * \theta_{gas}) \quad \text{.....Equation 2.4}$$

K_T is bulk thermal conductivity with additional subscripts denoting the thermal conductivity of the solid, liquid, and gas phases and θ is volumetric fraction of the phase (m^3/m^3). This equation is also applicable to HC by substituting with K_T. A value of K_{Tsol} and HC_{sol} for MSW was determined by the experiments performed by Faitli et al. (2015) based on mass fractions of different solid components and their respective density and thermal properties. The MSW tested was composed primarily of organics (21.6%), plastic (19.9%), soil-like fines (15.7%), and paper (12.7%). A comparison between K_T and HC for the three phases is provided in Table 2.3 (after Faitli et al. 2015). Density of the materials is included for comparison as volumetric heat capacity is dependent on the material density and specific heat capacity.

Thermal properties of the solid component was not calculated for the MSW tested by Hanson et al. (2000) but the needle probe experiments resulted in bulk properties ranging between 0.01 – 0.7 W/m·°C and 0.8 – 10 MJ/m^3·°C. The range of values from the box experiment were 0.24 – 1.15 W/m·°C and 0.9 – 2.1 MJ/m^3·°C (Faitli et al., 2015). The large spread in values from the needle probe tests was attributed to both the heterogeneity of the solid matrix composition and large void spaces that can exist in the field (Hanson et al. 2000).

Table 2.3: Thermal properties of MSW and void-space components (after Faitli et al., 2015)

Phase Material	Thermal Conductivity (W/m/°C)	Specific Heat Capacity (kJ/kg/°C)	Density (kg/m^3)
Solid MSW mixture	3.99	1.8	1297
Fresh water	0.60	4.2	1000
Fresh ice	2.18	2.1	931
Landfill gas (60% CH_4 by volume)	0.03	1.6	1.1

Because of the parallel conductance between the three phases in MSW, the high conductivity of the solid matrix has the most influence on bulk K_T, whereas the high specific heat capacity of water influences the bulk HC the most (Faitli et al., 2015). When considering the affects of consolidation on MSW properties, it is evident from Equation 2.4 and Table 2.3 that the low thermal conductivity and low volumetric heat capacity of landfill gas (accounting for the relatively low density of landfill gas compared to the other components) results in an increase in both thermal properties when the volumetric fraction of landfill gas decreases. A reduction in void ratio therefore results in an increase in bulk thermal properties of MSW proportional to the relative changes in the volumetric fractions of the bulk MSW using Equation 2.4.

Needle probe tests on laboratory-scale samples from four different landfills sampled at various depths were performed by Khire et al. (2020) and utilized in a numerical model. Ranges of bulk thermal properties for MSW utilized or output from various numerical models in the literature are presented in Table 2.4.

Table 2.4: Thermal properties of MSW as reported by various authors and studies

Source	Landfill Location	Waste Layer or Conditions	Thermal Conductivity (W/m·°C)	Specific Heat Capacity (kJ/kg·°C)	Bulk Density (kg/m^3)	Volumetric Heat Capacity (MJ/m^3·°C)
Hanson et al. (2008)	Anchorage, Alaska	Average	0.3	1.8	530	1.0
	Vancouver, British Columbia		1.5	2.2	1,000	2.2
	Canton, Michigan		1.0	2.0	1,000	2.0
	Las Cruces, New Mexico		0.6	1.6	760	1.2
Rowe et al. (2010)	Japan	Saturated	0.96	2.36	N/A	N/A
		Unsaturated	0.35	1.94		
Kutsyi (2015b)	Ukraine	Average	0.85	1.6	1,060	1.7
Megalla et al. (2016)	Ste. Sophie, Quebec	Minimum	0.3	2.26	930	2.1
		Maximum	0.7 - 1.1			
Emmi et al. (2016)	NE Italy	Average	1.2	2.38	840	2.0
Shi et al. (2020)	*Bioreactor*	Average	0.44	2.22	1,020	2.3
Khire et al. (2020)	NE USA	Upper	0.3	2.0	720	1.4
		Middle	0.6	2.3	930	2.1
		Lower	0.9	2.0	1,280	2.6
Overall Average for MSW			0.7	2.1	920	1.9

The properties published in the literature provide examples of the ranges and average values for thermal properties for MSW with varying magnitudes of VWC. These varied values promote modelling minimum and maximum potential values of K_T and HC that will result in either the greatest or least heat gain in the waste mass over long periods of time. This was ideal for predicting upper and lower limits of heat potential, as well as explore further the premise that thermal properties are heterogeneous in the Northern Landfill.

The properties of the glacial till deposits beneath the landfill site also needed to be defined but are less variable due to its natural deposition environment and mineralogical thermal properties being more well-defined in the literature (Abu-hamdeh, 2003; Hamdhan & Clarke, 2010). The subgrade glacial tills and its properties are described in Section 2.6.

2.3 Temperature Distribution in Landfills

Several landfills around the world have been instrumented to measure spatial and temporal waste temperature variations. Multiple detailed temperature studies by Hanson & Yeşiller (2005; 2010; 2015a; 2015b) took place at landfills in British Columbia, Michigan, New Mexico, and Alaska over almost a decade. The work done at these sites included both horizontal and vertical arrays being installed using thermocouples fixed inside flexible PVC conduits. The same authors later compiled temperature data from other published sources around the world and presented it as a summary (Yeşiller et al., 2015a). Gas and temperature data was monitored at instrument bundles beneath fresh MSW lifts placed under freezing conditions as well as non-frozen lifts in the summer months at a landfill in Ste. Sophie, Quebec (Bonany et al., 2013; Megalla et al., 2016). Typical temperature distributions, thermal gradients, and common factors that influence the magnitude and timing of maximum temperature reached within MSW landfills are reviewed in the next three sections.

2.3.1 Temperature Profiles and Ambient Influence

To compare the data from landfills of different total depths, a normalized depth can be used in which the position (depth) is divided by the total waste thickness. This results in the upper surface being assigned a value of 0.0, the landfill liner a value of 1.0, and the mid-depth a value of 0.5. The typical shape of temperature profiles within a completed cell is a convex profile with the greatest temperatures being measured in the middle third between 0.3 and 0.6 normalized depth (Hanson et al., 2010; Yeşiller et al., 2015). Temperatures consistently were observed to decrease from the warmer central zone towards the liner but remain higher than surrounding natural ground surface temperatures. Maximum and minimum reported temperature profiles in the literature for various landfills were plotted by Yeşiller et al., (2015a). In general, younger wastes displayed a more severe convex shape whereas older wastes were observed to be more linear. The addition of new waste lifts on top of older lifts generally results in an upward movement of the position of the maximum temperature (Yeşiller et al., 2015a).

Ambient atmospheric conditions consistently resulted in minimum waste temperatures being measured near the upper surface of waste in the studied landfills. As well, from horizontal array data, temperatures along landfill liners or between waste layers were greatest around the central portion of a cell and were lowest on the edges of the cell. Atmospheric influence of MSW near the

side slope intruded up to 20 m in some cases (Yeşiller et al., 2005). These reduced waste temperatures also displayed a lag in the timing of peak and trough values related to the peaks and troughs of seasonal atmospheric average temperature waves. The amplitude of these peaks and troughs within the waste was reduced when compared to the atmosphere. The observed time lag and reduction in amplitude (phase-lag) was more prominent with depth or distance into the cell until a certain distance (6 to 8 m) where stable temperatures persisted throughout the seasons (Yeşiller et al., 2005; Hanson et al., 2010). Steady temperatures consistently developed after the placement of the first overlying lift and it was found that a lift thickness of 4 to 5 m was enough to significantly reduce the observation of seasonal trends in underlying waste layers (Yeşiller et al., 2005).

A landfill studied in Ste. Sophie, Quebec provided waste temperature data commencing at the time of waste placement and for multiple waste layers placed in different seasons. Megalla et al. (2016) concluded from the field measurements that waste placed in the winter remained frozen at a depth greater than 3 m and for as long as 1.5 years after placement, even with ambient temperatures exceeding 30 °C within the study period. The lag time of frozen waste to reach and exceed 0 °C was attributed to the latent energy required to melt the ice present in the MSW (Bonany et al., 2013; Megalla et al., 2016). These findings are consistent with the temperatures measured at a landfill in Anchorage, Alaska by Hanson & Yeşiller (2010; 2015a). It was stated in later research that wastes frozen at placement could remain frozen for up to 2 years (Hanson et al., 2010; Yeşiller et al., 2015a).

For the purpose of geothermal energy recovery, studies proposing designs of heat extraction wells consistently describe the central region of the landfill as the optimal zone to install wells (Coccia et al., 2013; Grillo, 2014; Yeşiller et al., 2015b). Highest temperatures, and thus rates of microorganism activity, heat generation, and energy potential have consistently been observed to exist away from the side slopes by at least 20 m and beneath the upper 8 m zone subject to atmospheric cycling (Yeşiller et al., 2005). This is inconsequential for vertical extraction arrays which are typically constructed from the upper plateau and thus already directly above the central region of the landfill (for typical cell geometries). Horizontal configurations have advantages for energy extraction potential and applications to cooling landfill liners, however are at risk to damage due to settlement of the MSW with time (Coccia et al., 2013; Grillo, 2014). The common

pathways of thermal energy transfer within a landfill and climate or operational factors affecting maximum waste temperature are explored in the next sections.

2.3.2 Energy Transfer Mechanisms

When considering landfills as geothermal energy sources it is important to understand that the waste temperature trends and maximum temperatures reached are a result of energy being introduced or removed from the system, the relative magnitudes of each, and the rates of change throughout time. Temperature differences within the landfill and between the landfill and the surrounding media results in energy transport as conduction. Conduction of thermal energy by MSW and the pore fluids is influenced by the thermal conductivity of the materials as well as the thermal gradient across the area of interest.

Spatial and temporal temperature variation was measured by Yeşiller et al. (2005) and Hanson et al. (2010) at four landfills across North America. The sites were located near the cities of Anchorage, Vancouver, Canton, and Las Cruces and experienced different climates (Table 2.5). Average annual air temperature (AAAT), precipitation, Koppen-Geiger classification, and maximum waste temperatures are presented in Table 2.5 for a number of North American landfills (after Yeşiller et al., 2015a). Climate data for Saskatoon is included for comparison and the data is average annual values between 1988 and 2018 from the Environment Canada weather station identified in Figure 1.1. It should be noted that peak temperatures reported for the sites depend on the timeframe of temperature data collection as some sensors were trending upwards at the time of publication. The Koppen-Geiger term for ‘no dry season’ is represented by ‘NDS’ in the table.

Table 2.5: North American landfill climate data and Koppen-Geiger classification (after Yeşiller et al., 2015a)

Location	Peak Temperature and waste age	Climate Region	Average Annual Temperature (°C)	Average Annual Precipitation (mm)	Source
Vancouver, BC	92 °C at 2 years	Temperate, NDS, warm summer	9.9	1,167	Yeşiller et al. (2015a)
Canton, Michigan	62 °C at 3.5 years	Cold, NDS, warm summer	9.8	835	Yeşiller et al. (2015a)
San Luis Obispo, California	58 °C at 3 years	Temperate, dry, warm summer	8.7	354	Yeşiller et al. (2015a)
Anchorage, Alaska	55 °C at 10 years	Cold, NDS, cold summer	2.3	408	Hanson et al. (2010)
Las Cruces, New Mexico	30 °C at 4 years	Arid, steppe, cold	18.2	240	Hanson et al. (2010)
Philadelphia, Pennsylvania	30 °C at 1 year	Cold, NDS, warm summer	10.6	1,156	Koerner (2001)
Ste. Sophie, QC	4 °C at 2 years	Cold, NDS, warm summer	6.7	997	Bonany et al. (2013)
Saskatoon, SK	----------	Cold, NDS, warm/cold summer	2.7	351	Environment Canada historical data

In general, higher thermal gradients were observed at landfills in cooler, wetter climates that support high waste temperatures when compared to warm, dry climates with cooler peak waste temperatures (Hanson et al. 2010). In frozen wastes placed in Ste. Sophie, Quebec, researchers concluded that the initial flux direction of thermal energy was consistenly upwards through the liner from the subgrade into the lowest layer of MSW due to the positive temperatures in the subgrade and negative temperatures in the waste. This upwards flux was considered a critical source of energy required to thaw the frozen MSW (Bonany et al., 2013; Megalla et al., 2016).

In addition to conduction of thermal energy along temperature gradients, energy can be transported or introduced to the landfill through other mechanisms. Gasses present in the pore space of MSW will equilibrate in temperature to the surrounding waste but flow within the pore space is primarily due to pressure gradients (convection) and secondarily across concentration gradients (diffusion) (Ishimori et al., 2011). When the gas moves, it will either lose or gain heat to the surrounding waste it passes depending on the temperature difference. Similarly, leachate will transport thermal energy within a landfill or cover system when it moves as a result of hydraulic head gradients or under the influence of gravity (Hanson et al., 2013; 2008; Hao et al., 2017). Results from analyzing

pumped leachate volumes and waste/liner temperatures predicted only 5% of thermal losses to occur from convective leachate flow and the rest was attributed to conduction, as gas flow data was not available (Yeşiller et al., 2005). The atmosphere can introduce or remove energy via solar radiation and convection with air as a result of winds. Energy can also leave the upper MSW or cover layer via long wave radiation (Bonany et al., 2013; Megalla et al., 2016). These different mechanisms can be incorporated into numerical model boundary conditions or by coupling fluid flow and thermal energy equations together.

2.3.3 Factors Affecting Maximum Waste Temperature

Several mechanisms describing the thermal regime within a landfill have been reviewed in the preceding sections. Each mechanism comes with variables and properties that affect the magnitude of thermal energy introduced, stored, or removed from the landfill system. As well, it is evident that these variables are coupled to physical and chemical processes. Climate (precipitation and temperature) and site operating conditions both impact waste temperatures and, if the overall waste composition is considered comparable between sites, are the primary factors differentiating landfill temperature from one site to another. An interesting observation drawn from both Yeşiller et al. (2005) and Hanson et al. (2010) was that higher waste placement temperatures (for placement temperatures above freezing) correlated to higher final or maximum measured temperatures at any sensor at the Anchorage landfill. From this, the conclusion was also drawn that non-frozen wastes increased in temperature at similar rates across a cell, except in locations where aerobic heat generation contributed to rapidly increasing waste temperatures (Yeşiller et al., 2015a). This implies that waste layers placed in the warmest months of the year may reach higher maximum temperatures than layers placed in the cooler months, even if the waste is not frozen at placement. This also implies that on average, waste placed in warmer climates should reach greater temperatures than waste placed in cooler climate regions, however was not consistently the case for the studied landfills (Hanson et al., 2010) such as in Table 2.5.

As reviewed in Section 2.1.1, moisture content of waste affects the hydrolysis rates of cellulose (El-Fadel et al., 1996a; 1996b; 1996c) as well as being a component in the formation of acetic acid (Table 2.1). Provided the landfill is not a dry-tomb design, which uses an impermeable cover system designed to prevent infiltration, precipitation is another climate factor considered to affect waste temperatures (Yeşiller et al., 2015a). Higher magnitudes of annual precipitation contribute

to higher moisture contents in the waste over time and thus higher rates of heat generation, exemplified by higher temperature increases being observed at the landfill near Anchorage, Alasksa compared to Las Cruces, New Mexico (Hanson et al. 2010) despite the difference in AAAT. High heat generation rates and rate of temperature increase were attributed to high annual precipitation for the landfill in Vancouver (Hanson et al., 2010). The optimal precipitation for heat gain in MSW was reported as 2.3 mm/day (840 mm/yr) by Yeşiller et al. (2005).

From Table 2.5, Saskatoon most closely compares to the Anchorage, Alaska site in terms of AAAT and annual precipitation. A large contrast in temperature of 2-year-old waste between Ste. Sophie and Vancouver is evident (4 versus 92 °C), with only marginally greater atmospheric temperature and precipitation in BC. Colder climates may also experience a large portion of annual precipitation as snowfall, which can insulate the waste from the atmosphere (Hanson et al. 2010) but also be blown off the surface of the landfill by wind before infiltrating as meltwater. Although heat rates were greatest in the high precipitation Vancouver area, temperature increases were greater in Canton. This contradiction was attributed to the high moisture content in the Vancouver landfill increasing the bulk heat capacity and lowering the bulk density of the wastes when compared to what was determined for Canton (Hanson et al. 2010). The relationship between water content and thermal properties was reviewed in Section 2.2.2.

Operational conditions that influence waste temperature include waste placement rate, waste fill thickness, and introduction of oxygen from gas extraction (Yeşiller et al., 2005; Jafari et al., 2017). A linear relationship was reported between waste placement rate (m/y) and heat content of wastes (a measure of energy gain in the MSW in units of °C·d/d) (Yeşiller et al., 2005). This is attributed to the insulating nature of overlying waste layers as mentioned previously. This implies that a cell that is built vertically in a shorter time than another cell (ie. more time passes between placement of lifts) would increase in temperature at a greater rate and experience a greater peak temperature compared to similar aged wastes in the more gradually filled cell. Although waste thickness was mentioned in early studies to influence waste temperatures (Yeşiller et al., 2005; Rowe, 1998), no trend or correlation was mentioned in more recent studies. For example, the Vancouver landfill that reached temperatures of 92 °C has a thickness of only 19 m and the landfill in Philadelphia, Pennsylvania reached only 30 °C and has a thickness of 50 m (both locations have similar annual average temperature and precipitation). Aerobic activity in landfills can lead to unusually high

temperatures and even combustion and/or fires in the buried MSW. Apart from the oxygen present when the waste is placed, oxygen can be introduced to the upper waste layers via vacuum pressures within the landfill as a result of landfill gas recovery (Jafari & Stark 2016; Jafari et al., 2017; Reinhart et al., 2017; Khire et al., 2020). From comparison of temperatures and climate at multiple landfills in this section, the complexity and coupled nature of the landfill thermal regime is even more apparent. Numerical modelling is an important tool that has been used by various authors in the literature to predict temperatures or determine material properties within the landfill environment.

2.4 Numerical Modelling of Thermal Regime

Numerical models of landfills have been developed over the past three decades to predict problems ranging from rapid or uneven settlement and slope instability to predicting excessive liner and waste temperatures. A comprehensive review of coupled numerical models produced over this time period was published by Reddy et al. (2017) and discusses the different programs and equations used by various authors. A coupled model capable of accounting for several processes and mechanisms known to take place within an MSW landfill environment (such as unsaturated fluid flow, stress-strain response, biodegradation, and gas/heat generation) is an extremely challenging problem. This challenge is the reason most authors limit the number of mechanisms modelled and were required to make a number of assumptions without the supporting field data (Reddy et al., 2017). The review paper focusses on the coupled processes that occur in a bioreactor landfill, where leachate recirculation takes place and moisture contents are increased as a result. The interconnectedness of the processes is depicted visually in Figure 2.2 (after Reddy et al., 2017). The figure presented by Reddy et al. (2017) for bioreactor landfills was modified for geothermal extraction systems at conventional landfills (not bioreactor or dry-tomb applications).

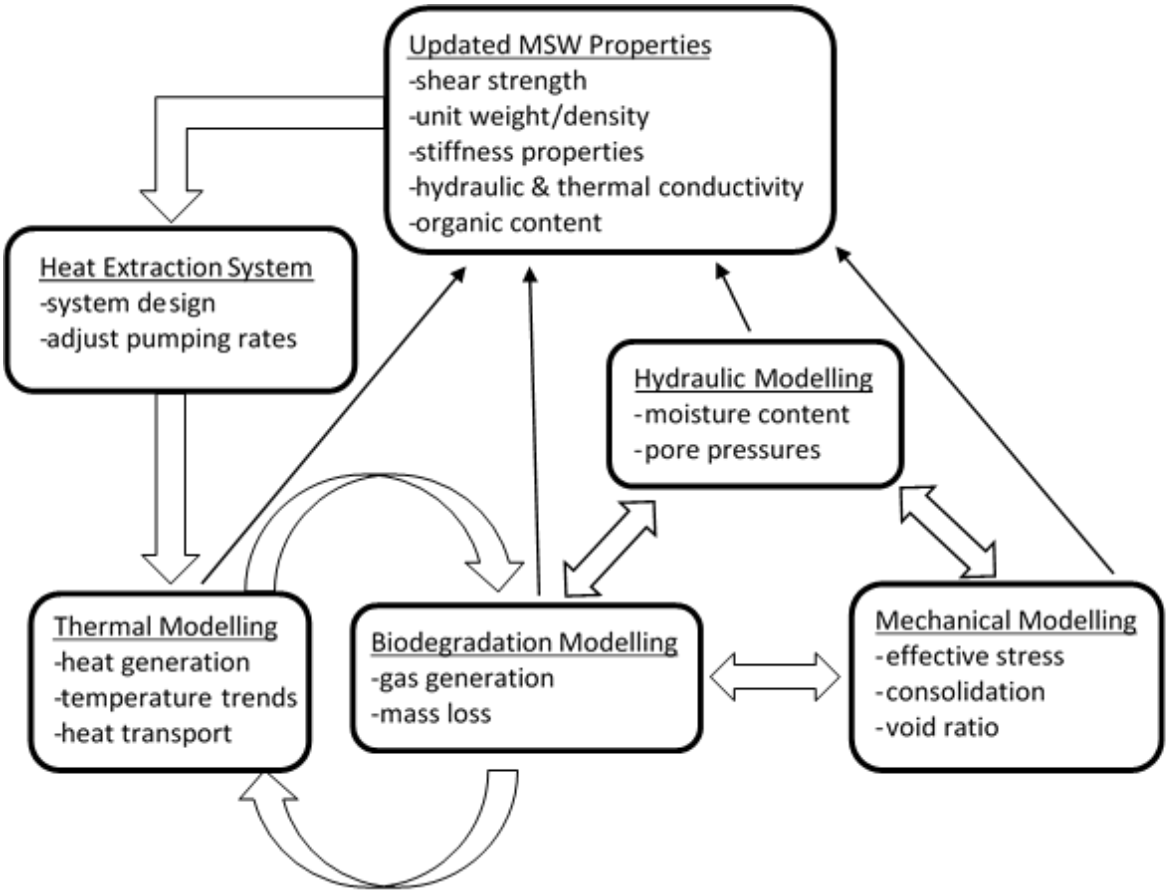

Figure 2.2: Flow diagram of coupled processes in landfill modelling (after Reddy et al., 2017)

Heat generation and gas generation are coupled as demonstrated by the relationships in Figure 2.2. Because of this relationship it is important to understand that void changes and transient physical properties directly affects hydraulic, biodegradation, and thermal modelling in MSW landfills. Additionally, increasing MSW temperature has been correlated to increases in compressibility, hydraulic conductivity, settlement rate, and total settlement in landfills (Yeşiller et al., 2015; Reddy et al., 2017). Of the many studies reviewed by Reddy et al. (2017), only those that focussed on thermal modelling and of relevance to my research at the Northern Landfill will be discussed in this section.

Biokinetic, gas, and heat generation modelling was done mathematically by El-Fadel et al. (1996a; 1996b; 1996c) and compared to field data from a landfill in California. These models demonstrated the coupled nature of microorganism digestion rates with gas and heat generation and the feedback of temperature and pH in the landfill environment. The authors also defined heat generation as proportional to gas generation via a conversion factor. Depletion of organic carbon was found to

be first order (hydrolysis rate) and is the rate-limiting step until methanogenesis supersedes the role once concentrations of acetate, methane, and CO_2 stabilize (El-Fadel et al., 1996a; 1996b).

Nastev et al. (2001) used a numerical model that accounts for fluid property changes with temperature to predict gas and heat transport in a Montreal landfill (CESM). The gas generation rate was an exponentially decreasing function using a decay rate measured from gas recovery wells on site. Heat generation followed this same shape based on a conversion using enthalpy per mole of CH_4 generated (Table 2.2). A 1D model defined the evolution of pressure, temperature, and gas composition in a 40 m thick waste profile using a constant AAAT of 6.6 °C as the top boundary and 20 °C at the bottom. Temperatures reached a maximum of 38 °C at depth after 20 years (Nastev et al., 2001). The published profiles were convex and related well to the theories explained in Section 2.3.1. This model was one of the earliest coupled heat and gas numerical models published in the literature.

A thermal numerical model was developed by Hanson et al. (2008) which included formulation of exponential growth and decay heat generation functions using empirical methods. A 1D vertical finite element analysis (FEA) was constructed with element sizes of 0.5 m, determined by a relative error analysis of mesh refinement with element size ranging from 0.1 to 6 m. Homogeneous thermal properties specific to four modelled landfill sites were based on MSW composition and needle probe tests performed (properties listed in Table 2.4). The subgrade material was included in the 1D geometry to a depth of 75 m below the landfill liners after iterating depths ranging from 10 to 200 m. The top boundary was a transient atmospheric temperature function that used modified air temperatures to account for incoming and outgoing radiation using freeze/thaw *n*-factors. These *n*-factors were calculated from measured near-surface (shallow) waste temperatures (Hanson et al. 2008).

The authors determined initial subgrade temperature profiles by simulating 7-10 years of atmospheric temperature cycling beginning with a uniform temperature profile set to the mean annual earth temperature (MAET). Waste placement was modeled in 3 to 5 m thick lifts until final height was reached. Placement times were based on site records, aerial surveys, and land-based surveys. Waste placement temperatures were equal to the daily average temperature on the day of placement. The geometry of the model simulating the thermal regime of a column of waste within the central region of the landfills, away from atmospheric edge effects, is visualized in Figure 2.3

(after Hanson et al., 2013). This figure represents the conceptual model for the 1D heat transport numerical model developed for my research.

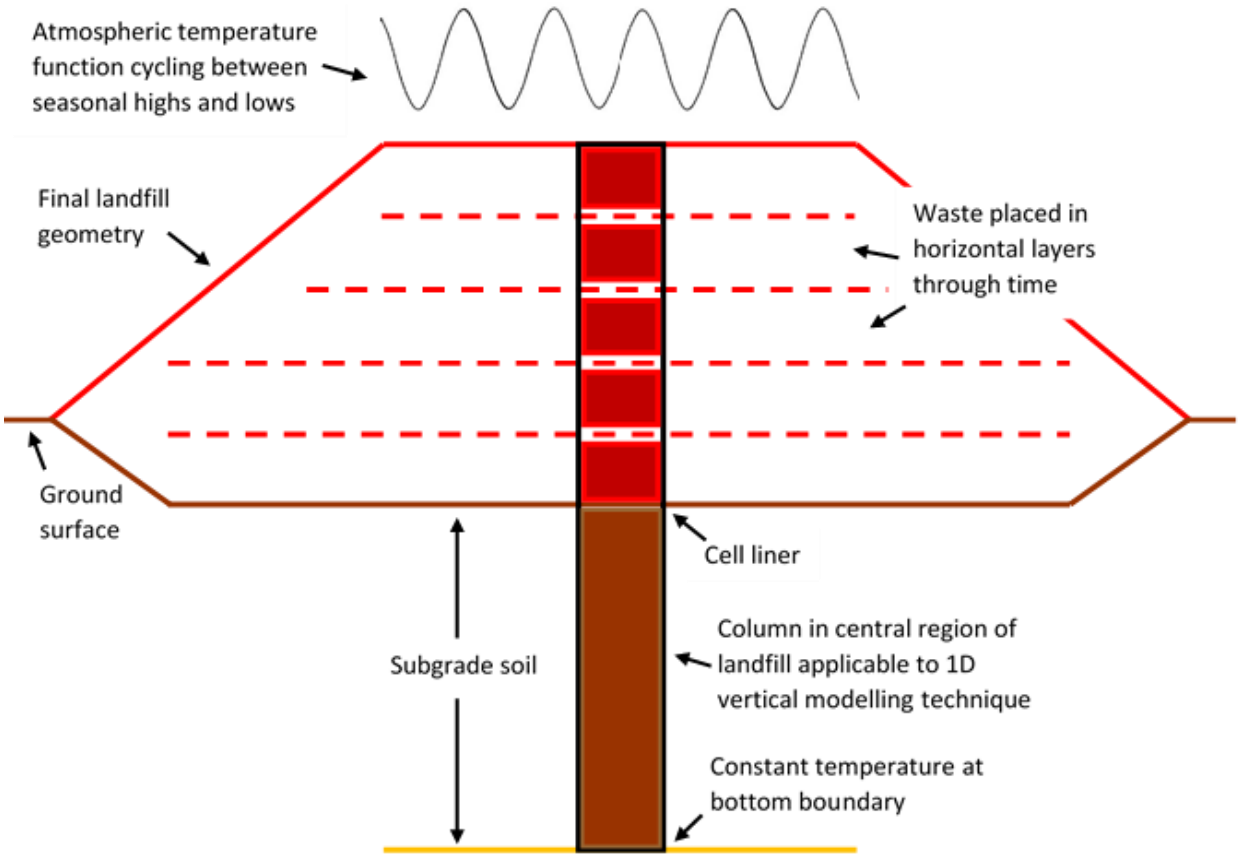

Figure 2.3: Visualization of 1D heat transport model theory and geometry (after Hanson et al., 2013)

The FEA model was used to determine empirical heat generation functions for each site by performing nonlinear regression analysis between modelled and measured temperatures. Model fitment was achieved at all four sites using an exponential growth and decay function (Hanson et al. 2008). The function defines heat generation rate (W/m^3) with time (d) and its shape is dependent on peak heat generation rate (W/m^3), a decay rate factor (d), and a shape factor (d). Peak heat generation rates and the shape factor were correlated to a composite climatic-operational component defined as the product of AAAT and annual precipitation divided by the MSW unit weight. The decay rate factor was correlated to average vertical landfilling rate (m/y). The resulting curves after calibrating the various fitting parameters for the four North American sites are shown in Figure 2.4 for comparison (after Hanson et al., 2008).

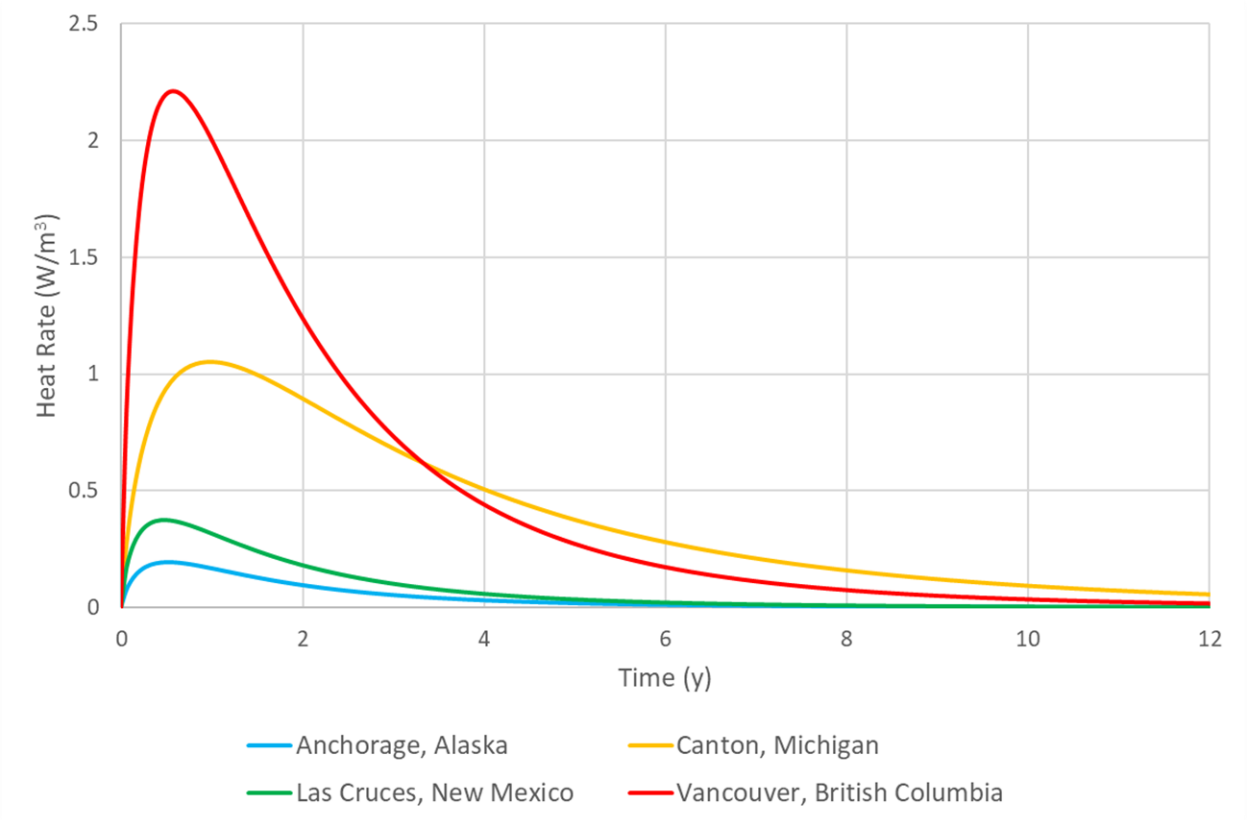

Figure 2.4: Transient heat rate functions for four landfills developed by Hanson et al. (2008)

From Figure 2.4, the BHP of the waste for the sites is the total area under each curve which varied between 15 MJ/m^3 (Anchorage) to 191 MJ/m^3 (Vancouver). Based on the formulation of the exponential growth and decay curves by Hanson et al. (2008) higher precipitation and warmer AAAT would result in higher peak rates of methanogenesis and heat generation, which is illustrated by the curves in Figure 2.4.

The model outlined by Hanson et al. (2008) was applied by Emmi et al. (2016) to a landfill in Italy for comparing and validating geothermal heat extraction designs. The authors used a sol-air temperature top boundary which combines solar radiation and convective heat transfer instead of *n*-factors and used the same exponential growth and decay heat generation formulation defined by Hanson et al. (2008) for the MSW with site-specific climate and operational factors applied. For comparison, the calculated heat generation curve had a peak of 0.64 W/m^3 which was between the Canton and Las Cruces curves in Figure 2.4. The model simulated the entire landfill geometry in 2D using finite element modelling (FEM) software with an average waste depth of 18.5 m

(reported landfill height plus landfill depth). No gas or leachate flow was modelled, and all the waste was assumed to be placed at the same time and at a uniform temperature of 12.5 °C.

Similar to the studies by Hanson et al. (2008; 2013), Bonany et al. (2013) and Megalla et al. (2016) developed 1D heat transfer models that were calibrated to field temperature data. The temperature data comes from sensors placed below and between waste lifts as a cell was landfilled in Ste. Sophie, Quebec. A heat budget was developed to calculate magnitudes of energy introduced to the MSW through different mechanisms including atmospheric convection and radiation, biological heat generation, and conduction from the subgrade. A 2D FEM with triangular elements was constructed to simulate heat transfer in the 6 m waste layer. The top boundary incorporated emissivity and black body radiation properties for the MSW as well as wind-governed forced convection (Bonany et al., 2013). Because temperature data was available immediately following the placement of lifts, and the model simulated a relatively short period of time (~325 d), the study was well-suited for calibrating model inputs (thermal properties, heat rate, density, and top boundary radiation/convection factors) provided that fewer degrees of freedom existed. A step-wise heat generation function marked by a threshold temperature (10 °C) for the onset of biological heat generation was formulated. Heat generation equalled zero below this threshold and was governed by a 2^{nd} order polynomial equation, dependent on MSW temperature and a scaling factor above the threshold.

The sensitivity analysis by Bonany et al. (2013) indicated that the temperature response at the uppermost instrument bundle (0.5 m below surface) was not sensitive to changes in K_T but the bundles below (~3 m below surface) were more sensitive as a higher K_T resulted in more heat reaching the greater depths (Bonany et al., 2013). The model was insensitive to changes in volumetric HC, but higher values did slightly reduce the rate of temperature change and heat transfer within the waste layer. The model was sensitive to the heat generation scaling factor but only the uppermost bundle exceeded the threshold temperature meaning much of the waste had a heat rate of 0 W/m^3 for the duration of the simulation. Lastly, the model was most sensitive to variance in the magnitude of latent heat of fusion due to most of the waste being placed in below freezing temperatures and the significant amount of energy required to thaw the ice in pore spaces over the modelling timeframe (Bonany et al., 2013).

Megalla et al. (2016) published further model results and temperature data for the same site. A detailed heat budget breaking down the energy lost or gained from the different mechanisms at waste layer placement intervals over a period of 4.6 years was included. Convection, solar radiation, and long wave radiation (emitted from top of MSW) all impacted the top boundary in terms of energy flux, with solar radiation increasing energy flux into the MSW and the other two mechanisms increasing flux out of the MSW. The net surface flux (sum of the three mentioned mechanisms) was initially positive (into the MSW) but became increasingly negative as a result of increasing top layer MSW temperatures through time. The top 1 m of waste was observed to generate heat aerobically and contributed to 36% of the total heat generation over the duration. Based on best-fit analyses, K_T was modelled as heterogeneous and was assumed to increase linearly with depth with the same initial value maintained at the top 1 m of MSW (Table 2.4).

A landfill in NE USA with an average thickness of 20 m was modeled by Khire et al. (2020) using 2D FEM software. The authors aimed to determine heat generation rates within the MSW by calibrating the model to temperature profiles measured on site. The model divided the MSW into 3 sequential layers from top to bottom defined as fresh waste (0 to 2 y and 4.4 m thick), intermediate (2 to 6 y, 9.8 m), and aged (6 to 9 y, 5.8 m). Thermal properties were applied to each layer based on observed changes in density and degradation (Table 2.4). The top boundary was a constant AAAT value of 15 °C. 20 m of subgrade below the liner was included with a constant temperature boundary of 15 °C applied at the bottom based on groundwater temperatures from nearby monitoring wells. Vertical leachate flow was incorporated and collection points along the model domain simulated leachate pumping. The heat generation rate was assumed constant over the simulation periods (5 to 9 y durations) to determine average representative values. Heat generation in the aged layer was assumed equal to zero and the upper two layers were assumed to have equal heat generation rates. The MSW initial temperature was assumed equal to the AAAT and the full waste thickness was present at time zero. Maximum measured temperatures at the site ranged between 71 and 79 °C.

Because Khire et al. (2020) modelled fluid flux at different rates and heat generation was maintained constant, the effects of leachate convection on the temperature profile in the waste could be observed. As downward leachate flow increased, the location of the peak temperature moves downward and the magnitude decreases (Khire et al., 2020). Through manipulation of the

leachate flow rate and constant heat generation rates of the upper layers, the best-fit to site data for heat generation was 0.7 and 0.8 W/m^3 for 9 and 5 y old waste columns respectively (with a leachate flux reported as 37 $m^3/ha/d$). Because temperature profiles were relatively stable over the monitoring period, a heat generation rate as low as 0.2 W/m^3 in both locations was demonstrated to offset the conductive and convective losses over the monitoring time frame and the authors concluded that heat generation rates decrease with waste age (Khire et al., 2020).

A box model presented by Hao et al. (2017) for heat generation and accumulation in landfills mentions the existence of heat generated due to aluminum corrosion, ash hydration, and thermal reactions. The bulk MSW decay rate for biodegradation used by the authors was 0.04 y^{-1}. The model also accounts for water (liquid and vapour) and gas (H_2, CH_4, CO_2) leaving and entering the landfill system. Modelled average waste temperatures were relatively stable from 20 to 50 years likened to a balance between heat sources and sinks (Hao et al., 2017).

2.5 Gap Analysis of Reviewed Literature

From the literature review, gaps in the knowledge were identified that refined the objectives of my research as well as exemplified the heterogeneity of example waste properties and complexity of modelling heat generation and transport in the landfill environment.

Despite agreement by many authors that methanogenesis from cellulosic material is the most representative reaction pathway associated with landfill gas and heat generation, a broad range of values for associated enthalpy of reaction (ΔH) were reported (Table 2.2). This is likely a result of different methods being used to estimate the heat generation in landfills, with various energy sources other than anaerobic methanogenesis being potentially included or omitted. As a result of this variety, a bounded approach was used for performing calculations requiring a value of ΔH.

By reviewing numerical heat transport models published in the literature, it was found that heat potential of the MSW (cumulative heat generated) and heat generation rates varied dramatically between sites studied and the modelling methods used. In some cases, a constant heat rate was applied as opposed to a transient function. The magnitude of heat potentials based on the empirical model developed by Hanson et al. (2008; 2013) were dependent on climatic and operational factors (AAAT, annual precipitation, and landfilling rate). When Saskatoon AAAT and annual precipitation data was applied to the empirically-derived equation proposed by Hanson et al.

(2008; 2013) the equation was unsolvable, and the energy-expended function proposed by Hanson et al. (2013) was not reproducible for the modelling methods used in this research.

A mechanistic heat generation function for the Northern Landfill had to be derived from gas generation theory as part of this research. It should be expected that nearly all degradable organic matter can eventually be converted to landfill gas and heat energy as time progresses and temperatures remain elevated within the core of the waste fill, although heterogeneity of organic content of MSW is expected. Therefore, the heat generation function should be formulated such that ultimate heat potential is achieved in eventuality, which was not evident in the literature. The long-term temperature trends and total energy potential of MSW are important factors for engineers to evaluate landfills as geothermal energy sources. Thus, it became the objective of my research to determine the heat potential of the MSW at the Northern Landfill with methods that can directly relate heat potential to measurable MSW properties such as BMP and organic content.

2.6 Northern Landfill Geology and Background

The subgrade soil represents a large heat sink for generated heat within the MSW. The subgrade is also a potential heat source to fresh wastes placed in cold temperatures (Megalla et al., 2016). The waste placement rate, AAAT, annual precipitation, landfill geometry, and groundwater temperatures are also influential on heat transport modelling (Hanson et al., 2008; 2013). The subgrade geology and groundwater temperatures were investigated along with a background study of the design and operation of the Northern Landfill.

A site investigation was published by Haug et al. (1989) for the Northern Landfill and detailed the subgrade stratigraphy. The uppermost soil layer on site is a stratified deposit of sand and gravel intermixed with oxidized, fractured, low plasticity till of the underlying Floral Formation. Depth to this stratified layer is a maximum of 5 m below ground and it is lenticular in nature. The Floral till beneath the surficial layer is unoxidized and extends a minimum of 30 m below ground surface. Beneath the Floral till is an unoxidized stratum of Sutherland till which extends up to 70 m depth. Under the Sutherland till is an aquifer of stratified sands and gravels of the Empress group which lie above the Bearpaw shale formation. The surficial deposit hosts a shallow water table less than 1.5 m from surface in some places (Haug et al., 1989; Yanful et al., 1990).

Physical properties of the Sutherland and Floral group tills were reported by Macdonald & Sauer (1970). Specifically, the grain size, bulk density, and water content of the tills were required for estimating the bulk K_T and HC from Hamdhan & Clarke (2010). The physical properties of the tills from Macdonald & Sauer (1970) and estimated thermal properties are in Table 2.6.

Table 2.6: Physical and thermal properties of the subgrade till soils

Formation	**Physical Properties** from Macdonald & Sauer (1970)			**Thermal Properties** from Hamdhan & Clarke (2010)	
	Clay content (%)	Bulk density (kg/m^3)	Water content (%)	K_T (W/m)	HC ($MJ/m^{3\cdot}°C$)
Floral	20	2,290	11	3.69	2.61
Sutherland	39	2,180	18	2.45	3.18

3.0 Research Methodology

This chapter presents the methodology of my research. This includes methods regarding the field work and data collection performed at the Northern Landfill, laboratory work with MSW samples, and the framework and details of the numerical heat transport model developed.

Field work was a key phase of my research for several reasons. Firstly, it provided in-situ transient temperature profiles of the MSW at the Northern Landfill. The temperature data was necessary for developing a numerical model as it provided initial conditions, top and bottom boundary conditions, and targets for calibrating model inputs and outputs.

Secondly, field work was required to collect semi-continuous MSW core sample from surface to the liner elevation. Laboratory testing of the MSW cores collected from multiple locations at the Northern Landfill provided an opportunity to calculate the MSW water content, bulk and dry density, as well as identification of dated objects that were visible in the extracted material. The dated objects revealed the earliest possible year of placement for MSW at specific locations across site. The density of the MSW was a useful property for calculating BMP and C_{eq} according to the equations presented in Section 3.3.

Thirdly, gas wells installed in the sampled boreholes allowed for sampling of the landfill gas and measurement of gas pressures and leachate levels at instrumented locations. The gas compositions and positive pressures measured from the boreholes verified that anaerobic conditions exist and that landfill gas is being generated at the instrumented locations.

The methodology used for developing the heat transport model for my research is also outlined in this chapter. The process involved components of subjectivity and required several assumptions to evaluate the heat potential property of the MSW, due to the number of unknown parameters and degrees of freedom that existed. The modelling performed simulates an energy balance, thus the resulting heat potential term encompasses heat generated from anaerobic digestion of cellulose and methanogenesis as well as abiotically and from other organic compounds. The field and laboratory measurements aided in reducing the number of unknown parameters however information regarding the MSW thermal properties and placement history had to be approximated. The methodology for the measurements is outlined at the end of this chapter in addition to other components of the heat transport model.

3.1 Field Work and Instrumentation

The selected instrument for measuring the waste temperatures at the Northern Landfill was a thermistor. Pictured in the left-most image of Figure 3.1, a thermistor consists of a two-strand tinned-copper wire electrically connected at the tip and coated by a small bead of epoxy. The resistance to current through the epoxy-coated tip (at constant voltage) is related to the temperature of the bead.

Time constraints and uncertainty of conditions within the Northern Landfill dictated that the instruments would be installed in different phases as opposed to all at once. Three separate drilling phases took place and a total of six vertical thermistor arrays were installed across the upper plateau of the landfill. Details of the instrument installations and timing of each drilling phase is in Table 3.1. Phase 1 and 3 used arrays made in the geotechnical laboratory (referred to as "manufactured"). Phase 2 used arrays purchased from a geotechnical instrumentation company (referred to as "purchased"). The different type of arrays are pictured in Figure 3.2 during installation in the field.

Locations of the instrument installations in plan view are identified in Figure 3.3. The locations of the instrument Clusters are intended to provide data from across the upper plateau as far west and east as possible. The final positions of boreholes depended on drill rig accessibility and being unobtrusive to day-to-day operations of the landfill (growing stockpiles, shredding operations, truck traffic, and machinery parking). Due to ongoing operations and waste placement on the east side of site, no instruments were installed in the oldest two waste cells (1 and 2). Cluster 4 on the north side of the active haul road became an option after placement of waste on the north side of site occurred between Phase 1 and 2. This Cluster was installed to contribute to spatial variability in the site temperature and landfill gas data. An overview of the instrumentation and the installation of the arrays is included in this section.

Table 3.1: Thermistor array identifier, type, location, and date installed with maximum thermistor depth included

Cluster	Instrument/Borehole	Phase
1 – *NW corner of cell 6*	**BH18-01**: PVC gas well with manufactured thermistor array to 20 m depth and unshielded atmospheric temperature	Phase 1 – July 2018
2 – *NW corner of cell 4*	**BH19-02A**: PVC gas well with purchased thermistor array to 24 m depth and unshielded atmospheric temperature **TH19-02**: 1" PVC disconnected from surface with purchased thermistor array to 24 m depth and shielded atmospheric temperature	Phase 2 – May 2019 Phase 2 – May 2019
3 – *NE corner of cell 4*	**BH18-03:** PVC gas well with manufactured thermistor array to 20 m depth and unshielded atmospheric temperature	Phase 1 – July 2018
4 – *SE corner of cell 5*	**BH19-04:** PVC gas well with purchased thermistor array to 24 m depth that **was damaged during installation** **TH19-04:** 1" PVC backfilled to surface with manufactured thermistor array to 24 m depth	Phase 2 – May 2019 Phase 3 – Nov. 2019

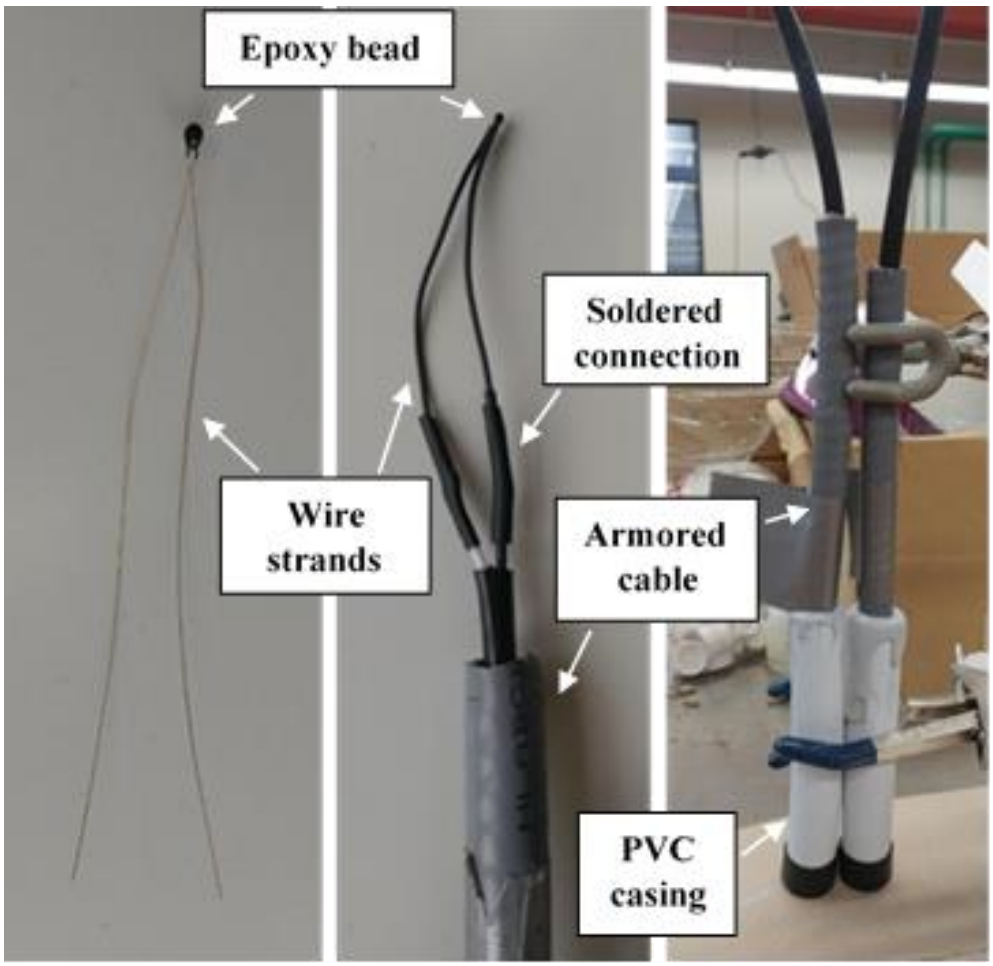

Figure 3.1: Thermistor assembly process in the laboratory for the manufactured arrays used in Phase 1

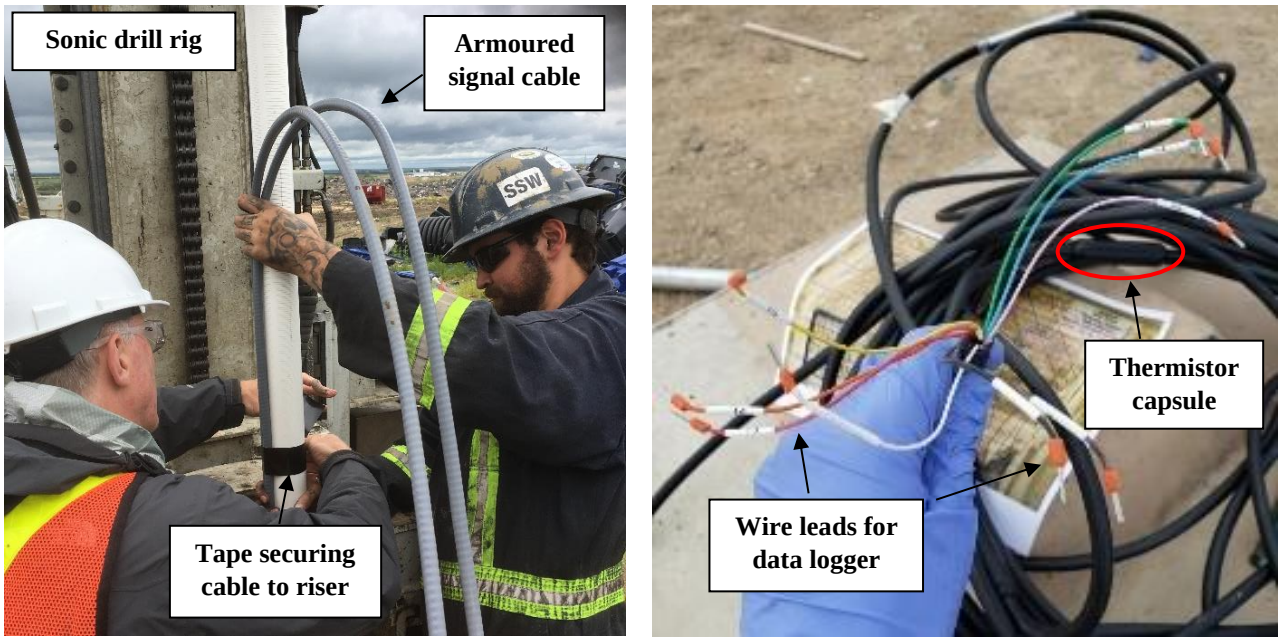

Figure 3.2: Left - Manufactured array during installation; Right - purchased array prior to installation

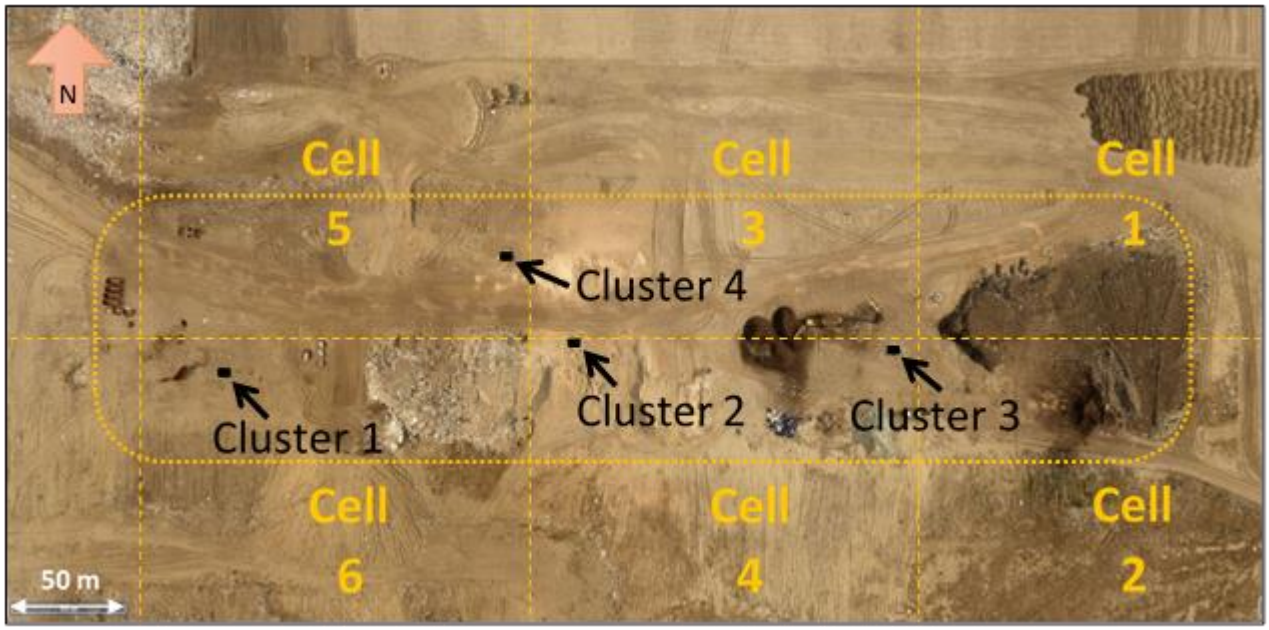

Figure 3.3: Instrument Cluster locations with the upper plateau and cell boundaries drawn as dashed lines. Note BH18-01 is located at Cluster 1, BH18-02 at Cluster 2, and BH18-03 at Cluster 3.

3.1.1 Thermistor Array Construction and Installation

Prior to any field work in Phase 1, temperature measuring instrumentation was assembled in the laboratory as depicted in Figure 3.1. The manufactured arrays used 10 kOhm thermistors which

were soldered to armoured cable, cut to length depending on the target depth of each thermistor. The thermistor target depths (1, 3, 5, 10, 15, and 20 m) were selected so that spacing was smaller in the top portion of the MSW where temperatures were expected to be more variable over the seasons. Each soldered thermistor was inserted into a 6-inch (15 cm) long, 1/2-inch (1.3 cm) diameter PVC tube capped at one end and filled with a self-leveling epoxy sealant that dries into a rubber-like compound to protect the wires from water and sand backfill. Figure 3.1 labels the components and depicts the steps of the thermistor manufacturing completed in the laboratory.

The purchased arrays were made with thermistors individually encased in plastic capsules along a bundled signal cable. The capsule protects the thermistors from water and sand and the bundled cable was reinforced with Kevlar stranding. The purchased instrument is pictured in the right-hand image in Figure 3.2. The thermistors were placed at specified locations along the cable. A thermistor at a target depth of 24 m below the 20 m depth was included in Phases 2 and 3 arrays once installation and drill rig capabilities were determined in Phase 1. Each thermistor (manufactured and purchased) was connected to a datalogger and tested for accuracy by submerging them in a laboratory water bath at temperatures of 5, 25, and 45 °C. The largest recorded error in the temperature values was ±0.4 °C and was acceptable for field application. The output temperatures from the water bath and calibration equations for each thermistor array are in Appendix A.

To install the thermistor arrays and collect MSW samples, a track-mounted sonic drill rig was contracted for each of the three drill phases. The rig advanced 6-inch (15 cm) outer diameter casing into the waste fill just behind a 4.5-inch (11 cm) outer diameter sample barrel in 10 ft (3.05 m) advancements. The MSW samples were extruded from the sample barrel into plastic sleeves (bags) by the drilling contractor. Weights of the bagged cores were recorded to the nearest 10 g using a scale in the field and were placed inside cardboard tubes for transport back to the laboratory. Several bagged samples existed for each 3.05 m run so that the samples were not an unmanageable length and weight. For example, the top 3.05 m advance of the sonic core barrel at BH18-01 resulted in two bags, identified as samples 1A and 1B. Advancement of the casing became slower and more difficult for the drill rig the lower into the waste fill the contractor advanced. The drill operator was able to advance the sample barrel and extrude core without the use of drilling fluid (water) in Phase 1 boreholes, but the operator in Phases 2 and 3 opted to use drilling fluid. As a

result, the wet weights of the core for Phase 2 and 3 boreholes were not usable to calculate moisture contents or in-situ bulk density.

The target depth of the boreholes was 0.5 m above the liner elevation, which is in the cross-sections in Appendix B. After reaching the target depth, the final depth of the borehole was reported to the nearest foot by the drilling contractor, which could differ from the targeted depth due to MSW sluffing into the borehole beneath the casing. In Phase 1 and 3, the manufactured thermistors were laid out on surface as individual lengths of cable alongside 2-inch (5.1 cm) diameter Schedule 40 PVC risers. The PVC risers were 10 ft (3.05 m) in length and slotted to accommodate gas sampling and pumping tests. The target depths for each thermistor was marked on the outside of the PVC, with the bottom cap of the deepest PVC section (first to be lowered down-hole) used as a datum. Sections of PVC pipe were threaded together as they were lowered vertically down the open borehole. The thermistors were secured to the PVC at the marked target depths using tape and zip-ties while the assembly was lowered down the open borehole. Every 2 or 3 m, tape was wrapped around the PVC and signal cable to secure the arrays in place until the first riser rested on the bottom of the borehole. The annulus space was backfilled with sand by the drill operator to within 3 m below surface. The remaining space was filled with bentonite chips and hydrated to inhibit gas migration around the PVC. Based on the position of the bottom of the PVC after settling into the loose MSW at the bottom of the borehole, the exact thermistor depths below surface were calculated to the nearest 10 cm. The exact depths of each thermistor varied slightly from the target depths and are listed for each array in Appendix A. The installation process for a manufactured string is photographed in the left-hand image in Figure 3.2. The added weight of the armoured cables and significant annulus space occupied by six cables outside of the PVC prompted the use of the purchased thermistor arrays for Phase 2, which proved to be lighter and easier to manage while lowering down the open borehole. Time constraints led to manufactured arrays being used in Phase 3 but a lighter weight signal cable was used compared to Phase 1.

Phase 2 and 3 field work proceeded in a similar fashion as Phase 1. Core sample was collected, weighed, and stored for transport. Thermistor arrays were secured to PVC risers and lowered down the open boreholes but two arrays (TH19-02 and TH19-04) were secured to 1-inch (2.5 cm) diameter solid PVC instead of the 2-inch (5.1 cm) slotted, as landfill gas sampling was not necessary at these locations. At TH19-02, the top two risers (20 ft, 6.1 m) of the 1-inch PVC was

pulled off the array after installation. At TH19-04 the riser could not be separated after installation and was instead backfilled with drilling sand. Without the need for gas sampling, these methods were used instead to reduce the vertical gas convection within the risers speculated to be caused by atmospheric temperature affects around the borehole stickup. Figure 3.4 is an installation diagram of the Phase 1 arrays BH18-01 and BH18-03. Depths are in imperial units as measured in the field. An upper and lower domain are delineated midway between the 5 and 10 m depth and is relevant to the data presented in Section 4.1.

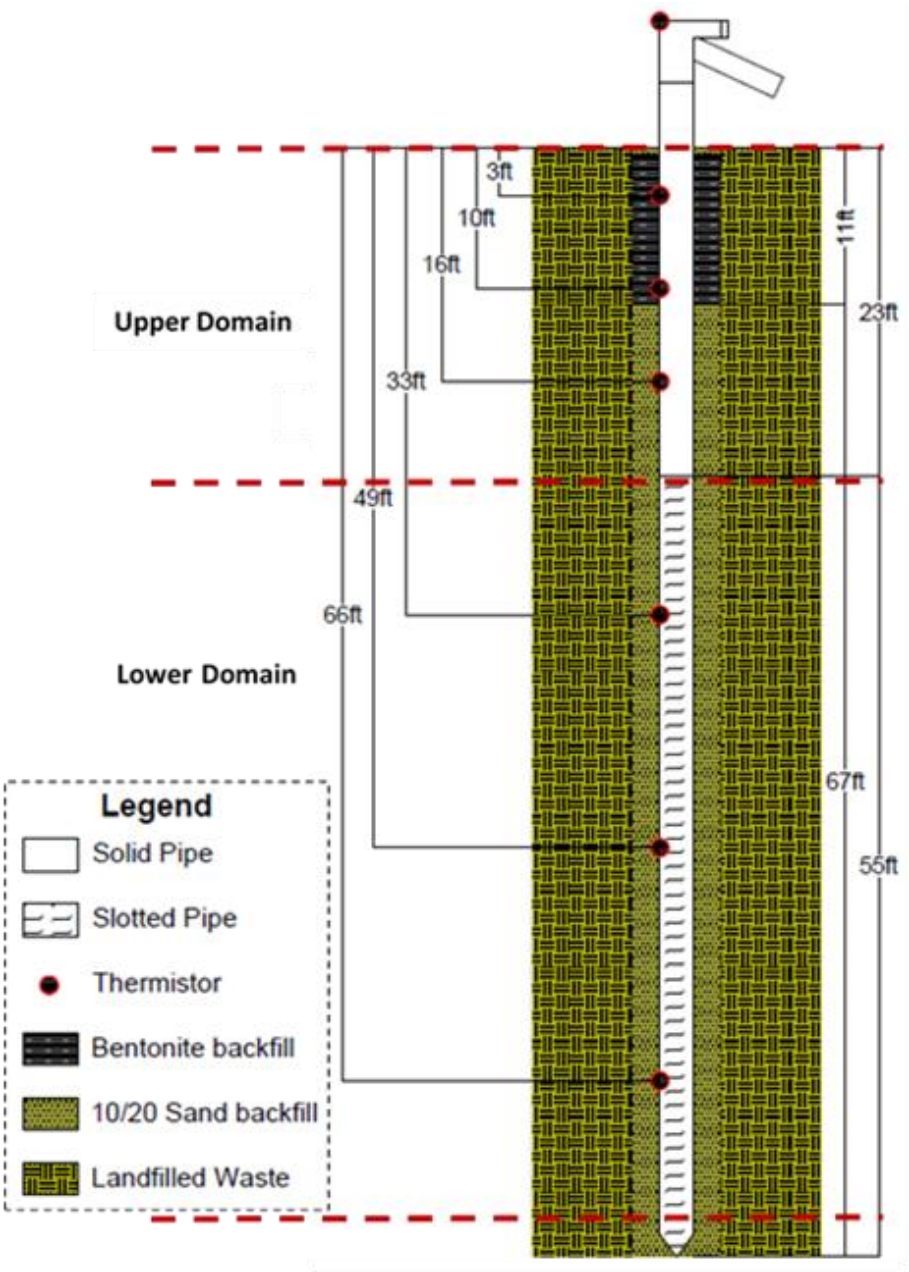

Figure 3.4: Phase 1 borehole construction and installation details.

During Phase 3, a geothermal heat exchange well was installed at Cluster 2 to undertake heat extraction experiments and assess the resulting thermal response of the MSW for future research. This research was outside of the scope of this research. The geothermal prototype well and associated analysis will expand upon the results of my research and the investigation into geothermal energy potential at the Northern Landfill and similar sites.

3.1.2 Laboratory Measurements and Methods

After Phase 1, the MSW core samples that were collected from the boreholes on site were air dried on the floor of the Environmental laboratory at the University of Saskatchewan. MSW core from Phase 2 and Phase 3 were dried on shelves in a canvas tent outdoors on University property. The dry weights were recorded for each individually bagged sample. The weight of all samples within each 3.05 m advance was summed (for example sample 1A plus 1B) and the volume calculated using the inner diameter of the sonic core barrel (9.02 cm) and the 3.05 m length advanced by the drill operators. The dry weight of the waste was divided by the core volume to calculate dry density. The difference between the wet weights and dry weights of the samples revealed both the mass and volume of water present (assuming a density of 1.0 g/cm^3) which was divided by the core volume to calculate VWC. Sources of error in this method of density estimation included the presence of residual moisture within the air-dried cores after four weeks and potential vertical compression of the MSW within the sonic core barrel during advancement would have resulted in a shorter total core length than 3.05 m being recovered each advance.

The MSW cores were to be homogenized into subsamples for analysis of BMP, thermo-graphic analysis (TGA), and loss on ignition (LOI) as part of future research. This presented the opportunity to search for evidence regarding the age of the MSW in the vertically oriented profiles that were recovered. The core samples were laid out on a table and the MSW was searched visually during the subsampling procedure for the various laboratory tests. While searching, objects with dates were picked out and the locations were recorded. Dated objects still identifiable within the MSW samples included copyright years on food packaging, expiry dates, and newspaper or other forms of print with publishing dates. Because the cores had been disturbed during extraction in the field, transportation to the laboratory, and handling during drying and weighing, the position of the objects with respect to the end of the core sample was recorded as being found within the top, middle, or bottom third of the core and the depth calculated to the middle of the respective third.

No dated objects were recovered from BH18-03. Dated objects from Phase 1 boreholes and their positions are included in Appendix C as well as being plotted in Figures 3.10 and 3.11 at the end of Section 3.2. Core weights and the results of calculated density and VWC values are included in Appendix C.

3.1.3 Data Acquisition and Tabulation

After each drilling phase, the installed gas wells or thermistor arrays were finalized for data acquisition during subsequent site visits in the weeks following. The PVC gas wells were topped with adjustable-flow gas wellheads that fit over the PVC risers, pictured in the left-hand image in Figure 3.5. Data logger enclosures were assembled and mounted to hollow aluminum conduits anchored in the MSW adjacent to the boreholes. The tail wires of the thermistors were secured to the ports on the datalogger and terminating resistors were inserted as required.

The datalogging assemblies for the thermistor arrays were powered by solar panels and proved to be reliable while exposed to the elements year-round. Each datalogger input channel was assigned a name corresponding to a thermistor and its depth. A sample frequency of 2 hours was applied to each datalogger. The dataloggers stored the temperature values with a date and time reference. The datalogger's internal clock was synced to the field laptop's but tended to drift approximately 1 minute every month, requiring correction. Data was downloaded to the field laptop during site visits and was imported to a spreadsheet for analysis. Figure 3.5 is an image of BH18-03 once completed and the components of the datalogging enclosure.

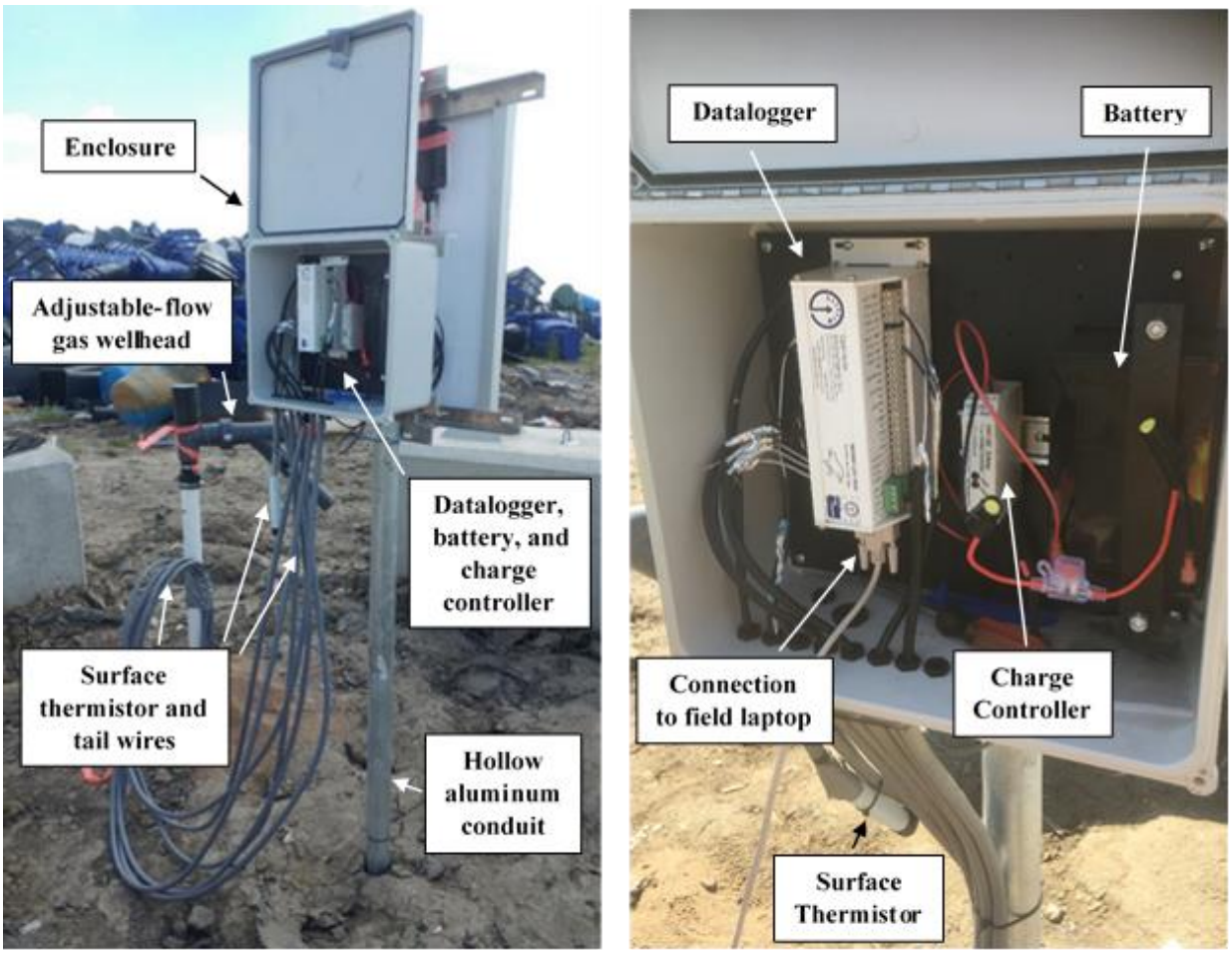

Figure 3.5: View of BH18-03 after completion and its datalogging enclosure

Using a spreadsheet, the raw data was tabulated for each array and the mean of 12 readings on any given date (daily average temperature) was calculated for noise and data pool reduction. The daily averaging of data also allowed for plotting temperatures with the calendar date on the time axis, and improved observation of seasonal temperature trends as opposed to diurnal responses. The resolution of the daily temperature values was also adequate for the numerical modelling boundary conditions that the data represented and therefore was not adjusted throughout the monitoring period.

Site visits occurred on a weekly basis in the summer months and transitioned to a monthly basis in the winter. Along with the temperature data being downloaded, the instruments were inspected and borehole gas pressures, gas composition, passive flow rates, and leachate levels were all recorded. The average leachate head above the liner elevation was measured to be 0.05, 2.48, and 2.25 m at BH18-01, BH18-02, and BH18-03 respectively. Passive gas flows were achieved by

fully opening the gas well heads and measuring the flow rate out of the borehole, driven by gas pressures in the borehole consistently greater than atmosphere, using a Landtec GEM2000™ handheld device. The same device was used to measure the composition of the landfill gas as percentage volume CH_4, CO_2, and O_2. Analysis and use of the gas data was out of scope for my research but the composition (60% CH_4 and $40^{\%}$ CO_2, ±5%) verified that all the boreholes were installed in wastes in the anaerobic phase of decomposition and that landfill gas was being generated.

3.2 Estimation of Waste Placement and Landfill Progression

An estimate of the age of MSW with depth at each of the instrumented borehole locations was needed for developing the numerical model timeframe. It was also necessary for the time-dependent heat generation function to be applied to the MSW material, which would initiate following waste placement. To predict the ages of different waste layers at the boreholes, the landfilled area and thickness on an annual basis from Cell 1 through 8 from 1987 until 2018 had to be estimated. The next section describes the operational information that was provided by Loraas engineers to guide the estimation of landfilling in the past and states any assumptions that had to be made.

3.2.1 Site History and Operating Practices

Engineers working at the Northern Landfill provided site drawings that outlined the time frame that cells were excavated into the native subgrade and reported the most up to date dimensions and elevations of the landfilled MSW. The cell construction schedule drawing provided is Figure 3.6. A contoured elevation map of the landfill was provided by Loraas and was dated spring 2016 with elevation data from 2015. This map is included with the provided landfill cross-sections, total volume estimates, and liner elevations in Appendix B.

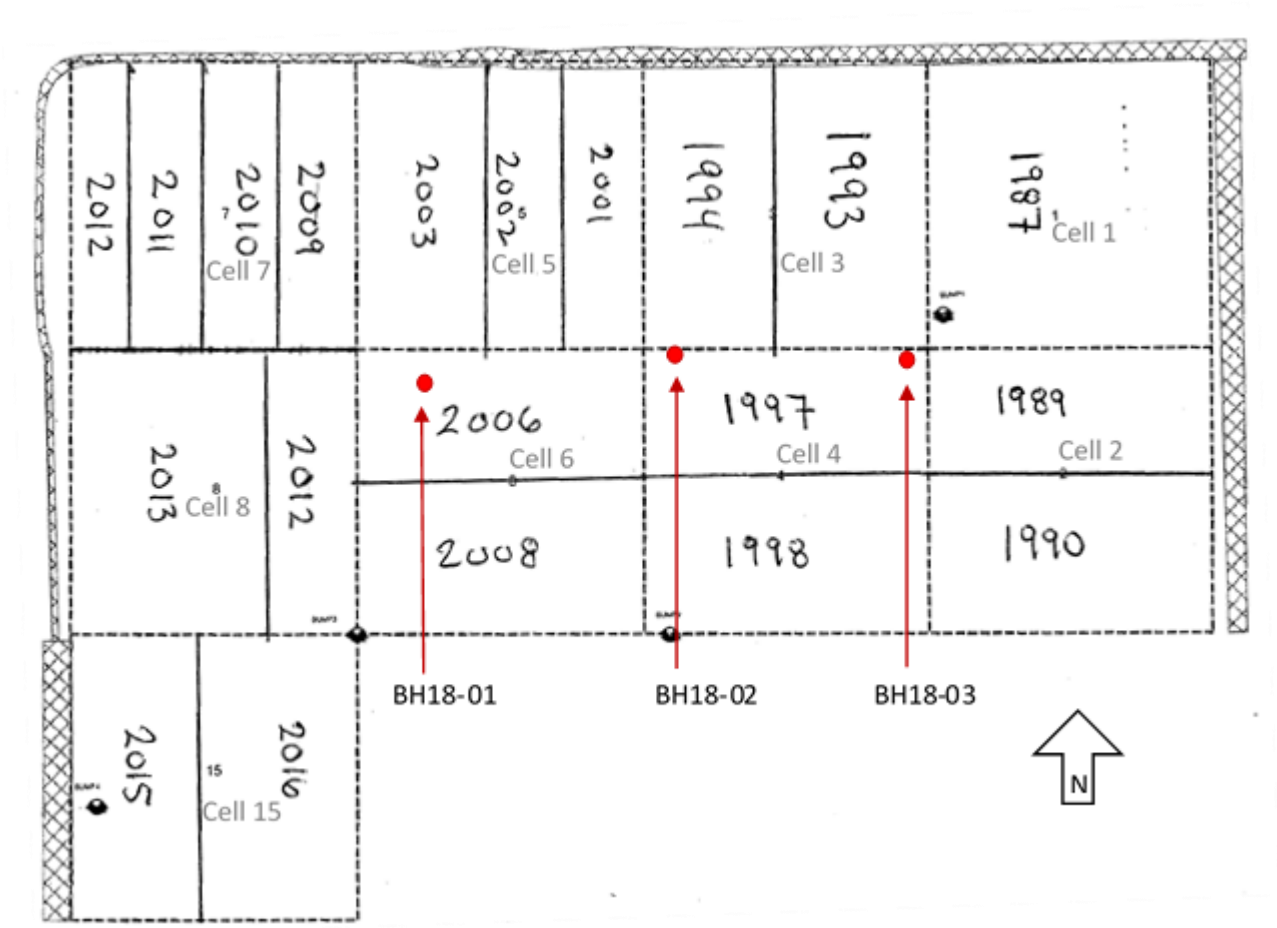

Figure 3.6: Construction schedule of cell liners at the Northern Landfill

From the cross-sections and contoured maps in Appendix B, the following metrics were calculated and/or measured:

- Average side slope downwards from the upper plateau was calculated to be 4.5:1
- Elevation of the upper plateau was 530 or 531 m above sea level (ASL) which was also the range of elevations measured during drilling in Phase 1
- Liner (bottom of MSW) elevation varies across site for drainage purposes
  - Lowest point is 505 m ASL at the southern edge of cell 6, south of Cluster 1
  - NW and NE from this location, elevation increases linearly up to 506 m in the NW corner and 507 m in the NE corner of site
- Depth from plateau to liner across cells 1 to 6 varies between ~26 and 24 m with an average of 25 m
  - Normalized to be from elevation 505 to 530 m ASL for all cells

- Natural ground surface is between elevation 511 and 512 m ASL
- Cell footprints are square and 170 m in length and width

The 2016 map reported a volume of fill within cells 1 to 8 of 3.3 Mm^3. This is an average annual volume of ~118 000 m^3 from 1987 to 2015. A meeting with the Loraas site engineers determined the following operational conditions:

- Cells 1, 3, 5, 7, and 8 were filled east to west and cells 2, 4, and 6 were filled north to south
- Cells were excavated during the late spring, summer, and early fall (construction season) and 5 to 6 m below natural ground surface
- Newly constructed liners were covered with one or two lifts of MSW as soon as possible, beginning in the fall after excavation
- The east side of site (cells 1 and 2) was observed to be at approximately half the present elevation above ground surface in 2001 (~520 m ASL)
- In 2019, annual tonnage was ~125 000 at an estimated 0.6 t/m^3 apparent density once placed and compacted (including daily cover soils)

3.2.2 Assumptions and Procedure for 3D Landfilling Drawing

A landfilling sequence beginning in fall of 1987 was developed with the information provided. To simplify the model, a tiered rectangular prism geometry was developed for creating the 3D drawing. Each tier represented a waste lift and is stacked upon the underlying tier (or the liner surface for tier 1). Exterior cell boundaries are those that are not shared with other cells. Shared boundaries are termed ‘interior’. The prism edges were offset from the cell boundaries such that the projection of the actual slope surface intersects the prisms at mid-height, resulting in an equal area of the prism protruding above the projected slope as is missing below. This area equalization minimizes error when simplifying the lift geometry as rectangular prisms and is visualized in a cross-section view of an exterior cell boundary in Figure 3.7.

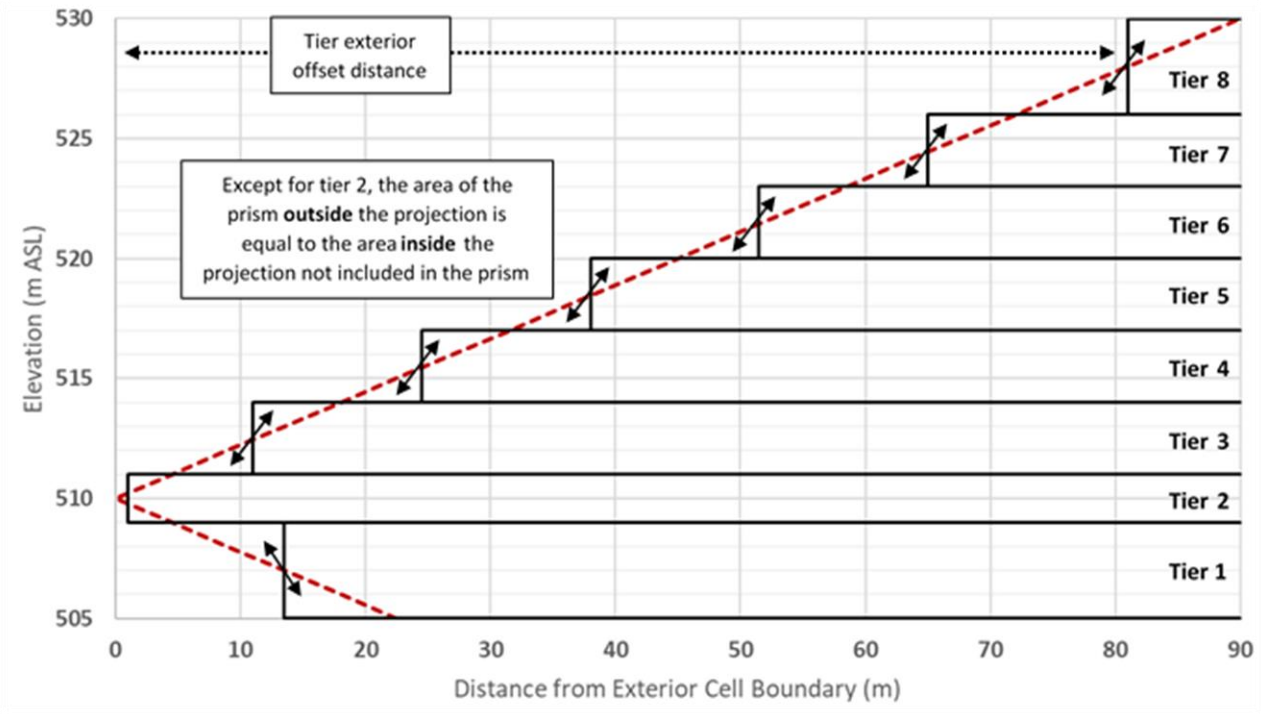

Figure 3.7: Example of prism geometry in cross-section with the actual 4.5:1 slope in red

Interior offset distances differ from exterior ones because the interior slope begins at liner elevation without a change in direction at ground elevation (510 m ASL). Tier offset, thickness, and elevation values are included in Appendix B. Other assumptions and procedures that apply to the 3D drawing (drawn using Autodesk Civil3D® software) are listed below:

- The landfilling year was assumed to be from the beginning of fall to the end of summer (mid-September to mid-September the following year)
  - The first year therefore was September 15th, 1987 to September 15th, 1988 and any waste filled in this period would be labelled 1987-88 or, for graphing purposes, 1988
- Across all cells the liner was assumed level at 505 m ASL and 5 m below natural ground elevation (510 m)
- Typical MSW lift thickness was assumed to be 3 m and any variation was maintained to the nearest whole metre
  - It was found through initial iterations of the 3D drawing that the first tier needed to be 6 m thick to satisfy the volume estimate in 1987-88 while only one cell existed in the first years of operation

    - Tier 2 is 2 m thick to fit within the wedge of the exterior slope (Figure 3.7)
    - To reach a final elevation of 530 m ASL, the uppermost tier was 4 m thick
- Airspace below ground level (newly excavated liners) was prioritized for placement of waste if present over the target landfilling year, and placement begins on the east or north cell boundary depending on the cell filling direction
    - Once up to ground level, priority was to bring newer cells up to the elevation of neighbouring cells
    - If all existing cells are at the same elevation, a new tier starts on the east boundary in cell 1 and 2 and proceeds west across the cells
- Annual fill volumes were calculated in a spreadsheet by summing individual prisms until the target volume was reached for a given year
    - Multiple prisms within the same landfilling year can exist in different tiers or locations (in other words, individual prisms in the same placement year do not need to be continuous or share edges or faces with one another)
- The waste filling rate was initially lower than the average (118 000 m^3/y) and increased beginning in the late 1990's
    - The annual fill volume beginning in 1987-88 was determined to be a maximum magnitude of ~87 000 m^3 as higher volumes exceeded the capacity of cell 1 prior to the excavation of cell 2
- Settlement of the MSW was not considered and prisms maintained their original height dimension
    - This assumption was necessary because incorporating consolidation of the waste was out of scope and would introduce an additional layer of iteration when generating the 3D model, without providing significant improvements to the predicted waste layer ages and thicknesses
- The position of temporary roadways and stockpiles throughout the years were not considered and it was assumed the entire cell widths could be landfilled, limited only by the slope angle (4.5:1) and final elevation of tier 8 (530 m ASL)

The annual fill volumes were increased when cell capacity allowed as well as to assure the total 3.3 Mm^3 landfilled volume in 2015 was achieved. The growth and magnitude of annual volumes that satisfied the target metrics is in Figure 3.8. Oblique views of the 3D drawing at the beginning

of each decade and in 2018 are in Figure 3.9. Different coloured prisms represent different years of placement and the 2018 view includes the borehole locations as vertical yellow lines. The Civil3D® drawing was reviewed by Loraas engineers and it was agreed upon that the assumptions regarding the landfill history and progression did not need to be changed. This method can be applied at other landfill sites if a similar level of information about cell progression (time and fill direction) and final geometry (side slope angle, surface elevations, and total volume) is known.

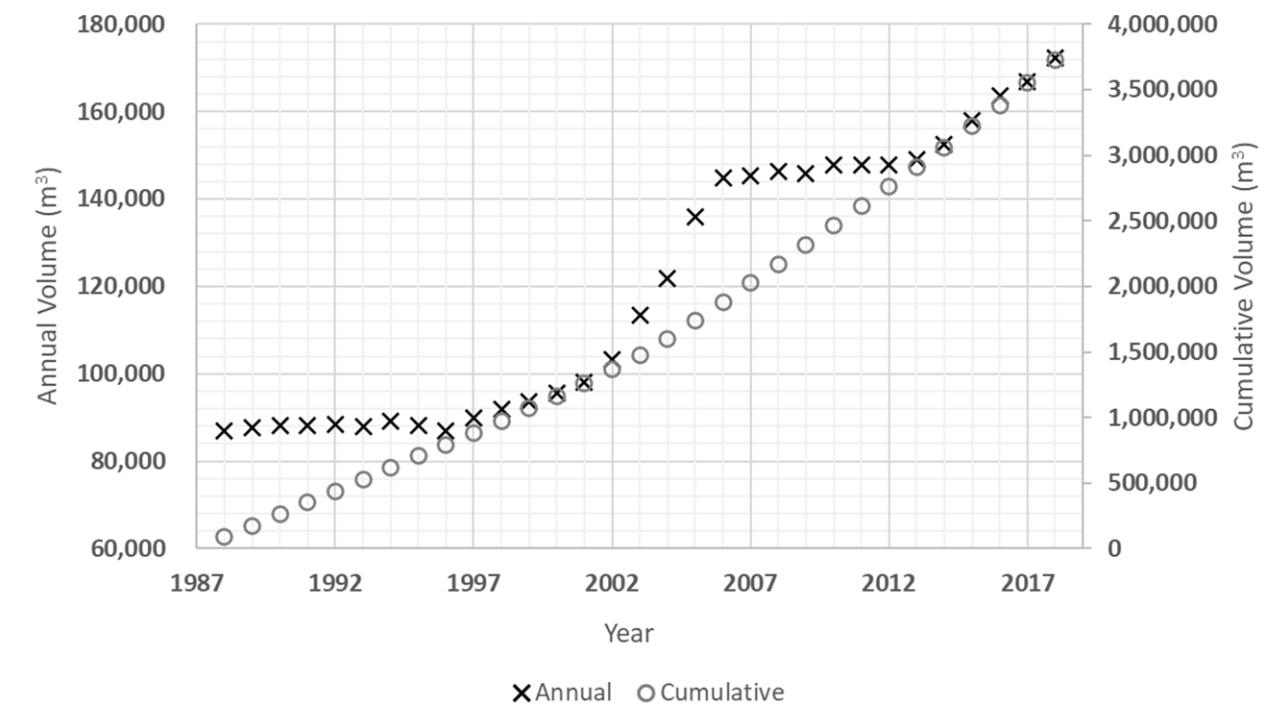

Figure 3.8: Annual and cumulative landfilled volumes from 3D prism model

Figure 3.9: Prism model as of A) 1990, B) 2000, C) 2010, and D) 2018 with instrument locations in yellow

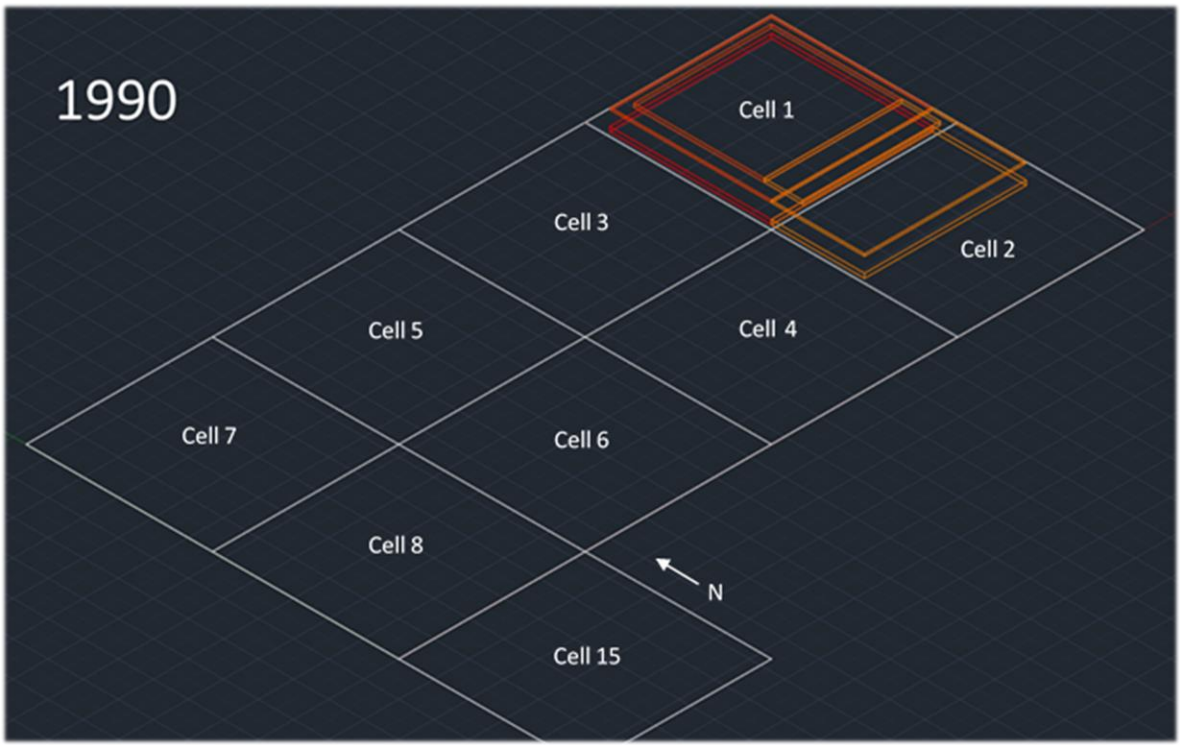

A) 1990 with cell locations labelled

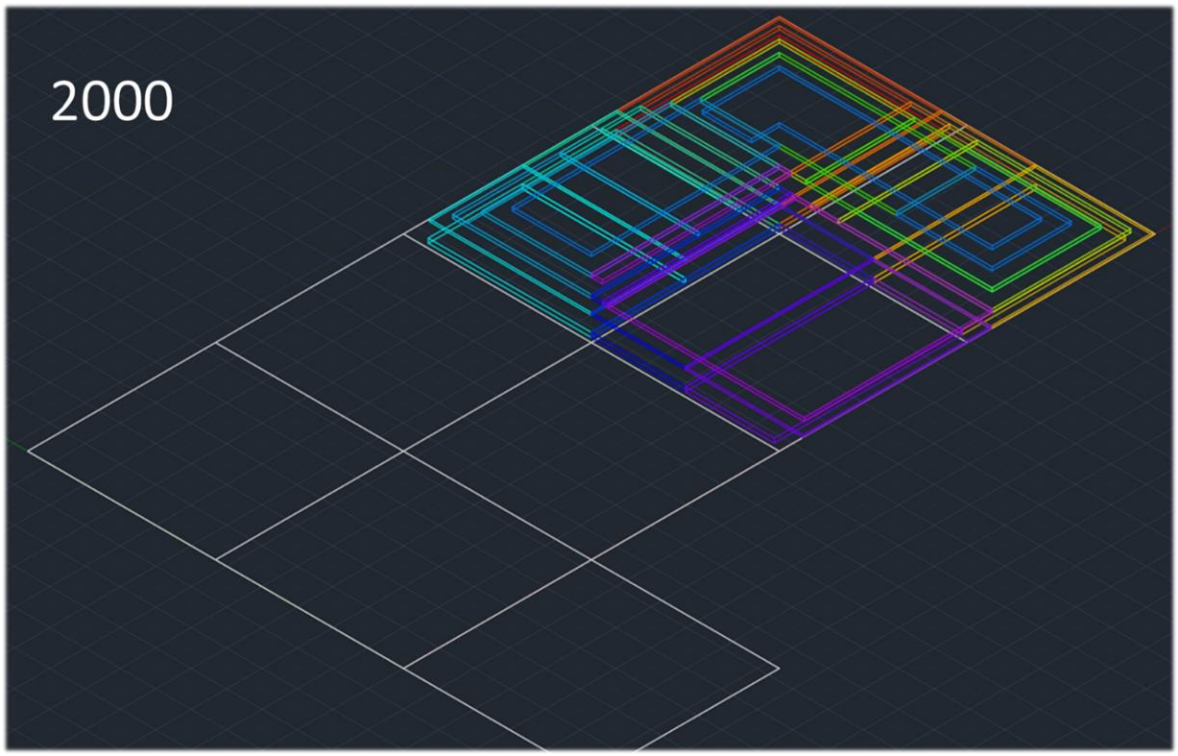

B) 2000

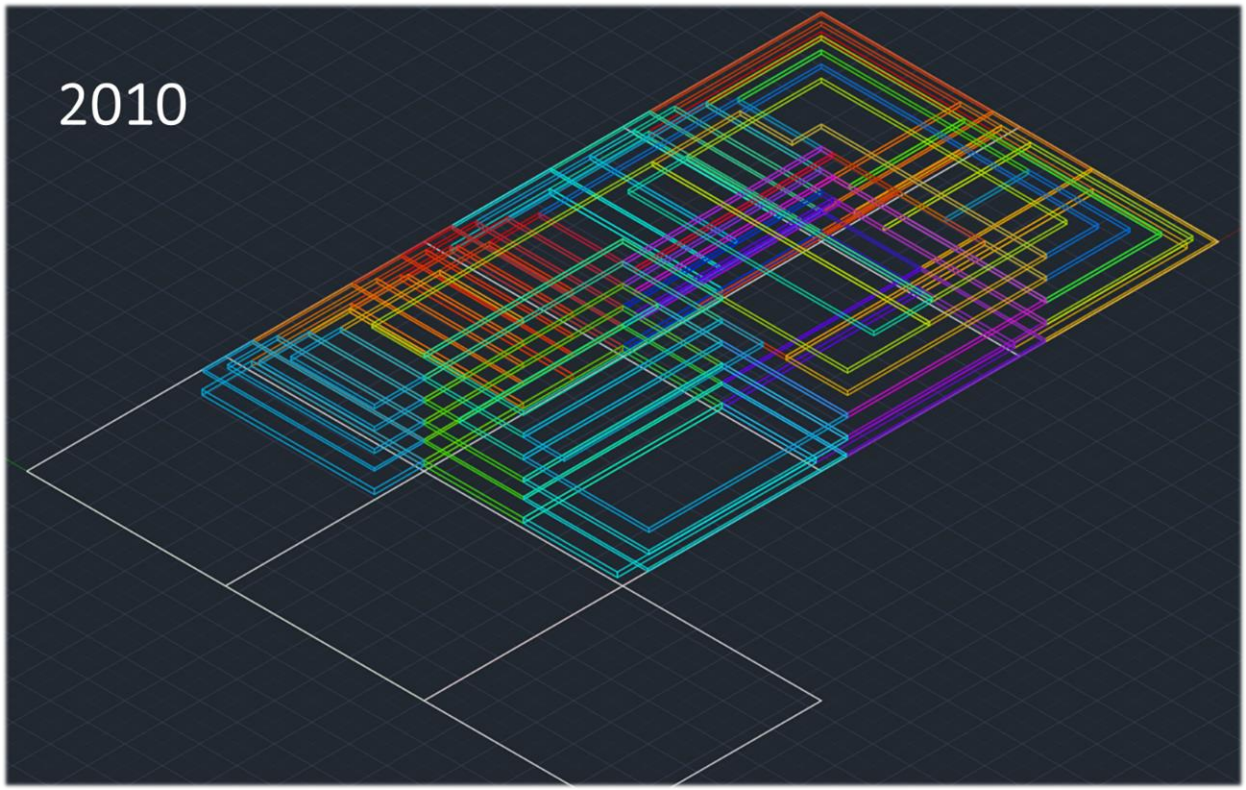

C) 2010

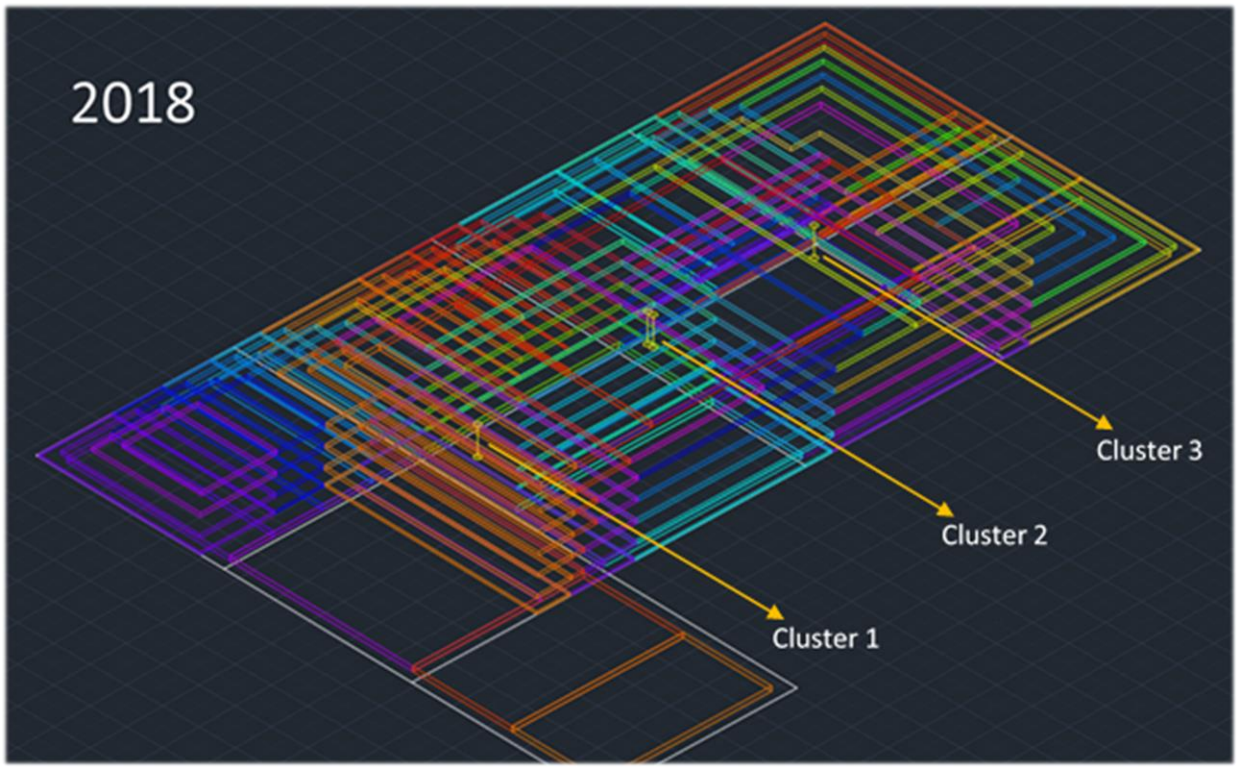

D) 2018 with instrument locations labelled

From this 3D drawing, two perpendicular cross-sections were created. One trending west to east that intersects all three Clusters most closely (just south of the interior cell boundaries) and extends 50 m on either side of the outer borehole locations. The other extends 50 m north and south from Cluster 2. The vertical faces of the prisms were converted back to a 4.5:1 slope to represent the interface of waste lifts more accurately. The cross-sections were compared to the dated objects identified from the recovered MSW core samples (in Appendix A) which were assumed to represent the minimum age that the waste could be at that depth. For example, an object with a copyright from 2009 could not have been landfilled in 2008 but it could have been landfilled as late as 2018. The depths of these 'object minimums' were compared to the cross-sections with good compatibility at Cluster 1 and 2. The locations of a few waste layer boundaries were shifted laterally to satisfy the object minimums, namely the 2009-10 layer at Cluster 2. The cross-sections are in Figures 3.10 and 3.11. Although the above methods and assumptions for estimating the waste layering across site introduces error, the timeframe and material placement times for 1D numerical modelling were based on these cross-sections as no other information was available regarding the landfill placement history at the instrumented locations.

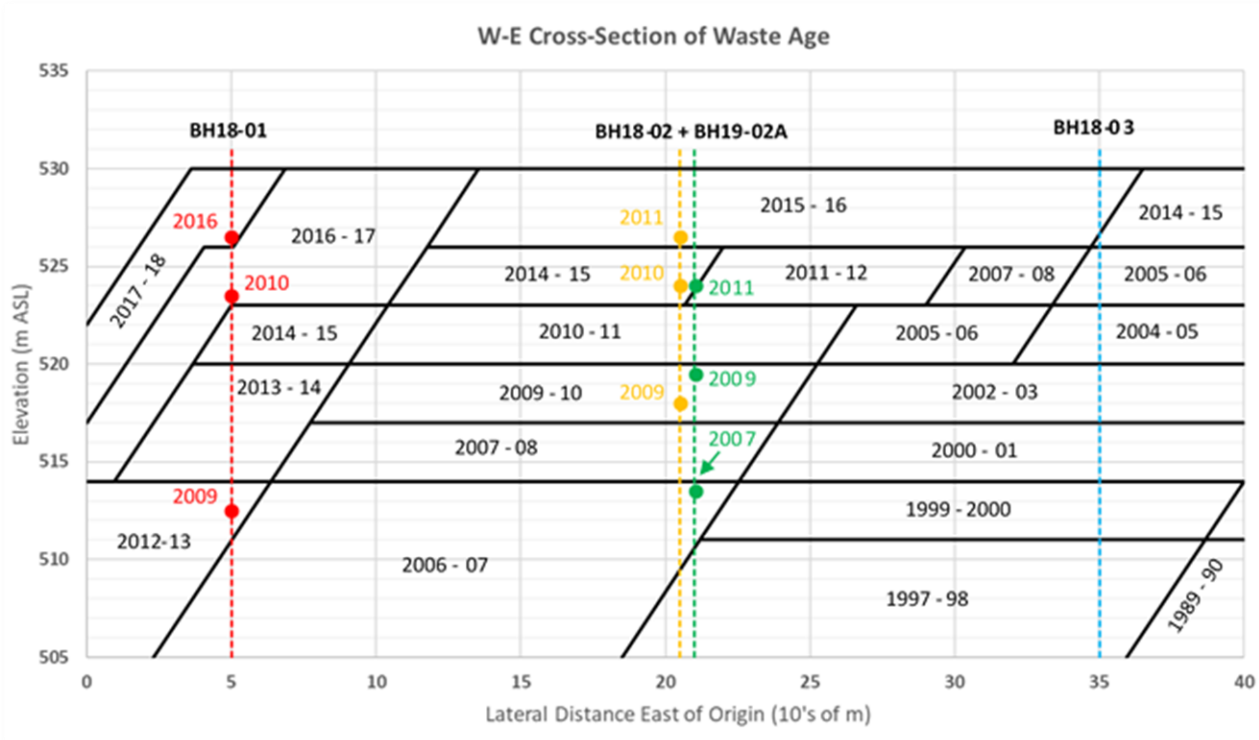

Figure 3.10: West to east cross-section of 3D drawing with object minimum locations labelled (10x vertical exaggeration)

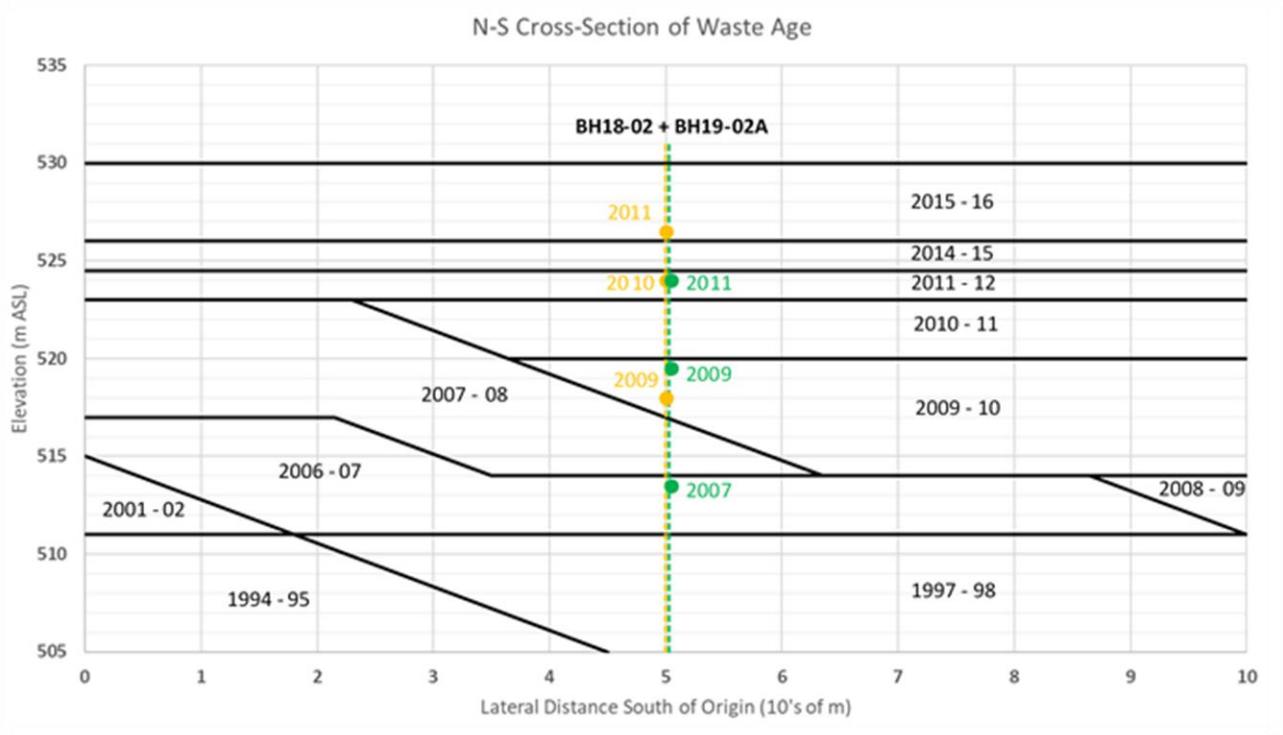

Figure 3.11: North to south cross-section of 3D drawing with object minimum locations labelled (2.5x vertical exaggeration)

3.3 Derivation of Waste Heat Generation Function

As identified in the gap analysis of the literature review, many authors used a constant rate of heat generation (typical for short-duration models) or the exponential growth and decay function presented by Hanson et al. (2008; 2013) as an empirical solution for landfill modelling. Annual average air temperature and precipitation values for Saskatoon did not produce a useable growth and decay function according to the mathematical definition presented by Hanson et al. (2008; 2013). In addition, the exponential growth and decay function resulted in vastly different total energy potentials (BHP_{ULT}) at different landfills, which was a function of climatic factors (precipitation, AAAT) as opposed to total degradable organics (C_{eq}) as theory would suggest. Because of this, and the research being undertaken at the Northern Landfill to assess BMP and gas generation, it was logical to derive a mechanistic heat generation function that can be directly related to gas generation based on stoichiometric and thermodynamic principles.

3.3.1 Conversion of Methane Potential to Heat Potential

The BMP of MSW can be converted to a proportional heat potential (BHP) or vice versa (Section 2.1). Because of the large number of unknown parameters and broad range of properties for MSW, a low and high enthalpy of reaction value was used to bound the conversion. Based on the values in Table 2.2, a high enthalpy value of 436 kJ/mol$_{C6H10O5}$ (145 kJ/mol$_{CH4}$) and a low enthalpy of 145 kJ/mol$_{C6H10O5}$ (48 kJ/mol$_{CH4}$) were selected to represent the ΔH limits for the anaerobic digestion of cellulose to landfill gas (LFG). Equation 3.1 is the conversion from BMP (L/kg$_{MSW}$) to a factor BHP$_f$ (kJ/kg$_{MSW}$) and is

$$BHP_f = \frac{BMP}{1000} * \frac{\rho_{CH4}}{M_{CH4}} * \Delta H \quad \text{.....Equation 3.1}$$

Where ρ_{CH4} is methane density (kg/m^3) at NTP (20 °C, 101 kPa) of 0.668 kg/m^3, M_{CH4} is molar mass of 0.016 kg/mol$_{CH4}$, and ΔH is enthalpy per mole of methane (either of the bounded values selected previously). Based on this equation, a litre of methane produced in a laboratory BMP test would release between 2.0 and 6.1 kJ of energy. This equation can be modified to estimate energy release on a field-scale from LFG volumes. At a 60/40 % by volume ratio of CH_4 to CO_2 in LFG, Equation 3.2 can be used to represent the energy released per volume of LFG generated and is

$$BHP_{LFG} = 0.6 * V_{LFG} * \frac{\rho_{CH4}}{M_{CH4}} * \Delta H \quad \text{.....Equation 3.2}$$

Where V_{LFG} is a measured or predicted volume of landfill gas at NTP. A cubic metre of gas produced would theoretically generate between 1.2 and 3.6 MJ of energy. These equations are useful for calculating BMP and potential LFG volumes based on the BHP$_{ULT}$ ranges determined through numerical modelling. The equations can also be used to predict BHP$_{ULT}$ from measured LFG volumes in the field. However, to model the MSW on a volumetric basis, these BHP factors must be converted from kJ/kg$_{MSW}$ or MJ/m$^3_{LFG}$ to MJ/m$^3_{MSW}$. The simplest means is by incorporating MSW dry density (ρ_{dMSW} in kg/m^3) into Equation 3.2 via multiplication. The result is Equation 3.3 and is

$$BHP_{ULT} = \frac{BMP}{1000} * \frac{\rho_{CH4}}{M_{CH4}} * \Delta H * \rho_{dMSW} \quad \text{.....Equation 3.3}$$

Where BHP$_{ULT}$ is the total heat potential of MSW (kJ/m^3) assuming anaerobic digestion of cellulosic organic matter. Dry density was calculated from the dry weights of MSW core samples

recovered for the BMP portion of the project as outlined in Section 3.1.2. Individual core dry weights and densities are tabulated in Appendix C. If MSW was lost from the sample barrel during recovery, dry densities would increase compared to those calculated. Calculated dry densities to the nearest 10 kg per core run were variable and no trend was observed with depth or between locations. The average dry density per borehole was comparable between BH18-01, 02, and 03 at 1050, 1020, and 930 kg/m^3 respectively. BH19-02A (5 m east of BH18-02) sampled in Phase 2 had a lower calculated average dry density at 780 kg/m^3.

3.3.2 Deriving Heat Rate Function from Cumulative Gas Production

Cumulative gas production from laboratory BMP experiments can be represented by the exponential decay function in Equation 2.3. For modelling purposes, the MSW material required a heat rate function rather than cumulative heat produced. Therefore Equation 2.3 was derived with respect to time. The resulting heat generation function after substituting BMP for BHP is

$$HR(t) = BHP_{ULT} * k(e^{-kt}) \quad \text{.....Equation 3.4}$$

Where HR is heat rate in kJ/d/m^3 and k and t are decay rate (d^{-1}) and time (d) just as in Equation 2.3. The t_{lag} term was removed from the equation as the initiation of heat generation is in theory dependent on the temperature and water content of the MSW as opposed to what was observed during laboratory BMP tests. The result is an exponential decay function beginning at a peak HR value equal to heat potential multiplied by decay rate and decreasing exponentially, approaching an asymptote of zero as time increases. The HR curves are defined per waste layer and shown graphically in Section 3.4.4.

The area under the HR curve as time approaches infinite is equal to BHP_{ULT}, which is the key parameter for estimating the heat potential value for MSW in landfills where decay rate is expected to be much lower on average than in warm, wet climates. This method is anticipated to be more portable between different landfill sites and models because BHP_{ULT} is a property of the MSW and heat generation curves can be defined depending on its magnitude and the representative average decay rate.

3.3.3 Estimation of Equivalent Cellulose Content

Heat generation was equated to CH_4 generation, and as reviewed in Section 2.1.1, CH_4 generation was attributed primarily to anaerobic methanogenesis from cellulose. Therefore, calculating an

equivalent mass of cellulose in MSW from BMP that encompasses all degradable organic matter was considered a useful index property to define. A higher BHP_{ULT} is proportional to a higher BMP which is proportional to a higher C_{eq}. This method assumes that all generated CH_4 is derived from cellulose molecules in the MSW. C_{eq} (as % mass) can be calculated by rearranging Equation 3.3 and converting moles and mass of CH_4 to cellulose, resulting in

$$C_{eq} = \frac{BHP_{ULT} * M_{cell}}{\Delta H * \rho_{dMSW} * 3} * 100\% \quad \text{.....Equation 3.5}$$

Where C_{eq} is $kg_{C6H10O5}/kg_{MSW}$, M_{cell} is molar mass of cellulose (0.162 kg/mol) and, in accordance with Equation 2.1, three moles of CH_4 are produced per mole of cellulose ($C_6H_{10}O_5$). In Section 4.2.1 the above presented equations and methods of conversion are used to predict BMP and C_{eq} for the borehole locations based on results of BHP_{ULT} determined through numerical modelling.

3.4 Finite Element Modelling of Thermal Regime

Numerical modelling was performed to predict a range of BHP_{ULT} magnitudes for MSW at the Northern Landfill. The upper and lower bound heat potential were a function of a minimum and maximum HC and K_T properties for MSW being applied. The model sensitivity to certain inputs or assumed properties was also evaluated. The modelling outlined in this Section is a back-analysis targeting measured site temperature data and the results were not compared to closed-form solutions.

The FEM software used was GeoStudio 2018® for its capabilities of modelling energy (heat), water, and gas transfer in 1D and 2D. The TEMP/W GeoStudio® package is based on conservation of energy such that the rate of change of thermal energy change in a unit volume must equal the net thermal flux into and out of the volume. Equation 3.6 presents the governing equation used by the modelling software for energy balance (based on conservation of energy) and Equation 3.7 represents the rate of energy change when ignoring forced-convection and latent heat of vaporization (GEOSLOPE, 2017).

$$E'_{st} = \frac{dE'_{st}}{dt} = E'_{in} - E'_{out} + E'_{g} \quad \text{.....Equation 3.6}$$

Where E'_{st} is the rate of change in stored thermal energy, E'_{in} and E'_{out} is the rate of heat flux changes across control surfaces, and E'_{g} is a heat sink or source in a control volume (GEOSLOPE, 2017).

$$C_{ap}\frac{\partial T}{\partial t} = \frac{\partial}{\partial y}\left(K\frac{\partial T}{\partial y}\right)$$ .....Equation 3.7

Where C_{ap} is the apparent volumetric heat capacity, T is temperature, t is time, and K is thermal conductivity in the y-direction. (GEOSLOPE, 2017).

The numerical modelling for this research involved several inter-related steps which were:

- A 'subgrade simulation' modelling temperatures within the glacial till prior to cell construction to predict initial temperature conditions for the long-term model
- A 'long-term' model simulating cell construction and waste placement up to 2019 to estimate the upper and lower range of values for BHP_{ULT} and assess the sensitivity of the model to various inputs and assumed parameters.
- A 'short-term' model simulating MSW temperatures to estimate the present-day heat generation rates and assess the sensitivity of the model to various inputs, assumed parameters, and heterogeneous MSW thermal properties that increased with depth.
- A predictive 'future' model extending ~11 years from the results of the long-term model was created to model the potential temperature trends over another decade at the modelled locations. The additional decade provided observation of the effects of different BHP_{ULT} and decay rate combinations using the HR function derived in this thesis (Equation 3.4).

3.4.1 Model Geometry and Timeframe

With the boreholes being located within the central region of the waste cells, a vertical flux direction was selected to model heat transfer in 1D within the MSW immediately surrounding the instrumented boreholes. It was assumed that the measured temperatures at each depth extended far enough laterally that the gradient was consistently vertical and the 50 m or greater distance to the edge of the upper plateau was enough to not observe temperature changes influenced by the side slope. As a result of the modelling software used, the geometry and analysis technique of the software was constructed in 2D (x and y-directions) for better visualization of the materials and contoured temperature outputs with depth. Though the 2D geometry analyzes energy transport in a plane, no-flux boundary conditions were applied on either side which limited fluxes to the y-direction after a brief period that temperature differences in the x-direction stabilized.

A column of material 5 m wide, 95.5 m tall (after MSW reached present elevation), and 1 m 'into the screen' represents the conditions within the core of the landfill centred around each instrumented borehole location. Each simulation except the short-term model includes 70 m of subgrade below the liner elevation (505 m ASL). The geometry and 1D technique supported the use of square elements, which were made to be 0.5 m wide in the MSW and upper portion of the subgrade to allow a node to exist within the center of each square metre in space. This was done because HR boundaries were limited to points in the software (on element nodes and not applicable to lines or areas) so one central point within a square metre of material is 1 m away from the next heat source point. This simplified the use of HR values in units of $MJ/d/m^3$.

A screenshot of the upper part of the long-term model (from elevation 530 to 495 m) and the short-term model (with no subgrade modelled) is Figure 3.12. The short-term model presented in the figure has heterogeneous MSW thermal properties depicted by different colours per 1 m of material. The model geometry and boundary conditions are based on the conceptual model in Figure 2.3 (after Hanson et al., 2013). To analyze the affect of mesh size on the model outputs, mesh sizes coarser than the selected 0.5 m were included as part of the sensitivity analysis. This included mesh sizes of 1.0 m and 2.0 m. An analysis of finer mesh sizes (0.25 m) was not included as it was not considered computationally efficient at such a fine size.

The timeframe and timesteps for each step in the numerical model is presented in Table 3.2. Timesteps were selected for each modelling step based on the resolution of the top atmospheric boundary functions (monthly for subgrade, monthly, and future; daily for short-term) as well as to reduce computation time of the models. Components of the numerical model timeframe as well as some of the graphs presented in Section 4.1.2 refer to specific seasons, which are based on the dates in Table 3.3. The cell liners were constructed over the summer season, as reported by current site operators. Therefore, it was assumed the first waste layer would be placed during the fall season at the borehole locations. The placement date was represented by the middle date of the season (October 31st). Layers above the first were assumed to also be placed in the fall season because exact placement times were unknown. Based on this assumption and Figures 3.10 and 3.11, the waste layer placement times and thicknesses applicable to the long-term model were calculated and are listed in Table 3.4

Table 3.2: Model timeframes and timesteps

Model	Borehole	Start Time	End Time	Timestep (d)
Subgrade	BH18-03	May 1987	March 1997	15
	BH18-01	March 1997	March 2006	
Long-term	BH18-03	March 1997	September 2019	30
	BH18-01	March 2006		
Short-term	BH18-03	September 2018	September 2019	4
	BH18-01			
Future	BH18-03	September 2019	December 2029	30
	BH18-01			

Table 3.3: Season definitions for modelling and graphing purposes

Season	Season Start	Season End	Duration (d)	Mid-Season
Spring	March 15th	June 14th	92	April 30th
Summer	June 15th	September 14th	92	July 31st
Fall	September 15th	December 14th	91	October 31st
Winter	December 15th	March 14th	90.25	January 31st

Table 3.4: Waste layer placement schedule for the long-term model

Borehole	Layer Number	Placement Time (y) relative to model start	Time (Calendar) October 31st of Year	Thickness (m)
BH18-03	L1	0.6	1997	6
	L2	2.6	1999	3
	L3	3.6	2000	3
	L4	5.6	2002	3
	L5	7.6	2004	3
	L6	8.6	2005	3
	L7	17.6	2014	4
BH18-01	L1	9.6	2006	6
	L2	15.6	2012	3
	L3	16.6	2013	6
	L4	17.6	2014	3
	L5	19.6	2016	3
	L6	20.6	2017	4

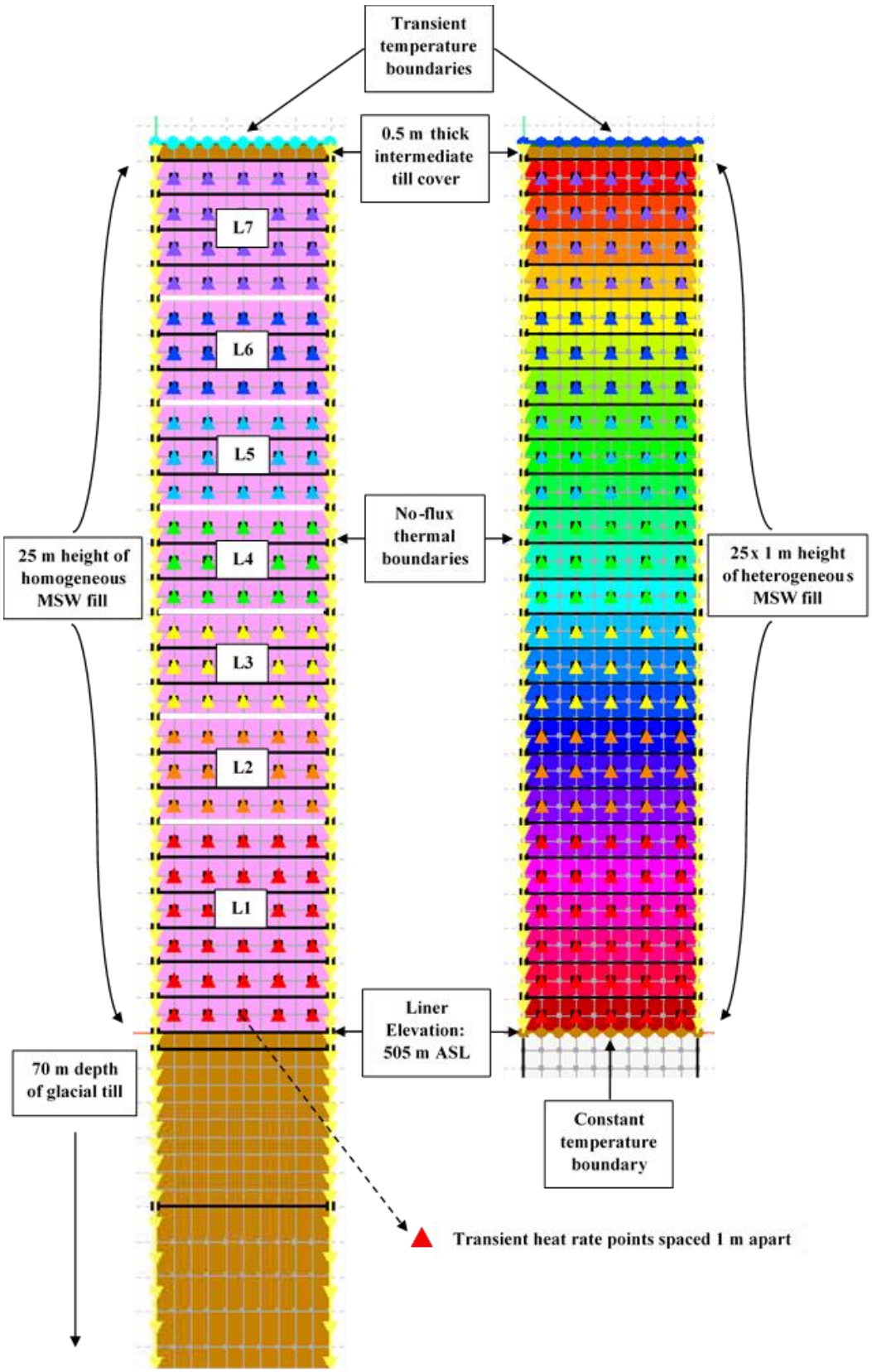

Figure 3.12: Visualization of model geometry, material extents, and boundary condition locations for Left; BH18-03 long-term model and Right; BH18-03 short-term model sensitivity analysis of heterogeneous thermal properties

3.4.2 Material Properties and Extents

The model materials and their positions within the model geometry are summarized below:

- Homogeneous MSW
  - Added in layers to the long-term model, above the liner elevation, according to Table 3.3 to a final thickness of 25 m
  - Present at a thickness of 25 m for the duration of the short-term model except for the sensitivity analysis of heterogeneity
- Heterogeneous MSW
  - 25 individual materials of 1 m thickness with different thermal properties applied to the short-term model as part of the sensitivity analysis
- Floral Till
  - The uppermost subgrade material which existed 5 m above liner elevation prior to cell construction and 30 m below liner elevation
  - Used to represent the intermediate cover (0.5 m thick) once 25 m of MSW was placed
- Sutherland Till
  - The lower subgrade unit was present from 30 m below liner to the bottom boundary of the model (70 m below liner)

Each material described above was applied to the 'Simplified Thermal' material model in the software, meaning all latent heat is released or adsorbed at the phase change temperature (0 °C). The software required definition of the bulk HC and K_T in the frozen and unfrozen state (GEOSLOPE, 2017). Frozen thermal properties were calculated from the unfrozen estimates using Equation 2.4 and the properties of ice and water from Table 2.3. VWC of the MSW was assumed constant for both the long and short-term models at a value of 0.2 m^3/m^3 based on the average estimated water contents of BH18-01 (0.22 m^3/m^3) and BH18-03 (0.18 m^3/m^3) calculated from the recovered core samples (Appendix C).

A range of unfrozen bulk thermal properties for the MSW were selected from Table 2.4 according to sites situated in North America and with comparable densities (780 to 1,050 kg/m^3). A lower and upper bound HC and K_T were chosen and paired together, creating two scenarios for the long-

term model. The scenarios represent a 'rapidly dissipating or high diffusivity' MSW material (upper bound K_T, lower bound HC) and a 'gradually dissipating or low diffusivity' scenario (lower bound K_T, upper bound HC). In other words, the high diffusivity scenario represents an MSW composition that would more easily increase in temperature and conduct the excess energy to the subgrade or atmosphere than would MSW in the low diffusivity scenario subjected to the same heat generation rate. Heat generation rates (and thus BHP_{ULT}) differed between the two scenarios to achieve the same target MSW temperatures that existed on September 1st, 2019. The unfrozen material properties applied to the models are presented in Table 3.5.

Table 3.5: Unfrozen thermal properties defining subgrade and MSW diffusivity scenarios

Material	**HC (MJ/m³/°C)**		**K_T (W/m/°C)**	
	Lower	Upper	Lower	Upper
Homogeneous MSW	1.2	2.2	0.3	1.1
Floral Till	2.61		3.69	
Sutherland Till	3.18		2.45	

3.4.3 Initial and Boundary Conditions

The activation or initial temperature for MSW in numerical models is typically assumed to be the average atmospheric temperature on the day of placement (Hanson et al., 2008; 2013). Because exact waste placement time at the modelled locations was unknown and cell construction was completed by the end of summer or early fall, waste layers were assumed to be placed over the fall season (represented by October 31st). The average monthly air temperature over fall 1997 was calculated to be 0 °C and was applied to all subsequent waste layers as the material was modelled as homogenous. Uniform waste placement temperatures of +10 and -10 °C were included in the sensitivity analysis, as well as alternating placement temperatures of +5 and -5 °C by layer. The waste placement time was not changed to correspond to the adjusted placement temperatures in the sensitivity analysis as otherwise the affect on final temperatures would not be isolated.

From models reviewed in the literature, subgrade temperatures were either determined from groundwater temperature data or modelled over a period of 7 to 10 years, subjected to an atmospheric temperature upper boundary (Hanson et al. 2008; 2013; Khire et al., 2020).

Groundwater temperature data was provided by Loraas from groundwater sampling events at several piezometers installed on the boundary of the site property. Groundwater temperature was measured as part of the annual water quality sampling program, after purging the wells for representative samples of the groundwater surrounding the wells (SNC, 2020). As a result, it cannot be determined what position along the screen would contribute the most to recharge and the temperatures measured once groundwater is sampled at surface may be influenced by atmospheric temperature, sunlight, and heat from the pump. The data was from May and October 2017 and May, July, and October 2019. The data was used to estimate the background natural groundwater temperature at the mid-depth of the piezometer screen. Piezometer locations, screen positions, and sampled groundwater temperatures can be viewed in Appendix D. Because there was only a small sample of groundwater data for the site, and none prior to 2017, a combination of the two typical methods was used, and the 'subgrade simulation' modelling step was created as a result.

Initial conditions and boundary conditions for each modelling step are listed along with brief descriptions in Table 3.6. The sides were set as no-flux thermal boundaries for each of the models. Initial conditions for the models are plotted in Figure 3.13 and 3.14. The dashed lines in Figure 3.13 represent the output of the subgrade simulations and are the initial conditions for the long-term model at the respective modelled location (BH18-03 at Cell 4, BH18-01 at Cell 6). Monthly average temperatures for Saskatoon, which were applied to the top boundary of all but the 'short-term' model, is included in Appendix D.

Table 3.6: Descriptions of initial and boundary conditions for each modelling step

Model	Initial Conditions	Top Boundary	Bottom Boundary	Heat Rate Points
Subgrade	May monthly average surface temperature, 6.5 °C at liner elevation, 0.05 °C/m increase to bottom (see Figure 3.13)	*Transient* monthly average surface temperatures on 15th day of each month (see Appendix D)	*Constant* 10 °C temperature based on 0.05 °C/m gradient, fit to piezometer data (see Figure 3.13)	
Long-term	**Subgrade:** final temperatures from Subgrade simulation **MSW:** 0 °C assuming placement on October 31st	*Transient* monthly average surface temperatures on 15th day of each month (see Appendix D)	*Constant* 10 °C temperature based on 0.05 °C/m gradient, fit to piezometer data (see Figure 3.13)	*Transient* function applied to nodes in each layer (see Table 3.4) defined by Equation 3.4, calculated at timesteps of 15 d and calibrated for fitment (see Figure 3.15 and Table 4.3)
Short-term	**MSW:** daily average temperature from thermistor array (see Figure 3.14)	*Transient* daily average surface temperature among all Clusters (see Figure 4.7)	*Constant* temperature based on extrapolated liner temperature from deep thermistors (see Figure 3.14)	*Constant* value applied to the nodes in each layer (see Table 3.4) and calibrated for fitment (see Table 4.5)
Future	**Subgrade:** final temperatures from Long-term model **MSW:** final temperatures from Long-term model	*Transient* monthly average surface temperatures on 15th day of each month forecast with average increase over previous decade (see Appendix D)	*Constant* 10 °C temperature based on 0.05 °C/m gradient, fit to piezometer data (see Figure 3.13)	*Transient* function applied to nodes in each layer (see Table 3.4) defined by Equation 3.4, calculated at timesteps of 15 d and based on variable BHP_{ULT} and k values (see Table 4.6)

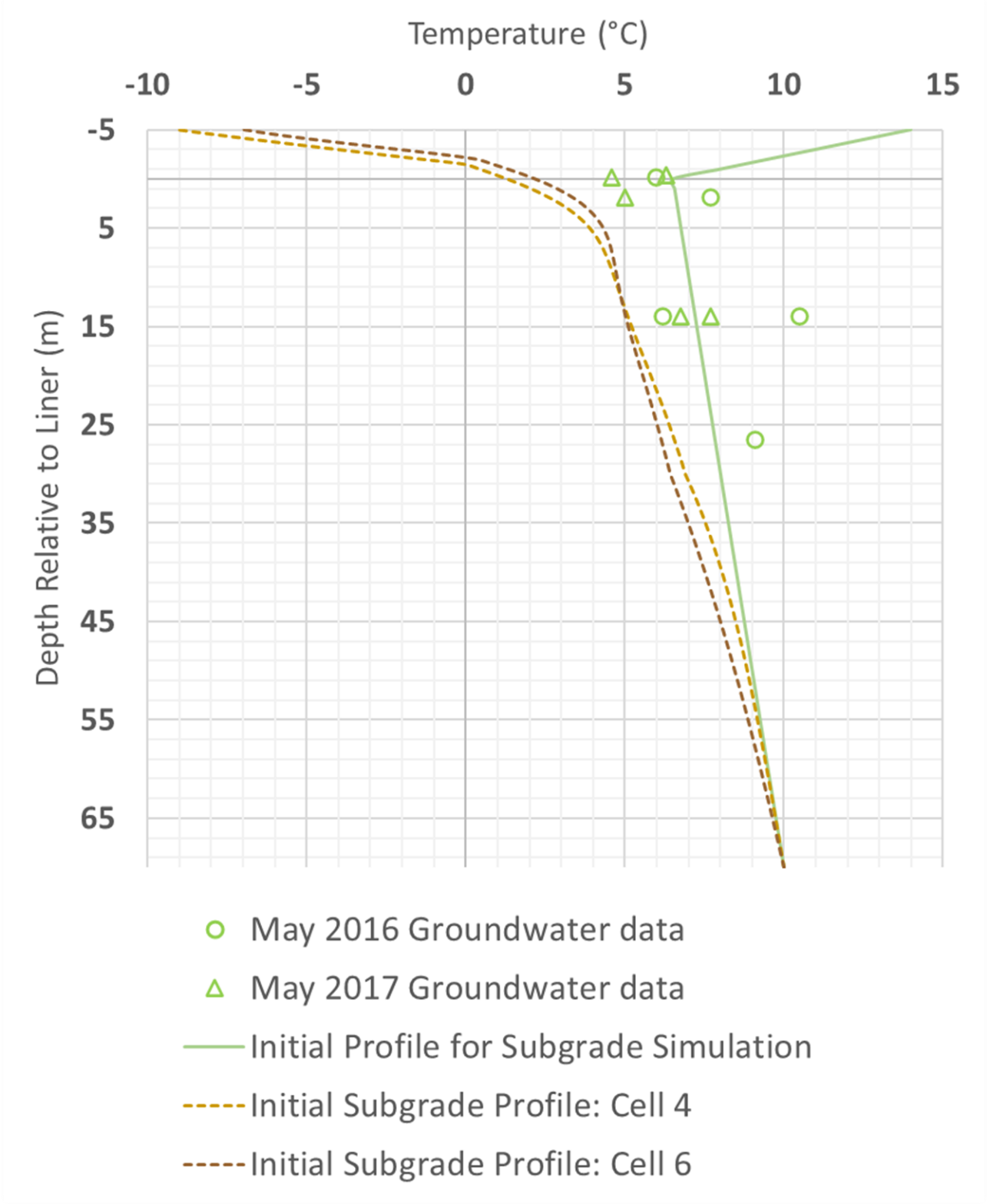

Figure 3.13: Initial conditions and groundwater temperature data used for subgrade and long-term models

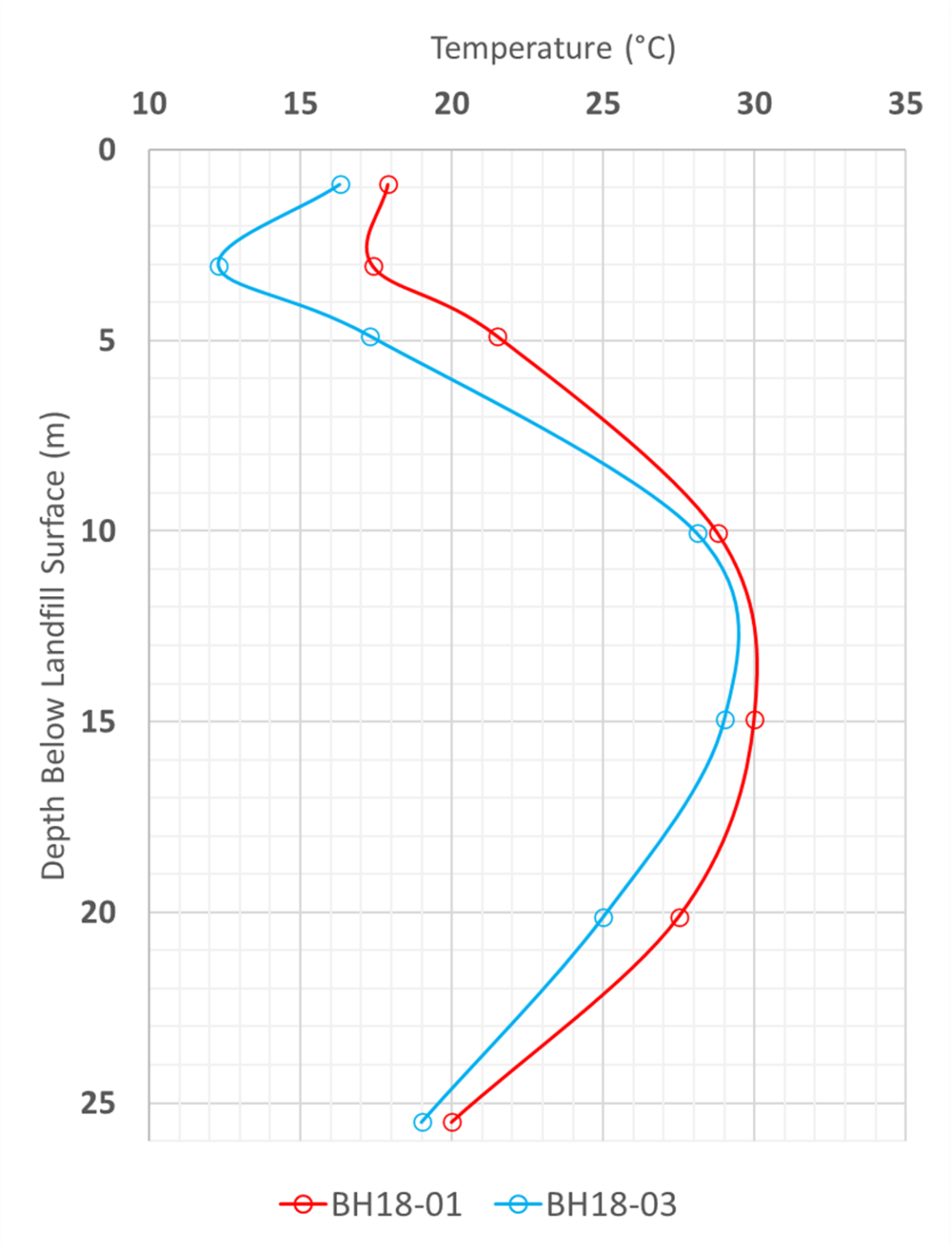

Figure 3.14: Initial MSW temperatures for short-term model based on thermistor measurements

3.4.4 Procedures for Estimating Heat Potential

The determination of BHP_{ULT} values in the model was an iterative process and the following assumptions had to me made:

- A constant decay rate *k* had to be estimated to isolate BHP_{ULT} for calibration and a value of $1x10^{-4}$ d^{-1} was selected as it was slightly less than the field estimate for gas generation at CESM ($1.5x10^{-4}$ d^{-1}) presented by Nastev et al. (2001) and was equal to the bulk MSW decay rate for an energy balance box model selected by Hao et al., (2017);
    - because the selection of an average decay rate is subjective, a sensitivity analysis was performed to assess the model results if a decay rate as low as $7.5x10^{-5}$ d^{-1} or as high as $1.25x10^{-4}$ d^{-1} was selected.
    - the software was unable to incorporate a HR boundary where the decay rate variable *k* in Equation 3.4 was a function of temperature as theory suggested, and it was impractical to perform this operation in a spreadsheet for the large number of model iterations performed.
- The HR function for each layer was assumed to begin at the start of spring (March 15th) following burial (136 d following placement of the overlying layer)
    - based on sources in the literature suggesting 4 m of MSW is adequate for insulation and stabilization of temperatures (Yeşiller et al. 2005), it was assumed for 6 m thick waste layers that the bottom 3 m would reach anaerobic conditions and begin methanogenesis independent of burial under additional waste lifts.
    - the 6 m thick layers were divided into two separate HR functions applied to 3 m of MSW each (denoted as L1T and L1B for top and bottom of layer one) and followed the assumptions of the other 3 m layers for initiation of heat generation.
    - the 4 m top layer of MSW at each borehole followed the assumptions of the 3 m layers and thus was assumed to not generate any heat for the duration of the models due to cooling from air temperatures in the winter months.

An example of the HR curves applied to the long-term model at BH18-03 with the initial estimated BHP_{ULT} value of 100 MJ/m^3 and a constant *k* value of $1x10^{-4}$ d^{-1} is Figure 3.15. The cumulative heat generation function with the same parameters is Figure 3.16. The peak HR in this example is 0.01 $MJ/d/m^3$ or 0.12 W/m^3 which is comparable to the peak heat rate modelled by Hanson et al.

(2008) for the Anchorage landfill (similar annual precipitation and temperature as Saskatoon). It is evident from Figure 3.16 that the cumulative energy produced at the end of the model period is less than ~52 MJ/m^3 of an eventual BHP_{ULT} value of 100 MJ/m^3 for each waste layer.

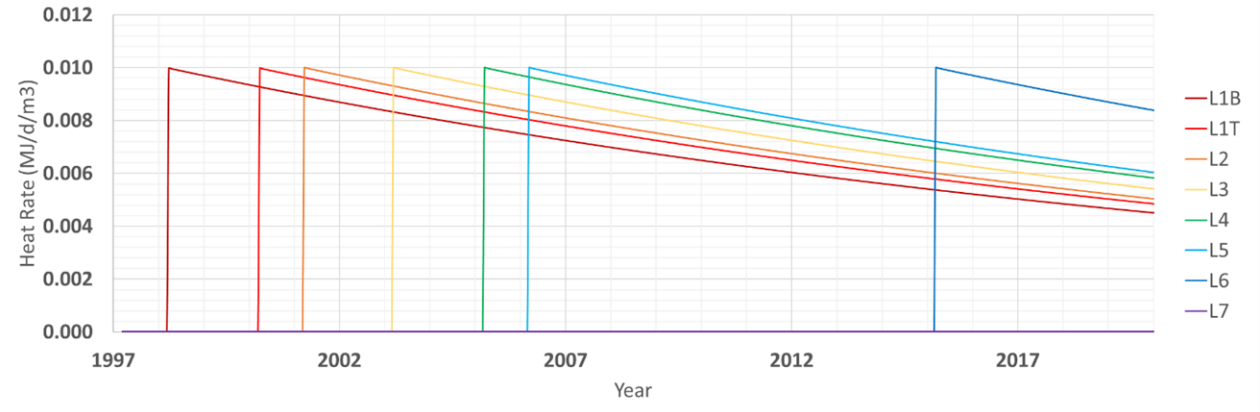

Figure 3.15: Example heat rate transient boundary condition for BH18-03

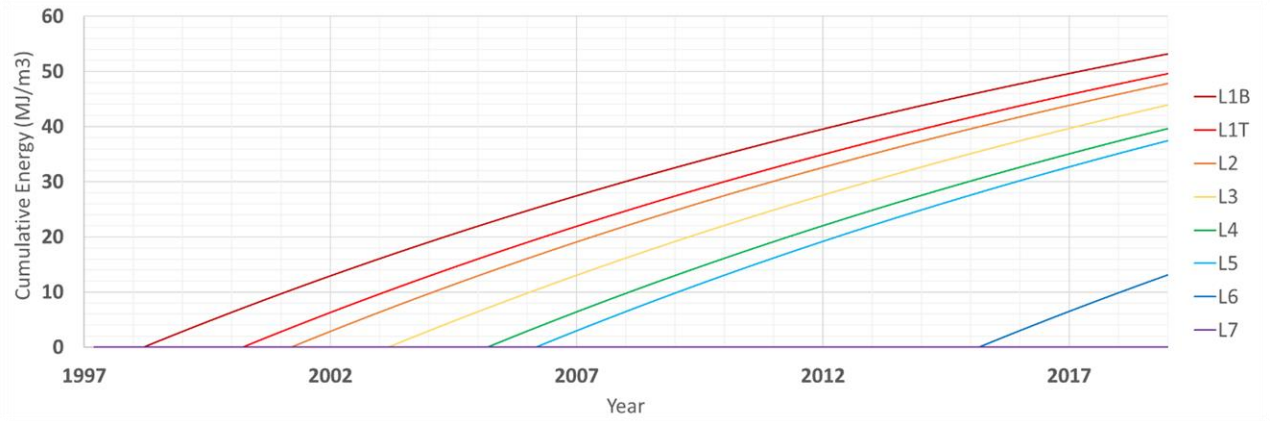

Figure 3.16: Example cumulate transient heat produced for BH18-03

Beginning with the HR function in Figure 3.15, the temperature profile of the MSW at the end of the long-term model (September 1st, 2019) was compared to the temperatures at depth measured on site at that time. The measured daily temperatures from August 14th, 2019 through September 15th, 2019 were used to calculate a monthly average to represent the target profile for the model. The following procedure led to the development of bounding BHP_{ULT} values, estimation of present-day heat generation rates, and several decay rate scenarios for the future model:

- The magnitude of BHP_{ULT} was increased from the initial 100 MJ/m^3 estimate until the maximum temperatures in the mid-depth region of the MSW aligned with the maximum temperatures measured on site for both the high and low thermal diffusivity scenarios
    - each borehole and diffusivity scenario had a unique BHP_{ULT} to develop present-day MSW temperatures with an assumed constant decay rate of $1x10^{-4}$ d^{-1}
- The short-term model with the long-term HR functions applied consistently overestimated the MSW temperature over the modelling period due to its high sensitivity to values of heat generation
    - heat rate boundaries in the short-term model were set to 'constant value' for each waste layer due to the short time frame
    - the average HR over the timeframe of the short-term model (7840 to 8225 d) was calculated from the calibrated long-term functions and were then adjusted to be a percentage of the long-term values to better fit the final temperature profile and transient trends, according to the measured temperatures on site
    - this calibration was performed using the average thermal properties of the high and low diffusivity cases (K_T of 0.7 W/m and HC of 1.7 $MJ/m^3/°C$) and the resulting temperature profile represented the base case for the short-term model for which to perform a sensitivity analysis and simulation of heterogeneous thermal properties with depth
- The calibrated short-term heat rates were used to back-calculate three variable decay rate and BHP_{ULT} scenarios that all produced similar estimated present-day heat rates. The scenarios were then applied to the long-term and future models for comparison
    - the first scenario assumed the average BHP_{ULT} at each borehole between the two diffusivity scenarios was constant and variable decay rates per waste layer were calculated
    - the second scenario assumed the original estimated decay rate of $1x10^{-4}$ d^{-1} was constant and variable BHP_{ULT} values per waste layer were calculated
    - the third scenario assumed a constant, more rapid decay rate of $3x10^{-4}$ d^{-1} and variable BHP_{ULT} values per waste layer were calculated

4.0 Results and Discussion

4.1 Site Temperature Data

The daily average temperature recorded by each thermistor at the four Clusters between July 13th, 2018 and October 1st, 2020 were continually plotted throughout this research. Data 'blackouts' occurred at BH18-01, BH18-03, and TH19-02 due to temporary datalogger errors or power supply issues.

4.1.1 Transient Thermistor Array Data

Figure 4.1 presents the plots per instrument array in the order of installation (Phase 1 through 3). The time period of data presented depends on the Phase that arrays were installed on site.

Figure 4.1: Transient daily average temperature over monitoring period at A) BH18-01; B) BH18-03; C) BH19-02A; D) TH19-02; E) TH19-04

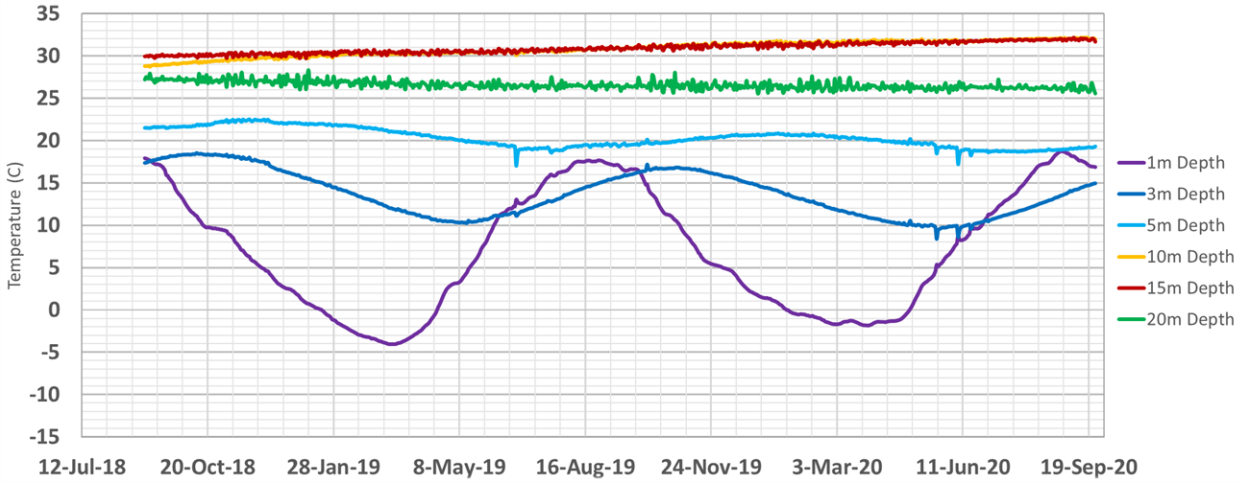

A) BH18-01

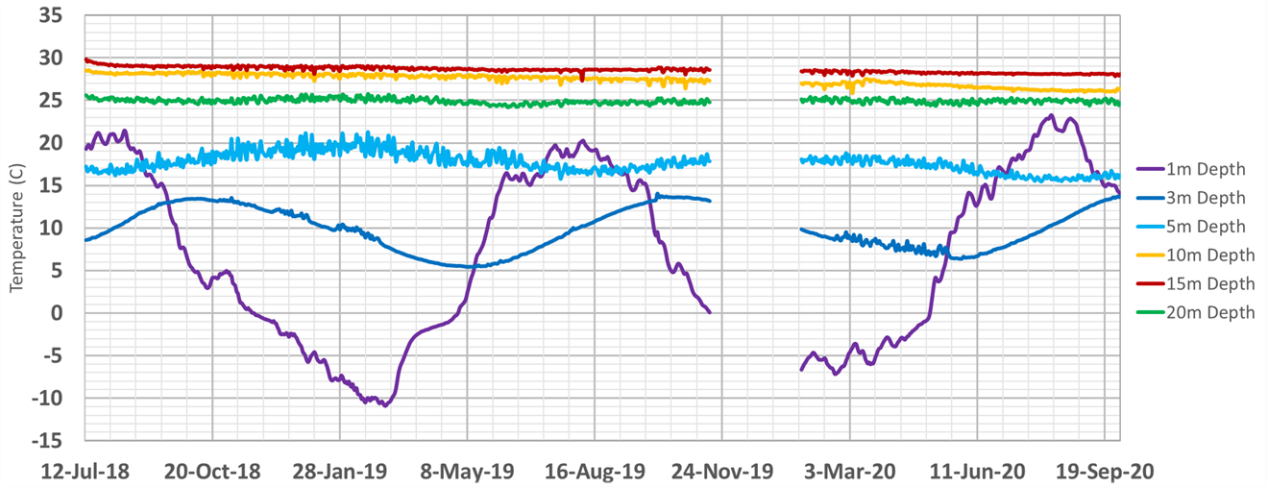

B) BH18-03

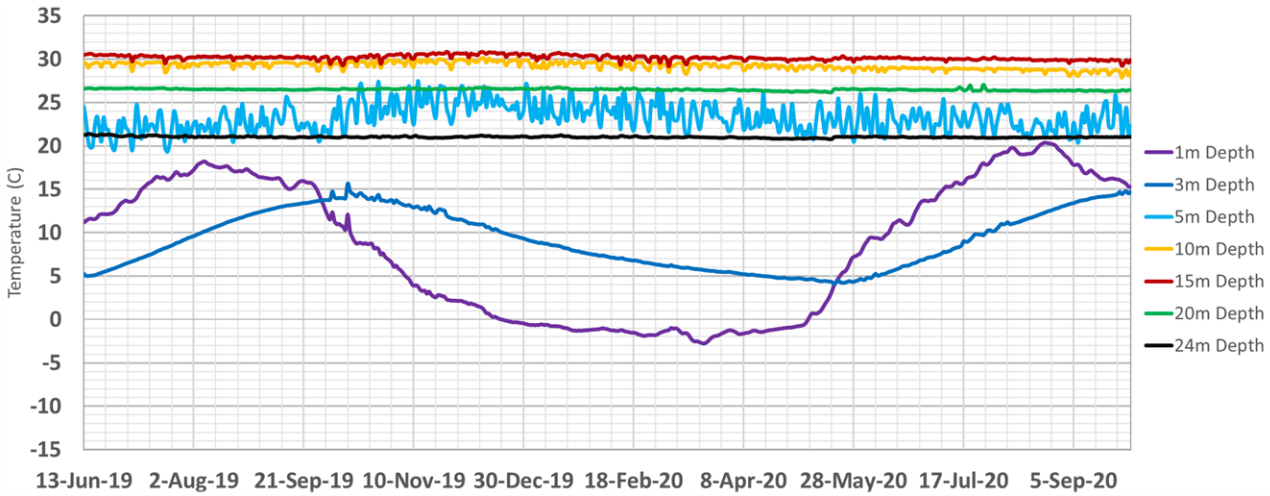

C) BH19-02A

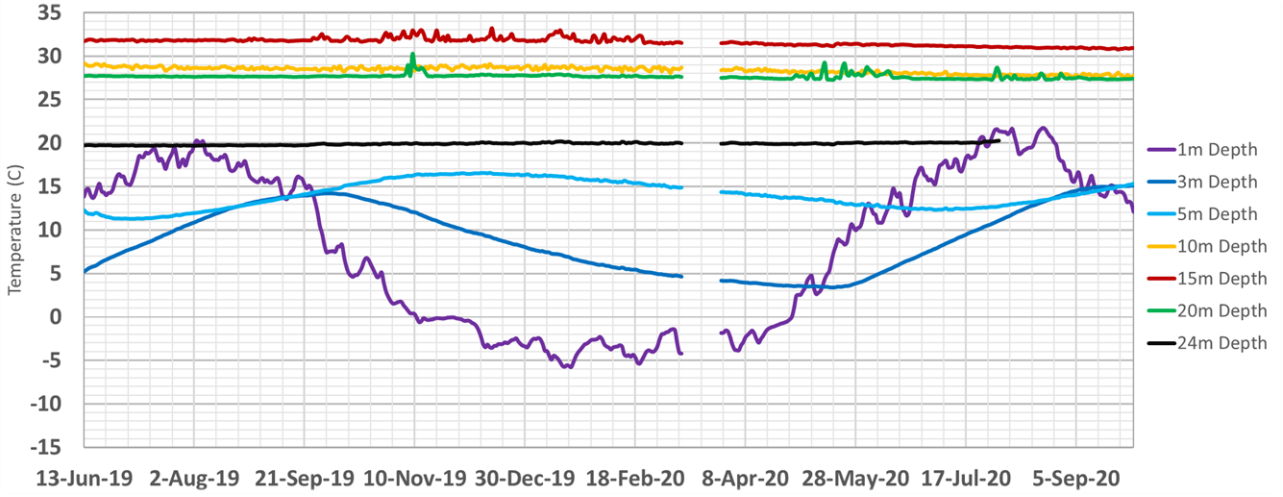

D) TH19-02

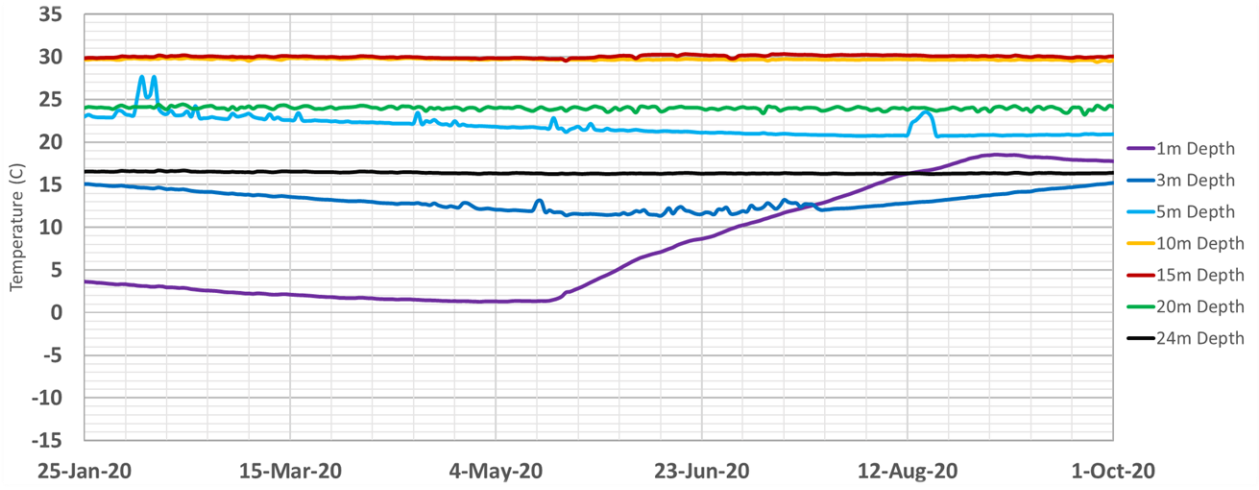

E) TH19-04

From Figure 4.1, a trend of increasing temperature at the 10 and 15 m thermistors at BH18-01 is evident (from 30 to 32 °C). A decreasing trend at the same depths at BH18-03 is observed from 29 to 28 °C (at 15 m depth). Cluster 2 (BH19-02A and TH19-02) demonstrated a relatively constant temperature trend that decreased slightly over the monitoring period, at around 31 °C (15 m depth). The peak temperature of 32 °C is within waste at an estimated age of 4 to 6 years (waste layer L3 at BH18-01). This is most similar to the observations at the landfill in Las Cruces, New Mexico from Table 2.5, where annual precipitation is 111 mm less and AAAT is 15.5 °C greater than in Saskatoon. The trends indicate that the peak temperature is increasing at BH18-01 and is unknown at BH18-03, as it appears to be decreasing from what would have been its peak. The peak temperature reached later in time at BH18-01 will offer a better comparison to the various sites across North America (Table 2.5).

The noise in the data such as that at the 5 m depth at BH18-03 and BH19-02A and the 20 m depth at BH18-01 was speculated to be a result of convective currents within the gas wells that the instruments were secured outside of. TH19-02 and TH19-04 do not have a gas well adjacent to the thermistors for this reason. After comparing the data from TH19-02 and BH19-02A to each other as well as to BH18-01 and BH18-03, it could not be concluded that the PVC gas well directly caused the noise. The noise was more likely caused by a poorly backfilled annulus space or unsaturated bentonite plug than the 2” PVC specifically. The condition of the bentonite plug at BH18-03 and the actual installed depth of the 1 m (target) depth thermistor being much shallower (0.36 m) at TH19-02 are considered the causes of the more variable 1 m depth curves when compared to the other arrays. Regardless of the array installation, the shallowest thermistors

generally recorded temperatures below 0 °C from early November to late May over the monitoring period. More discussion of the thermistor results and comparisons of the temperatures measured at the different array locations are discussed in Section 4.1.3, as the temperature differences are more easily observed by plotting data as vertical profiles.

4.1.2 Atmospheric Temperature Influence

The daily atmospheric temperature measured at the surface thermistor is plotted in Figure 4.2 with the upper domain thermistors at BH18-03 for observation of the atmospheric influence on shallow waste temperatures.

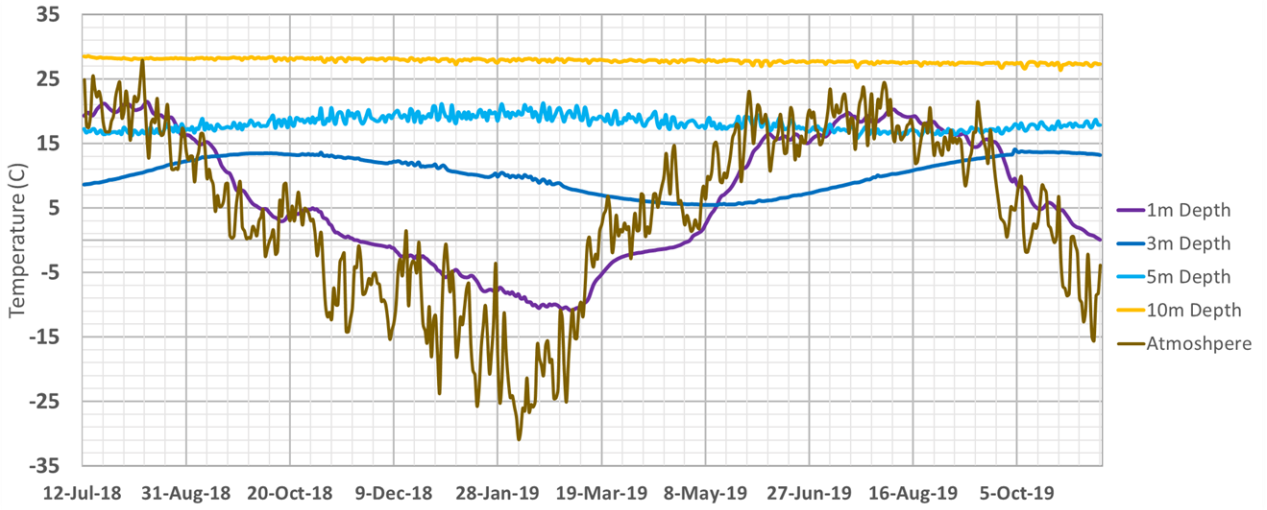

Figure 4.2: Visualization of phase-lag induced by atmospheric temperatures at BH18-03

From Figure 4.2 it is observed that the individual thermistors at 1, 3, and 5 m depth demonstrated the phase-lag phenomena identified by Yeşiller et al. (2005) and Hanson et al. (2010). The lag time between peak atmospheric and waste temperatures increases with depth and the amplitude of the temperature change due to atmosphere decreases with depth. The depth of atmospheric influence is between the 5 and 10 m thermistor, which coincides with the reported 6 to 8 m depth of atmospheric influence reported by Yeşiller et al. (2005). The phenomena is a result of insulation from the thermal properties of the MSW preventing instantaneous conductance of energy from the atmosphere to the waste. This was an expected observation if the thermistor arrays were properly installed and was observed at each of the thermistor arrays installed at the Northern Landfill.

It appears from the data in Figure 4.2 that the phase-lag could be used to determine thermal properties of the shallow MSW using an analytical solution or 1D model. However latent heat effects (evaporating, thawing), solar radiation, and environmental factors (wind, rain, and snow) as well as potential heat generation and potential for aerobic conditions complicate the upper boundary and the influence of atmospheric temperature on shallow waste temperatures. If these factors were considered in a future model, it is likely that thermal properties of the shallow MSW could be calibrated from the data collected.

4.1.3 Seasonal Profiles

The daily temperatures at each depth were averaged among the days within each season (outlined in Table 3.3) and are displayed in Figure 4.3. The plotting software interpolated curved lines between thermistor positions for better visualization of an entire vertical profile.

Figure 4.3: Seasonal average profiles over monitoring period for A) BH18-01; B) BH18-03; C) BH19-02A and TH19-02; D) All arrays over Summer periods (periods that data was available for all arrays)

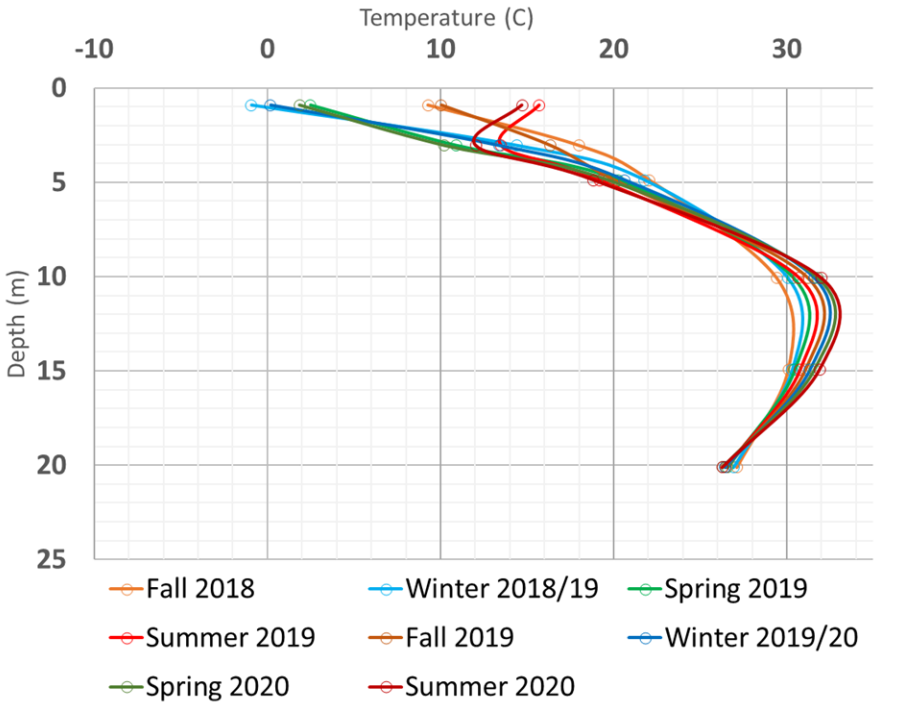

A) BH18-01

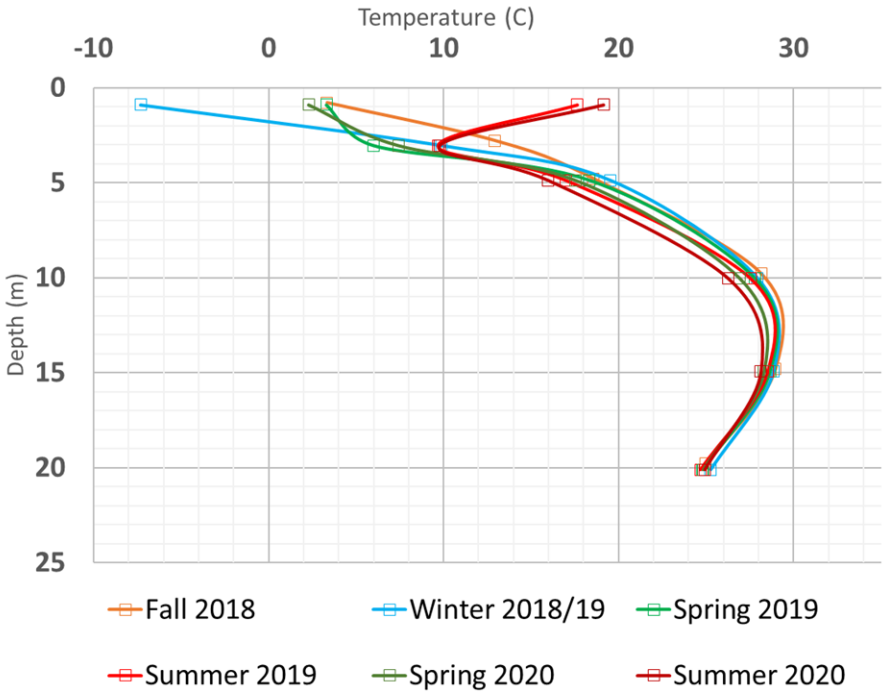

B) BH18-03

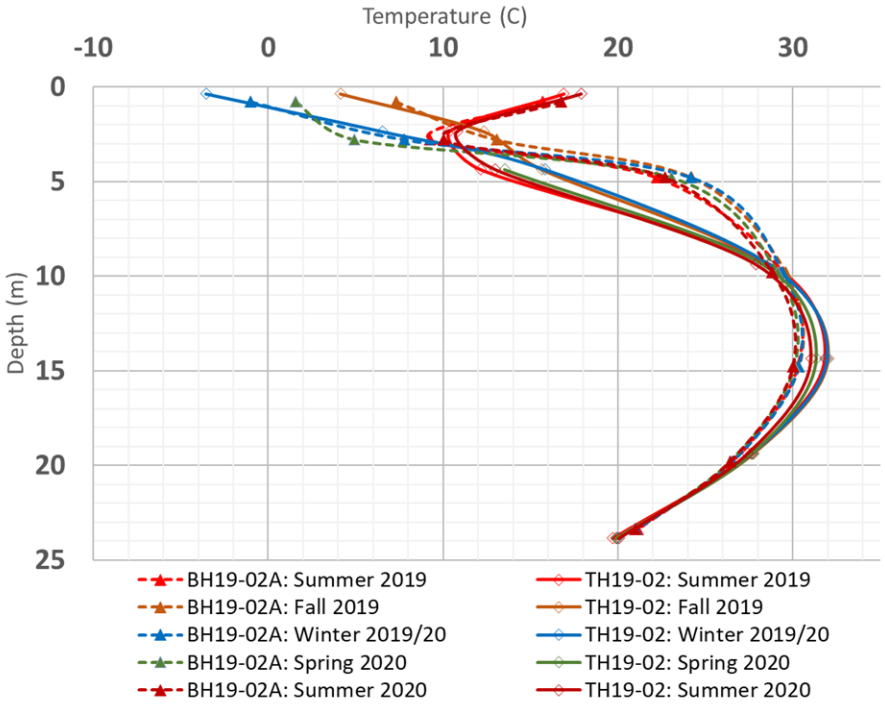

C) BH19-02A and TH19-02

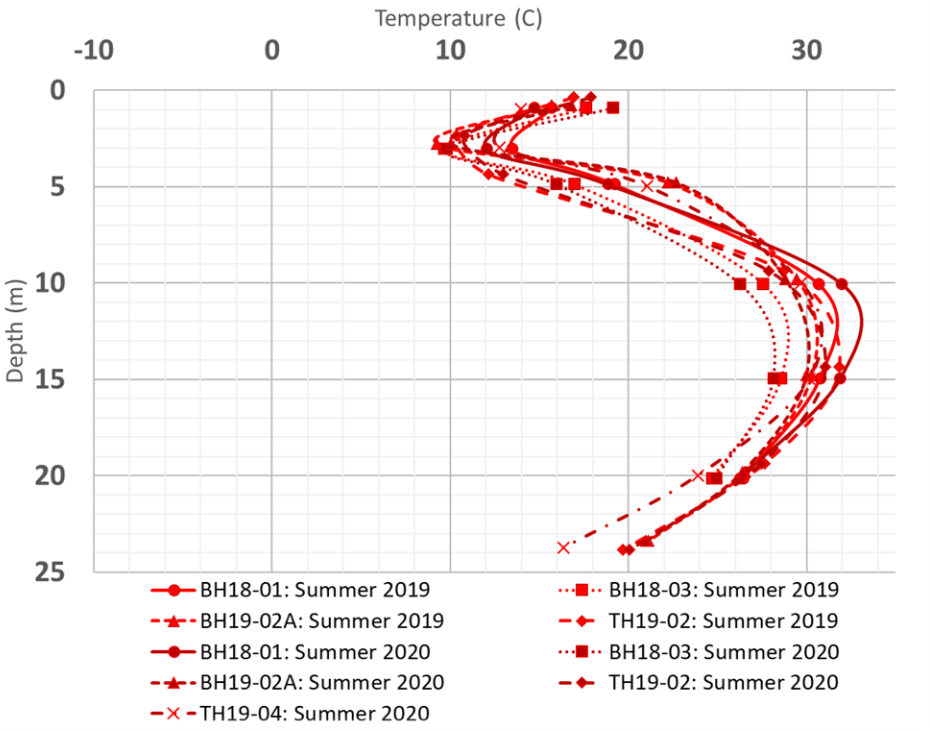

D) All arrays

From the profiles, it is evident that the temperature from season to season at the 10 and 15 m depth has consistently increased at BH18-01 and decreased at BH18-03, BH19-02A, and TH19-02. This is a strong indication of higher heat generation rates at Cluster 1, attributed to younger waste layers present at this location compared to Cluster 2 and Cluster 3. The variability of waste temperatures over very short distances is evident by comparing the profiles of BH19-02A and TH19-02 in Figure 4.3C as the arrays are 3.4 m apart on surface. The warm temperatures at 5 m depth at BH19-02A and cool temperatures at 24 m depth at TH19-04 when compared to the other arrays are evident in Figure 4.3D, where all five arrays are compared over the same time period. The average shallow thermal gradients are of the same direction (energy out of the landfill) in all seasons except summer, where the gradient between the 1 m and 3 m depths is downwards (energy into the landfill). This is consistent at all the arrays and the direction of the gradients is as expected in the cold average temperature of Saskatoon, after discovering the warm waste temperatures that exist at depth.

Temperatures at 20 m depth at BH18-01 consistently decreased over the monitoring period (from 27.1 to 26.3 °C), increasing the convexity of the profile through time in combination with the increases at 10 and 15 m depth. This is an indication of much lower heat generation rates at greater

depth at this location, although the magnitude of the downwards thermal gradient and expected heterogeneity of thermal properties are additional factors. Interestingly, temperatures at the 20 m and 24 m depth (if included) at the other arrays were all relatively constant over the monitoring period in comparison. This may be an indication of leachate mounding (2.25 to 2.48 m above liner) and the associated increase in bulk heat capacity stabilizing temperatures in the lower layer of waste at these locations in comparison to BH18-01 where an average of 0.05 m of leachate mounding has been measured.

Maximum recorded temperatures were consistently between the 10 and 15 m depth. The profiles at each Cluster demonstrate a convex shape. Both the convex shape and position of the warmest temperatures (0.3 to 0.6 normalized depth) correlates well with what was reported for multiple landfill sites (Hanson et al., 2010; Yeşiller et al., 2015a). As demonstrated by the shape of the interpolated curve, higher maximum temperatures may exist between the 10 and 15 m thermistor locations. The approximate position and magnitude of the maximum temperatures at each array from Figure 4.3 are in Table 4.1.

Table 4.1: Position and magnitude of maximum waste temperatures from seasonal profiles

Array	**BH18-01**	**BH18-03**	**BH19-02A**	**TH19-02**
Maximum interpolated temperature **(°C)**	32.9	29.3	30.6	32.1
Depth of interpolated maximum temperature **(m)**	11.8	12.6	13.0	14.2
Normalized depth of maximum interpolated temperature	0.47	0.50	0.52	0.57

The depth of the maximum temperature is shallowest at BH18-01, which agrees with the theory presented by Yeşiller et al., (2015a) in which the youngest waste at surface correlates to an upward translation of the position of the maximum temperature compared to the older locations. However this theory is not demonstrated when comparing Cluster 2 and Cluster 3, where TH19-02 has a deeper location of the maximum temperature but is located within younger wastes than at BH18-03. The deeper maximum temperature position at Cluster 2 could be a result of higher rates of downard leachate flux (Khire et al., 2020), higher heat generation at depth in the past, or variability of the thermal properties when compared to other locations. Because Cluster 2 boreholes were not

modelled, no further conclusions can be made regarding the deeper maximum temperature at TH19-02 or the less pronounced convexity at BH19-02A.

4.2 Modelling Results and Calculations

The results of the 1D vertical heat transport models described in detail in Section 3.4 are presented in this section. The objective of the long-term model was to determine BHP_{ULT} values at each modelled location (BH18-01 and BH18-03) that resulted in present-day temperatures in the mid-depth region being reached. Results of the long-term model are presented as vertical profiles to demonstrate the temperature distribution at the end of the modelled timeframe. Transient data throughout the simulation was only presented for the 'short-term model' as the initial conditions were known for only that step. The BHP_{ULT} values were used to calculate BMP and C_{eq} based on the equations presented in Section 3.3.

4.2.1 Results of the Long-Term Model and Sensitivity Analysis

The temperature profiles and 'base case' for each long-term model scenario is plotted with the results of a sensitivity analysis in Figures 4.4 and 4.5 and the waste temperatures measured at each location. The maximum MSW temperature reached at depth from the long-term model as of September 2019 for the base cases and sensitivity analyses are compared in Table 4.2. As mentioned in Section 3.4, the base case had the following parameters:

- Initial MSW temperature of 0 °C based on average waste placement date of October 31st
- Timesteps of 30 d based on resolution of the data used for upper boundary condition
- Decay rate of 1.0×10^{-4} d^{-1} based on initial reference values in the literature
- Mesh size of 0.5 m

The sensitivity analysis compared the following modelling parameters:

- Initial MSW temperatures of -10 °C, +10 °C, and alternating between -5°C and +5°C from the bottom waste layer to the top
- Timesteps in the model solver of 15 d and 45 d
- Decay rates of 7.5×10^{-5} d^{-1} and 1.25×10^{-4} d^{-1} using the BHP_{ULT} values in Table 4.3 from the base case
- Increased mesh sizes of 1.0 and 2.0 m

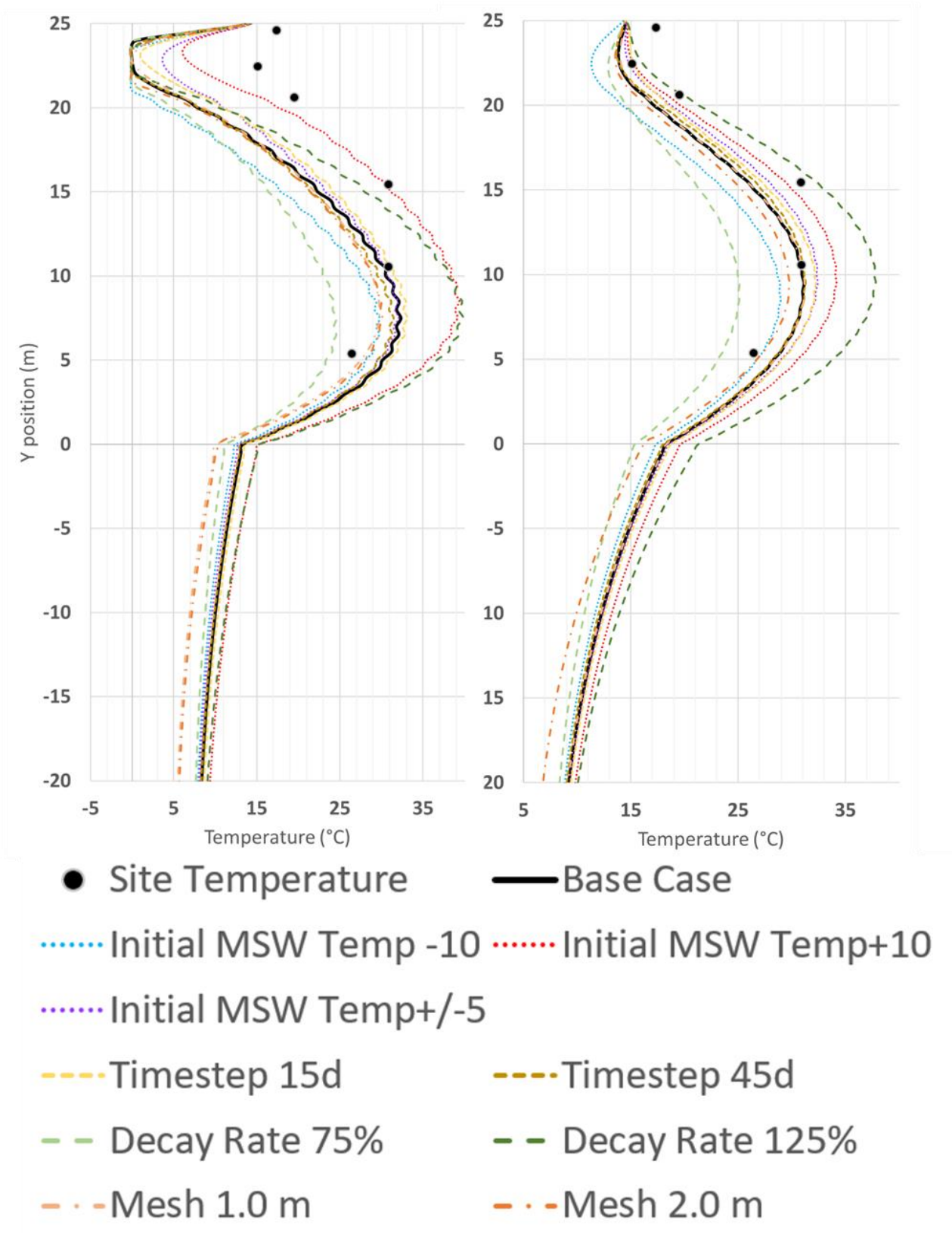

Figure 4.4: BH18-01 long-term model base case compared with the results of the sensitivity analysis for Left; low diffusivity scenario and Right; high diffusivity scenario. ***Note****: Y-position of 0 m corresponds to the liner elevation in the model.*

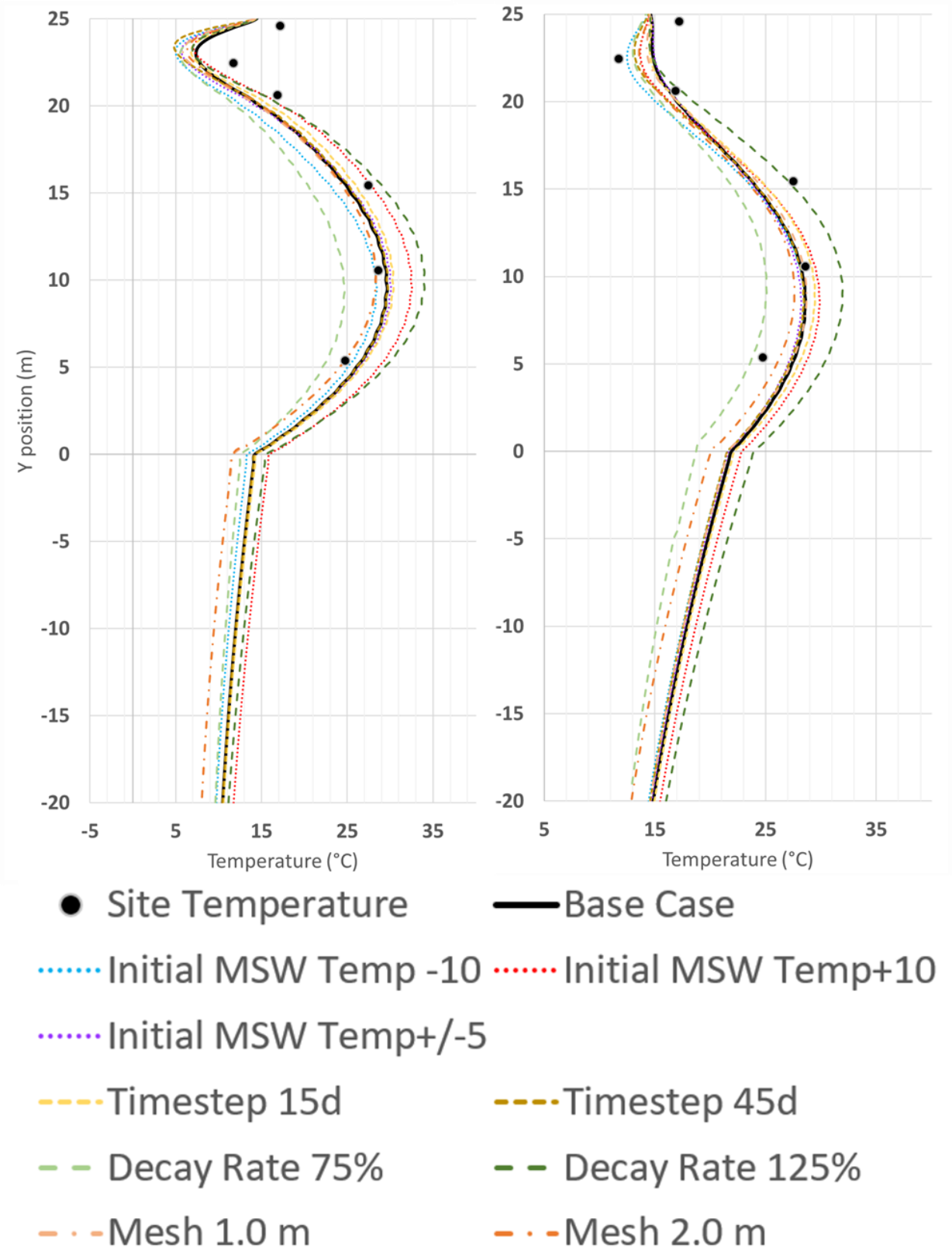

Figure 4.5: BH18-03 long-term model base case compared with the results of the sensitivity analysis for Left; low diffusivity scenario and Right; high diffusivity scenario. ***Note****: Y-position of 0 m corresponds to the liner elevation in the model.*

*Table 4.2: Difference in maximum temperature reached in the MSW from long-term model sensitivity analysis. Values in **bold** are the greatest differential from the base case by analysis (column).*

Borehole	Thermal Diffusivity	Base Case (°C)	Initial Temperature (°C)			Timesteps (d)		Decay Rate (d^{-1})		Mesh Size (m)	
			-10	+10	±5	15	45	$7.5x10^{-5}$	$1.25x10^{-4}$	1.0	2.0
BH18-01	High	31.1	-2.1	+3.1	**+1.3**	**+1.1**	+0.2	-6.0	+6.7	+0.1	-1.3
	Low	32.3	**-2.5**	**+7.1**	-0.3	+0.8	**-0.8**	**-7.7**	**+7.5**	**-2.5**	**-2.2**
BH18-03	High	28.6	-0.2	+1.3	-0.4	+0.8	-0.1	-3.5	+3.4	+0.1	-1.0
	Low	29.7	-1.3	+2.8	+0.4	+0.7	0.0	-5.0	+4.3	-1.3	-1.4

From the base-case curves in Figures 4.4 and 4.5, the convex shape of the temperature profile was successfully reproduced by the long-term model, however the depth of the maximum temperature is consistently lower than what was observed on site. The position of the maximum temperature is shallower for the high diffusivity MSW compared to the low. Considering the position is low in both diffusivity scenarios and at both boreholes and does not translate upwards or downwards in any of the sensitivity analyses, the discrepancy is likely caused by the thickness and timing of the waste layer placement in the model compared to reality. Thicker waste lifts or younger waste ages in the middle to upper layers should in theory translate the position of the maximum temperature upwards (Yeşiller et al. 2015a).

The diffusivity scenarios were also observed to have different depths of maximum temperature when compared to one another. The potential heterogeneity in thermal properties with depth being present at the modelled locations is another factor that would affect the location of the maximum temperature. Using the thermal properties applied to the short-term model analysis for both high and low heterogeneity (K_T from 0.3 to 1.1 W/m, HC from 1.2 to 2.2 $MJ/m^3/°C$), thermal diffusivity would hypothetically increase slightly with depth in the MSW when compared to the homogenous material approach. The actual heterogeneity of both K_T and HC and the affect on both the maximum temperature and its position in profile would have to be assessed with further modelling, in which the transient thermal properties due to reduction in void spaces are coupled with heat transport.

Also observed from Figures 4.4 and 4.5 is the poor fitment of the long-term model to site data in the shallow MSW (upper 5 m). The fitment is worse in the low diffusivity scenario compared to the high. At BH18-01 in the low diffusivity scenario, latent heat effects causing the uppermost

layer of MSW to remain frozen is evident. In all cases, an upwards translation of the maximum temperature location would improve the fitment in the shallow MSW in addition to the mid and lower regions.

From Table 4.2 it is evident that differences in maximum temperature from the sensitivity analysis were more pronounced at the younger BH18-01 compared to BH18-03 and greater in the low diffusivity scenario compared to the high. The greater sensitivity at BH18-01 is attributed to the shorter modelling period compared to BH18-03, where thermal energy had more time to dissipate when modelled heat generation rates have reduced. The higher sensitivity of the low diffusivity MSW is attributed to the thermal properties making the material inherently store rather than transmit thermal energy.

The greater magnitude of maximum temperature modelled in the +10 °C placement temperature analysis in all cases agrees with the field observations made by Yeşiller et al. (2005) and Hanson et al. (2010) that increased placement temperatures leads to increased waste temperatures. Interestingly, an initial temperature of -10 °C had less of an affect on the final magnitude of the maximum temperature than did +10 °C. Based on the framework of the model and software used, this is likely caused by the difference between the frozen and unfrozen thermal properties of the MSW.

Also of interest is the symmetry of the affect on maximum temperature that decay rate has compared to the base case. Despite higher heat generation rates in theory producing steeper thermal gradients than would be expected with lower heat generation rates, the magnitude of the temperature difference is comparable for both diffusivity scenarios and locations. Therefore, when using a first-order decay heat generation function, a direct correlation may exist between the peak heat generation rate and the maximum temperature reached when all other variables are unchanged.

The analysis of increasing mesh sizes revealed that in all cases the 2.0 m mesh size reduced the maximum temperature reached at depth and a 1.0 m mesh size had no affect on the high diffusivity scenarios but had comparable sensitivity as the 2.0 m mesh on the low diffusivity scenarios. This suggests that the high diffusivity MSW can be modelled with a coarser mesh size than the low

diffusivity MSW if required. The 0.5 m mesh size was therefore acceptable for modelling the wide range of thermal properties used in this research though computation time was reduced at 1.0 m.

The sensitivity of the model to changes in the till thermal properties was also analyzed as the subgrade represents a large heat sink for the warm MSW. The base case thermal properties of both the Floral and Sutherland tills were either increased by a factor of 125% or reduced by a factor of 75%. The resulting subgrade and MSW profiles are plotted in Figures 4.6 and 4.7.

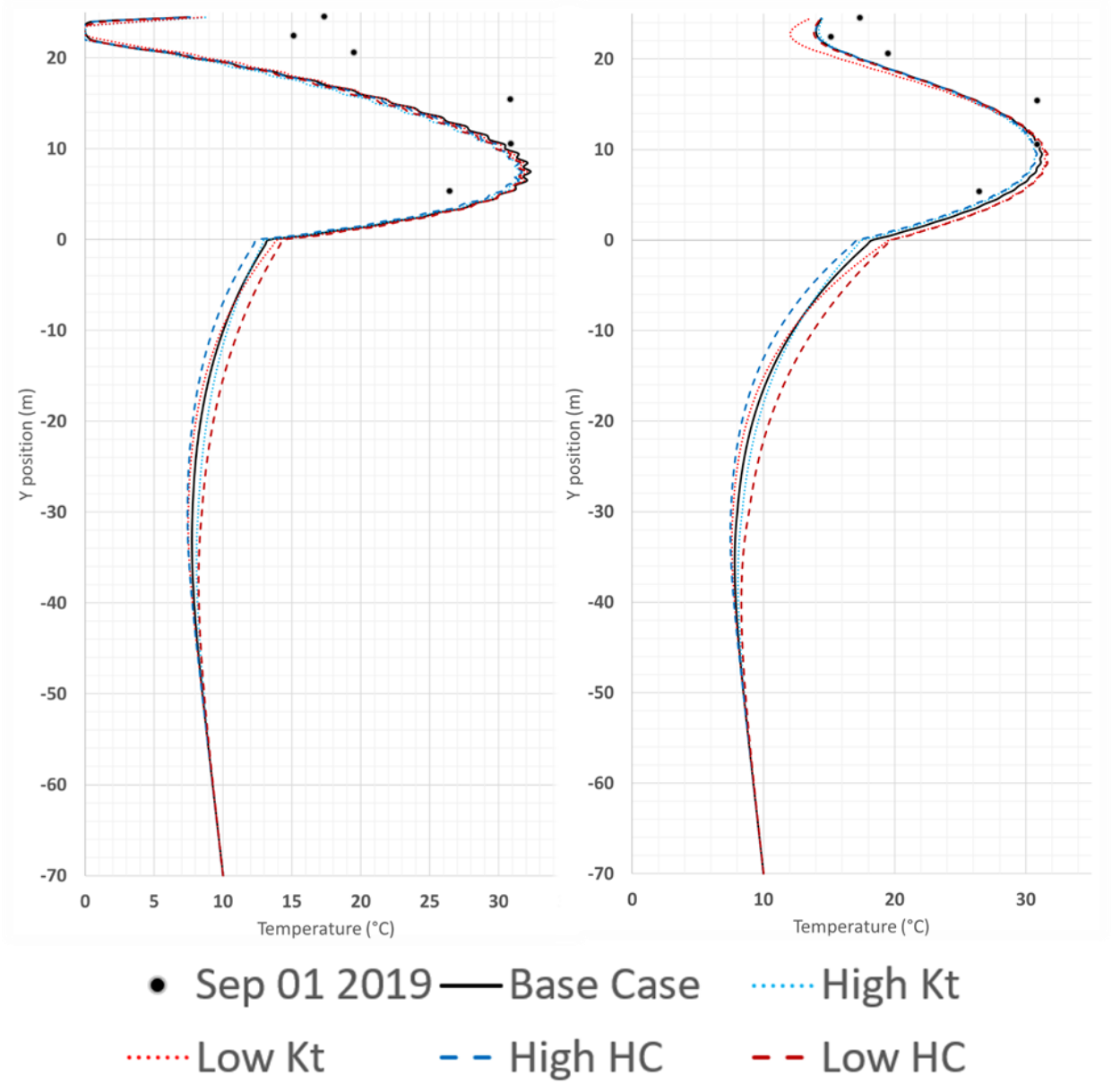

Figure 4.6: Long-term model sensitivity to subgrade properties (BH18-01); Left - Low Diffusivity; Right - High Diffusivity; ***Note****: Y-position of 0 m corresponds to the liner elevation in the model*

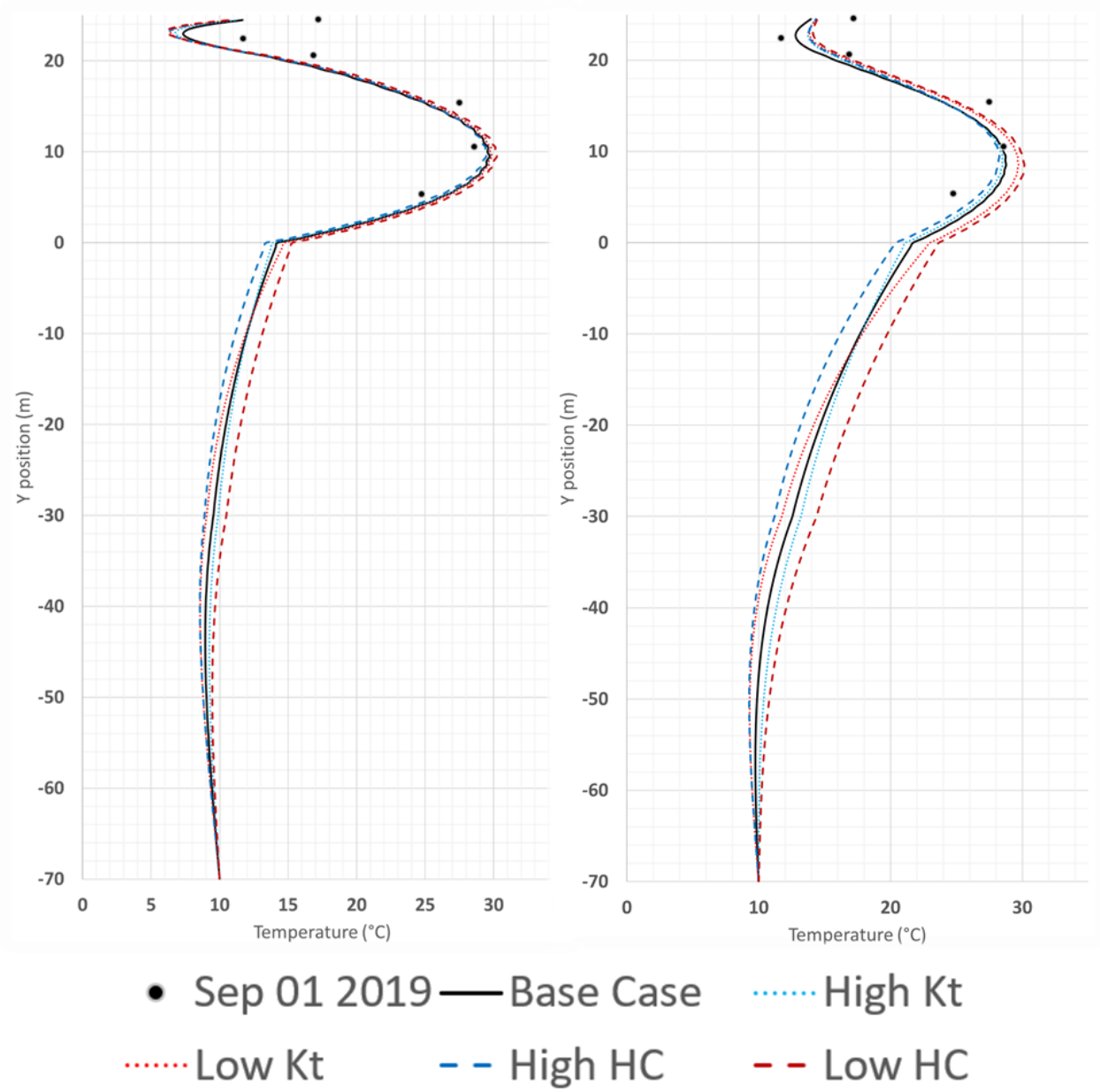

Figure 4.7: Long-term model sensitivity to subgrade properties (BH18-03) for Left: Low Diffusivity and Right: High Diffusivity.
***Note**: Y-position of 0 m corresponds to the liner elevation in the model*

From Figures 4.6 and 4.7, similarly to the sensitivity analysis of the long-term model, the high diffusivity MSW properties resulted in the greatest change to both the subgrade and MSW temperatures when compared to the low diffusivity scenario. Sensitivity was also greater at BH18-01 compared to BH18-03, attributed to the same reason as above (shorter time period). In all cases the subgrade temperatures were more sensitive to the percentage change to HC than they were to K_T.

There is potential error in the groundwater temperature data used for estimation of the initial subgrade temperature profile and the temperature at 75 m depth may be less than the value of 10 °C used as the model's bottom boundary condition. As well, with increases in atmospheric temperatures attributed to climate change, the shallow subgrade temperatures may not be as consistent as in the past. Thermistors or similar temperature-measuring instrumentation would have to be installed into the native subgrade materials on or near the Northern Landfill to observe the actual transient temperature trends of the subgrade in the region and measure the temperature at 75 m depth. This would also allow for samples of the subgrade to be collected for measurement of thermal properties, which in combination with the temperature data would be valuable for improving the analysis of geothermal energy potential at the site.

The BHP_{ULT} values for BH18-01 and BH18-03 calibrated for each diffusivity scenario of the MSW are presented in Table 4.3. The calculated lower and upper bound BMP and C_{eq} contents, using the relationship to BHP_{ULT} in Equations 7 and 9, are also in Table 4.3 along with the peak (initial) heat generation rates from the heat generation function. The cumulative energy produced by the end of the long-term model (September 1st, 2019) for each waste layer is included in Table 4.4.

Table 4.3: Results of heat potential estimate using Long-term model and associated methane potential and organic content

Borehole	**Diffusivity**	**Peak Heat Generation Rate** (W/m^3)	**BHP_{ULT}** (MJ/m^3)	**BMP** (L/kg_{MSW})		**Equivalent Cellulose** ($kg_{C6H10O5}/kg_{MSW}$)	
				UE	LE	UE	LE
BH18-01	**High** K_T =1.1W/m HC =1.2 $MJ/m^3/°C$	0.28	240	40	120	9%	27%
	Low K_T =0.3 W/m HC =2.2 $MJ/m^3/°C$	0.27	235	39	117	9%	26%
BH18-03	**High**	0.21	180	30	90	7%	20%
	Low	0.13	115	19	57	4%	13%

Table 4.4: Cumulative energy produced at the end of the Long-term model for each diffusivity scenario; ***Note –*** *LD is low diffusivity and HD is high diffusivity*

Borehole	**Waste Layer**	**Cumulative Energy Produced** (MJ/m^3)	
		LD	HD
BH18-01	L1B	86.5	88.3
	L1T	50.1	51.2
	L2+L3B	43.4	44.3
	L3T	36.0	36.8
	L4	21.2	21.7
	L5	13.0	13.3
BH18-03	L1B	62.7	98.1
	L1T	58.6	91.8
	L2	56.6	88.6
	L3	52.3	81.9
	L4	47.5	74.3
	L5	45.0	70.5
	L6	17.8	27.9

The high diffusivity MSW resulted in higher BHP_{ULT} values when compared to the low diffusivity case at both boreholes as expected. However, the difference in BHP_{ULT} values calibrated for each diffusivity scenario was smaller at BH18-01 (5 MJ/m^3) compared to BH18-03 (65 MJ/m^3). Because thermal properties are the same at each location in the long-term model, the only factor to cause this difference is the waste age (placement times). Because BH18-03 is older, a longer total elapsed time is modelled, and the high diffusivity scenario conducts more energy out of the column of MSW than does the low diffusivity scenario. As a result, a greater amount of energy (higher BHP_{ULT}) is required in the high diffusivity scenario to bring the MSW up to present-day temperatures. At BH18-01, it appears the modelled period is not long enough for the higher diffusivity waste to require a greater energy production (to reach target temperatures) than the low diffusivity scenario.

The results for BHP_{ULT} and peak heat generation rate from Table 4.3 were compared to values reported in the literature. Cumulative energy potentials from Hanson et al. (2008) were reported between 15.0 and 191.0 MJ/m^3 and peak heat rates between 0.19 and 2.21 W/m^3 among the four landfills studied (via numerical modelling). As mentioned in Section 2.5 the lower energy potentials reported for Anchorage and Las Cruces were considered to be much lower than in

reality, as they are based on climatic and operational factors as opposed to available organic matter within the MSW. The updated model published by Hanson et al. (2013) reported total expended energy at two cells of the Canton landfill to be 104 and 174 MJ/m^3 and peak heat generation rates of 1.52 and 1.16 at two different cells, respectively. Although not explicitly stated, the total energy expended in the 2013 paper appears to be the energy expended over the modelling period (such as in Table 4.4) as opposed to the total potential energy of the MSW (as in Table 4.3). Therefore, total potential energy for the studied sites could be greater than the expended energy reported.

Few other energy potentials of MSW were available in the literature. A value of 180 MJ/m^3 based on enthalpy of biochemical reactions from field data was reported in Yeşiller et al. (2005) from a conference proceedings by Zanetti et al. (1997), however the paper could not be found to assess the methods. The calibrated values from my model are in the same order of magnitude as what has been reported in the literature. The cumulative energy produced by the lower waste layers over the long-term model duration (in Table 4.3) demonstrate that the relatively low average decay rate applied to the model base case results in less than half of the total potential energy being expended by 2019 for each waste layer. Additional peak heat generation rates from the literature for comparison include a value of 0.64 W/m^3 determined by Emmi et al. (2016) at an Italian landfill based on the formulation proposed by Hanson et al. (2008). Khire et al. assumed constant heat generation rates between 0.3 and 1.0 W/m^3 and Rowe et al. (2010) assumed constant values of 0.44 and 0.76 W/m^3 above and below the leachate level, respectively. The peak values resulting from my model calibration (0.13 to 0.28) are comparable to the peak values determined by Hanson et al. (2008) for the Anchorage and Las Cruces landfills (0.19 and 0.38 respectively). Based on the theoretical relation to BMP, another indication of the accuracy of my model results can be reviewed by comparing the values in Table 4.3 to BMP values reported in the literature.

A review of BMP by Krause et al. (2016) reported BMP values for MSW determined experimentally ranged between 35 and 167 L/kg_{MSW}. Values based on models and waste composition data ranged between 20 and 223 L/kg_{MSW}. Ivanova et al. (2008) determined a BMP of 167.4 L/kg_{MSW} experimentally with a total initial cellulose content of the MSW sample of 24.9% by mass, however only ~79% of the cellulose was digested. Because of other heat sources being included in the energy balance and heat being generated from sources other than cellulose, the values of C_{eq} are not directly comparable to actual cellulose contents, but laboratory procedures

and experimentation could be developed in the future to evaluate a correlation. The BMP range from the model results presented in Table 4.3 (19 to 120 L/kg$_{MSW}$) is comparable to values reported by Krause et al. (2016), though the upper bound is lower than that reported in the literature. Based on the significant C/D waste stream received at the Northern Landfill as reported by operators, a lower organic content (C_{eq}), BMP, and BHP_{ULT} than the typical municipal landfill can be expected. The results of future research determining BMP of MSW samples recovered from the Northern Landfill will provide a sample of results to compare to values determined using this heat transport model.

4.2.2 Results of Short-Term Model and Sensitivity Analysis

The short-term model simulated the MSW at both borehole locations between September 1st, 2018 and September 21st, 2019. The final profile at the end of the model on September 21st, 2019 was graphed and different constant heat rates for each waste layer were iterated until the final profile most closely matched the measurements on site. The HR functions from the long-term model overestimated the heat rates significantly, except the functions for L4, L5, and L6 at BH18-03 which did not need to be adjusted when calibrating the short-term model. The estimated present-day heat rate values are listed in Table 4.5 for each waste layer.

Table 4.5: Estimated present-day heat rate values for the waste layers from the short-term model

Borehole	**Waste Layer**	**Calibrated Heat Rate** *MJ/d*	*W*
BH18-01	L1B	7.67×10^{-4}	0.009
	L1T	9.55×10^{-4}	0.011
	L2+L3B	5.95×10^{-3}	0.069
	L3T	1.23×10^{-2}	0.143
	L4	1.77×10^{-2}	0.205
	L5	1.61×10^{-2}	0.186
Thickness-Weighted Average:		8.53×10^{-3}	0.099
BH18-03	L1B	1.72×10^{-3}	0.020
	L1T	2.22×10^{-3}	0.026
	L2	2.68×10^{-3}	0.031
	L3	5.36×10^{-3}	0.062
	L4	8.87×10^{-3}	0.103
	L5	9.20×10^{-3}	0.107
	L6	1.28×10^{-2}	0.148
Thickness-Weighted Average:		6.12×10^{-3}	0.071

From Table 4.5, the heat rates at each location are predicted to be much lower at depth than the long-term model predicted. The long-term model HR function did however reasonably predict the heat rate in the upper layers at BH18-03. The lower heat generation rates predicted in the bottom layers than were modelled by the long-term model is attributed to either a much lower organic content in the lower waste or a higher average decay rate in the past than $1x10^{-4}$ d^{-1}, leaving very little degradable organic matter remaining. The higher predicted rates in the lower layers at BH18-03 compared to BH18-01 is surprising considering the difference in waste age, however the leachate mounding at BH18-03 may encourage greater rates of methanogenesis than the drier BH18-01 can support. The highest heat rates being present in L4 and L5 at BH18-01 (4 to 10 m depth) is an affirmation of the expectation that higher heat rates exist in the youngest waste layers, below the surficial layer influenced heavily by atmospheric temperatures. The calibrated HR values represented the base case for the sensitivity and heterogeneity analysis which was performed. The base case had the following parameters:

- Homogeneous average thermal properties (K_T = 0.7 W/m, HC = 1.7 MJ/m^3/°C)
- Constant heat rates according to Table 4.3
- Liner temperature of 20 °C and 19 °C for BH18-01 and BH18-03 respectively
- 0.5 m Floral till intermediate cover

The sensitivity analysis simulated the following scenarios using homogeneous, average thermal properties:

- 0.25 m thick till cover at the top of the MSW
- No till cover at the top of the MSW
- Liner temperatures 2 °C colder than the initial estimate
- Liner temperatures 2 °C warmer than the initial estimate

The heterogeneity analysis simulated the following scenarios:

- High heterogeneity with K_T and HC increasing linearly with depth from 0.3 W/m and 1.2 MJ/m^3/°C in the top 1 m to 1.1 W/m and 2.2 MJ/m^3/°C in the bottom 1 m (25 m depth)
- Low heterogeneity with K_T and HC increasing linearly with depth from 0.5 W/m and 1.45 MJ/m^3/°C in the top 1 m to 0.9 W/m and 1.95 MJ/m^3/°C in the bottom 1 m (25 m depth)

The output profiles from the short-term model are plotted in Figures 4.8 and 4.9. Note that HD, LD, and AD refers to high, low, and average diffusivity MSW thermal properties. The 'long-term HR' curves refer to the first-order decay heat rate functions from the long-term model base case.

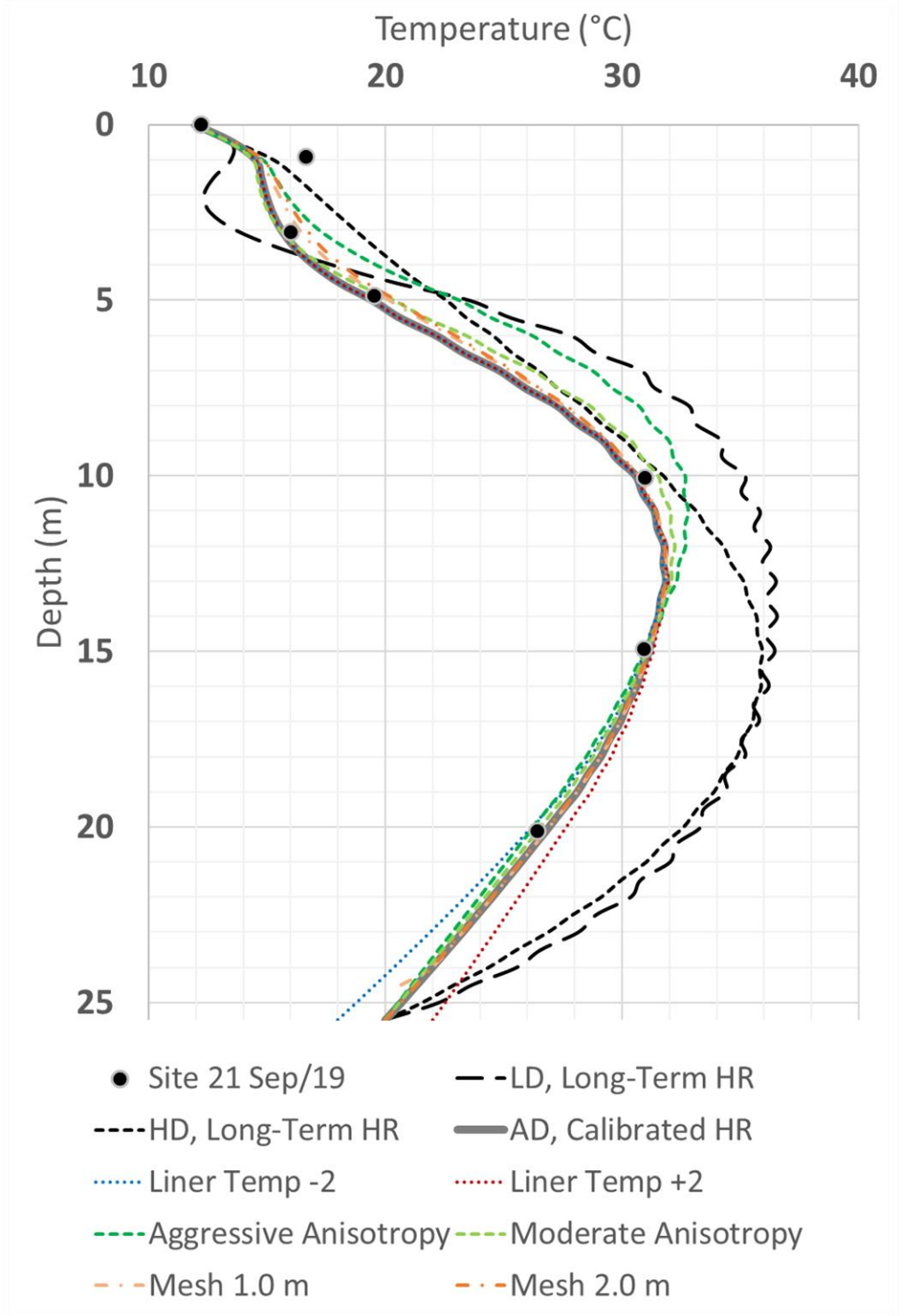

Figure 4.8: BH18-01 short-term model results and sensitivity analysis

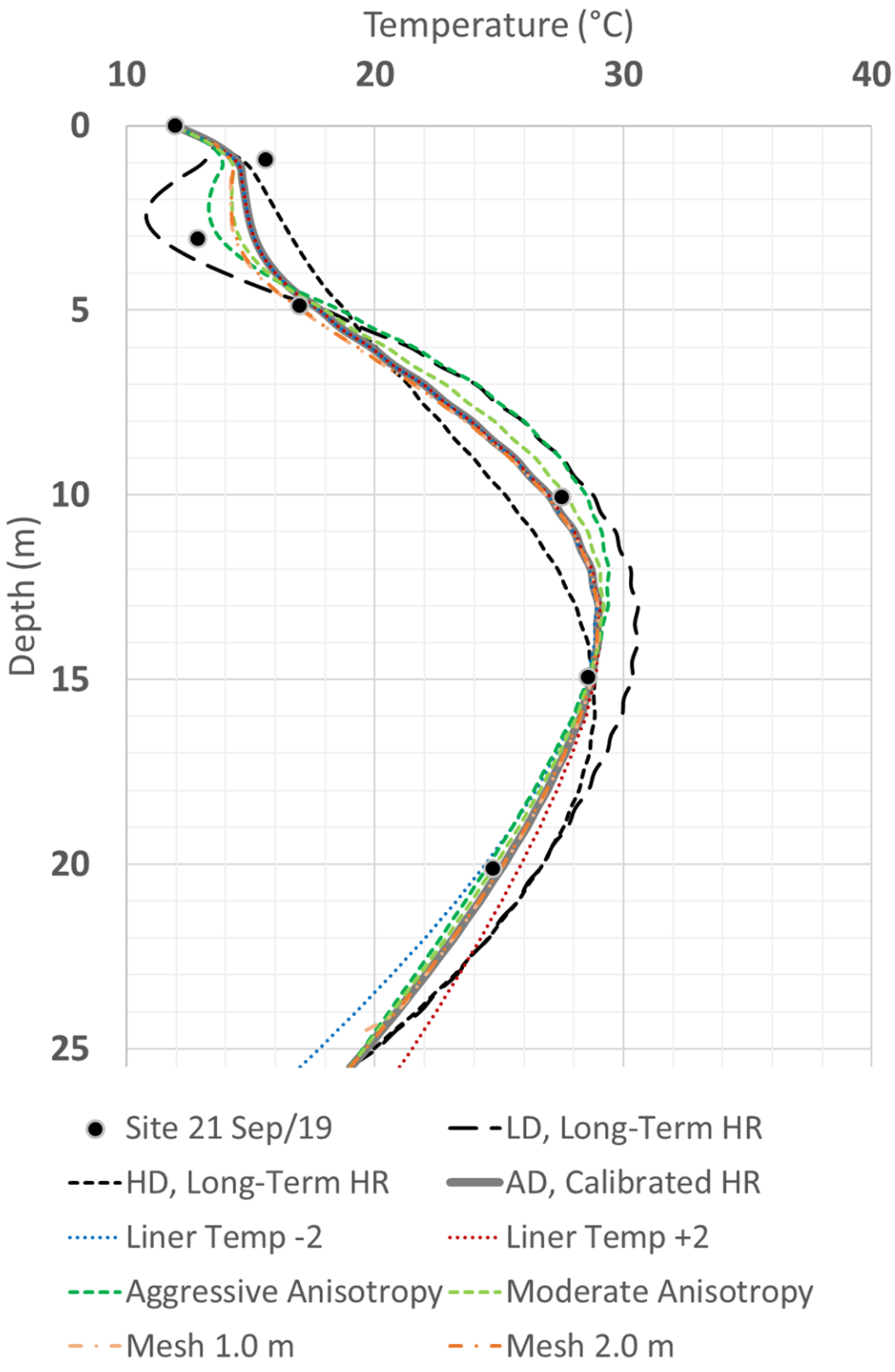

Figure 4.9: BH18-03 short-term model sensitivity analysis results

The over-estimation of maximum waste temperatures when the long-term heat generation functions were applied over the short-term modelling period are evident from Figures 4.8 and 4.9. Waste temperatures using the long-term HR values from both diffusivity scenarios significantly overestimate the temperatures from 5 m depth downwards at the younger BH18-01. The error is observed to be less pronounced at BH18-03.

The calibrated HR for both locations results in a reasonable fit to site data from 5 m depth downwards. The poor fitment of the short-term model to shallow temperatures above 5 m depth is attributed to a temperature-only boundary being used in the model. Other environmental factors such as solar radiation, wind, and snow cover have been demonstrated to affect energy transfer at the landfill surface (Hanson et al., 2010; Megalla et al., 2016). Implementation of a modified temperature boundary using *n*-factors or other boundary terms is recommended for future modelling, as the temperature in the shallow MSW may have influence at depth due to heat conductance and impacts on thermal gradients.

The increased mesh sizes of 1.0 and 2.0 m had comparable affects on output temperatures. The short-term model was only sensitive to the coarser mesh sizes in the upper 7 m of MSW, and an increase in shallow temperatures was observed at BH18-01 while a decrease in shallow temperatures resulted at BH18-03. This difference is attributed to the greater calibrated rates of heat generation in the upper two layers at BH18-01 when compared to BH18-03 (Table 4.5). This suggests that though the model sensitivity is low over the relatively short timeframe, a coarser mesh may be more sensitive to heat generation rates in the MSW, and in the shallow MSW nearer the transient top temperature boundary.

The application of heterogeneous thermal properties only induced observable changes to the MSW temperature from 1 m below surface downwards to the mid-depth (~13 m depth). The variable liner temperatures affected the MSW temperature most significantly at the liner elevation but was insignificant above ~15 m depth. The significance of the cover thickness on the MSW temperature was not demonstrated well in profile but can be viewed in the transient graphs for each shallow thermistor which is plotted in Figures 4.10 and 4.11.

Figure 4.10: BH18-01 transient site data and short-term model comparison at A) all depths; B) 1 m depth; C) 3 m depth; D) 5 m depth; E) 10 m depth; F) 15 m depth; G) 20 m depth

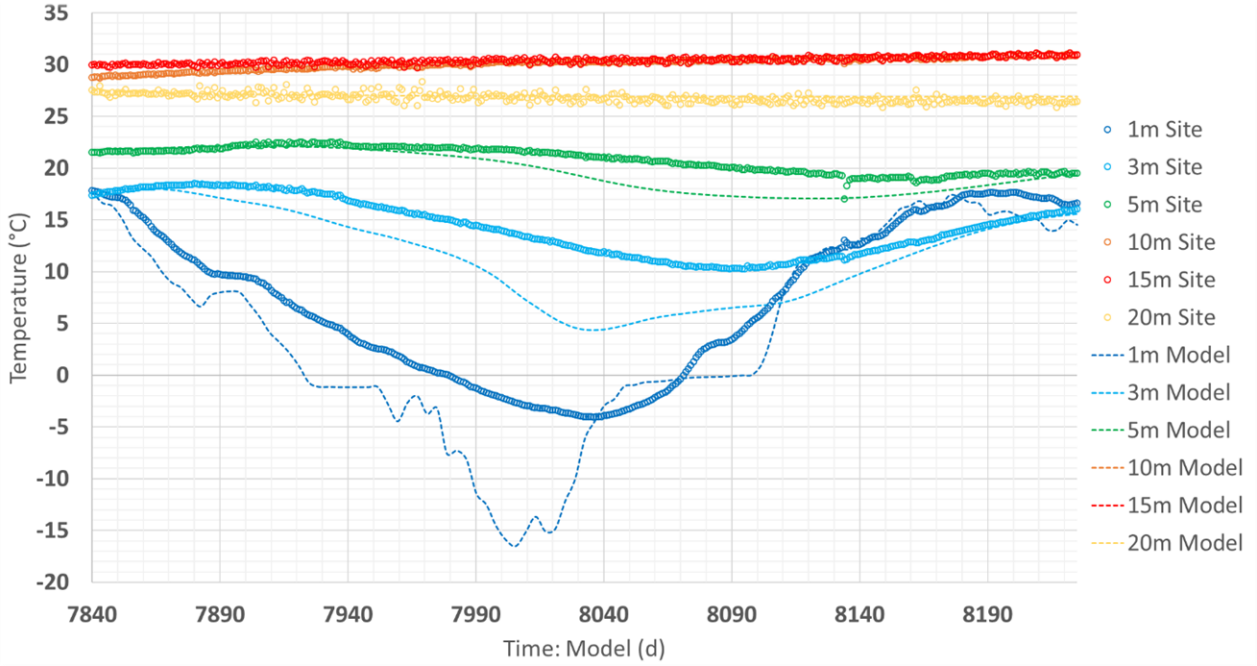

A) all depths

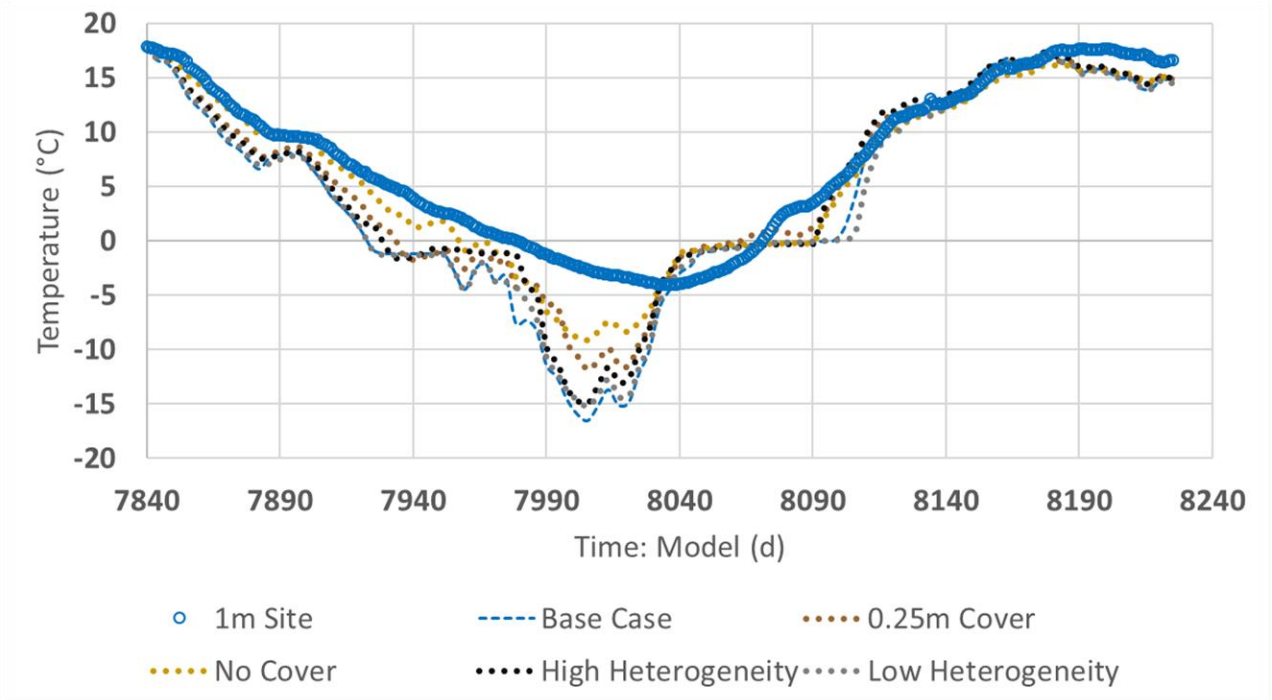

B) 1 m depth

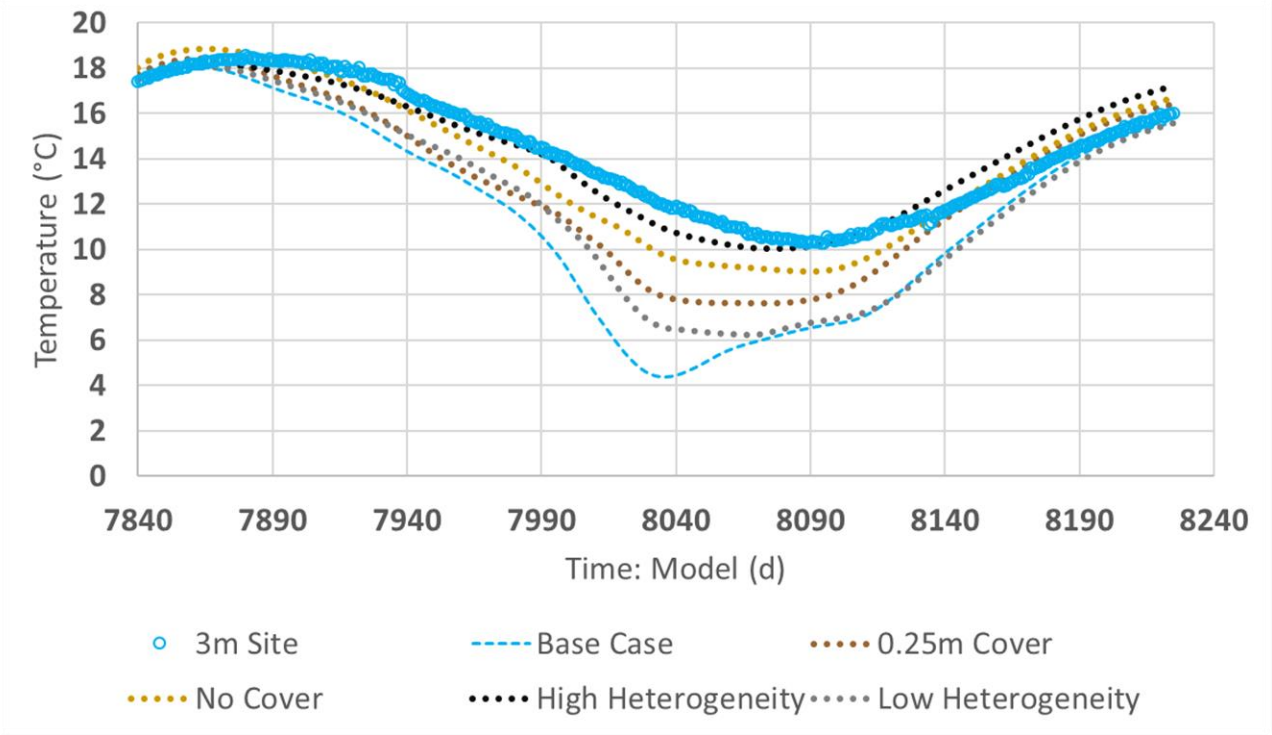

C) 3 m depth

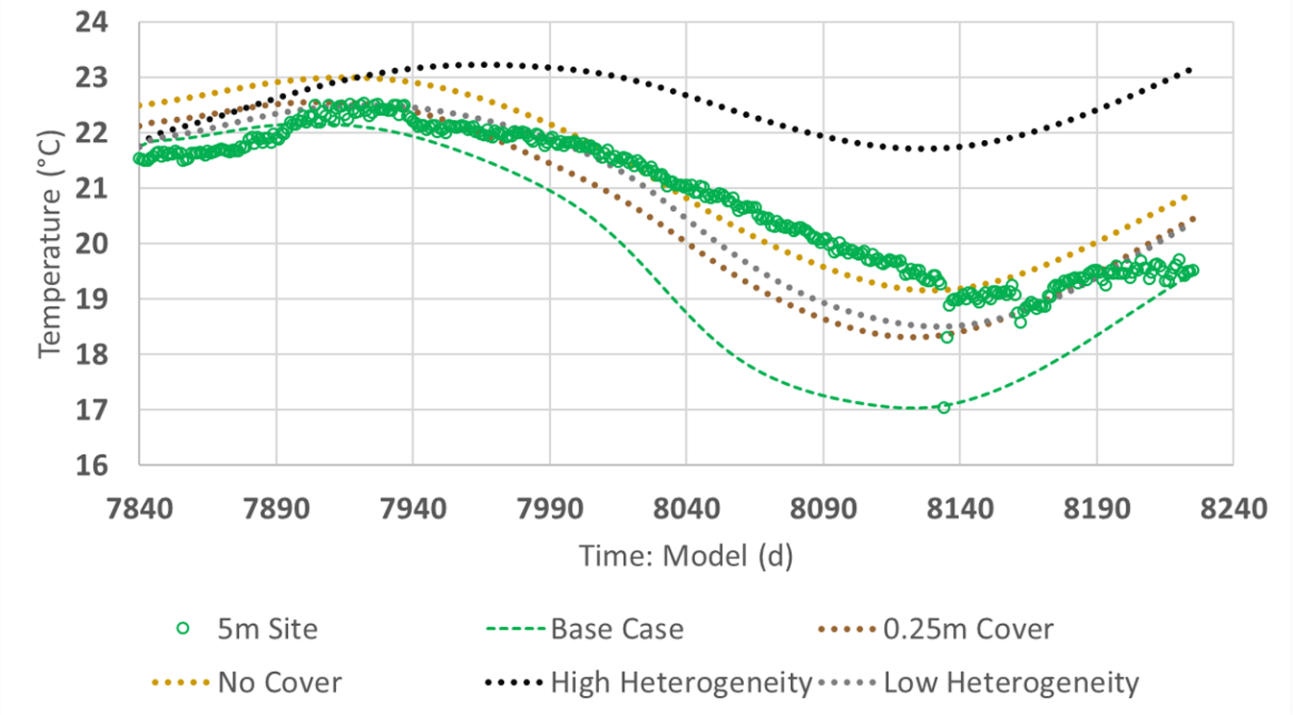

D) 5 m depth

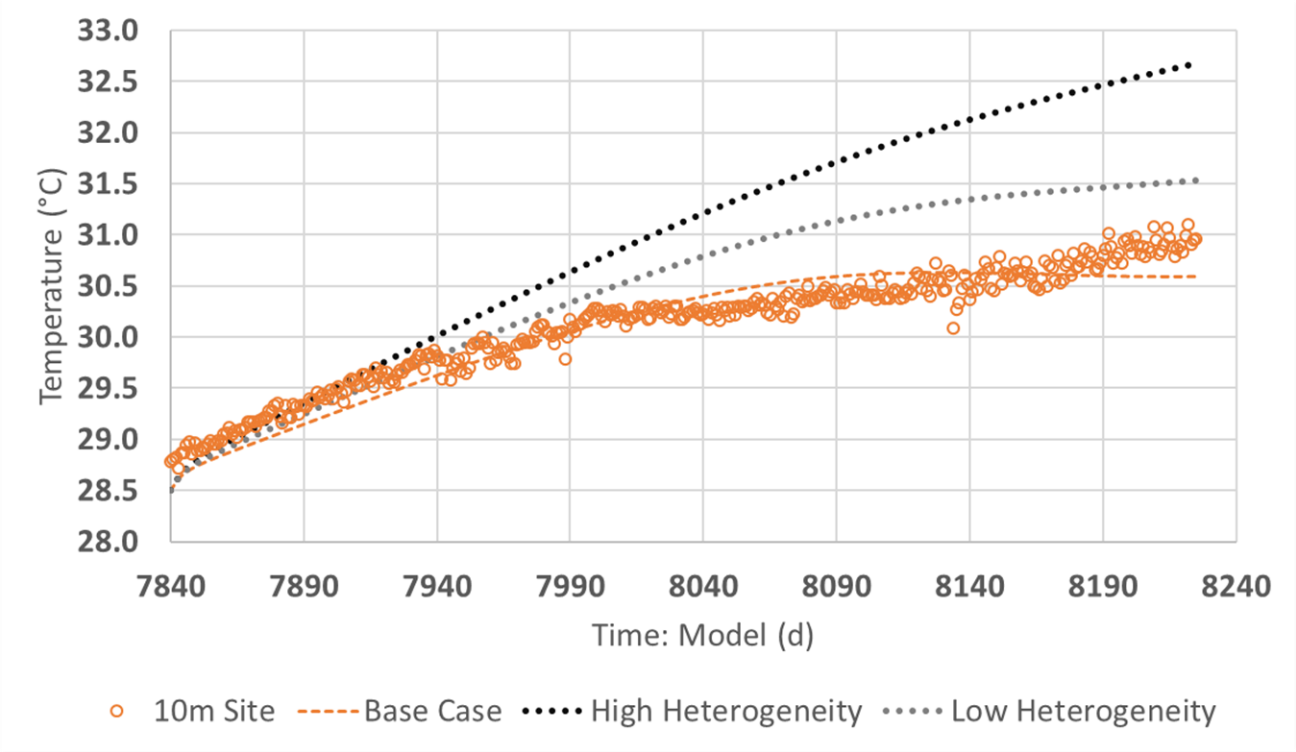

E) 10 m depth

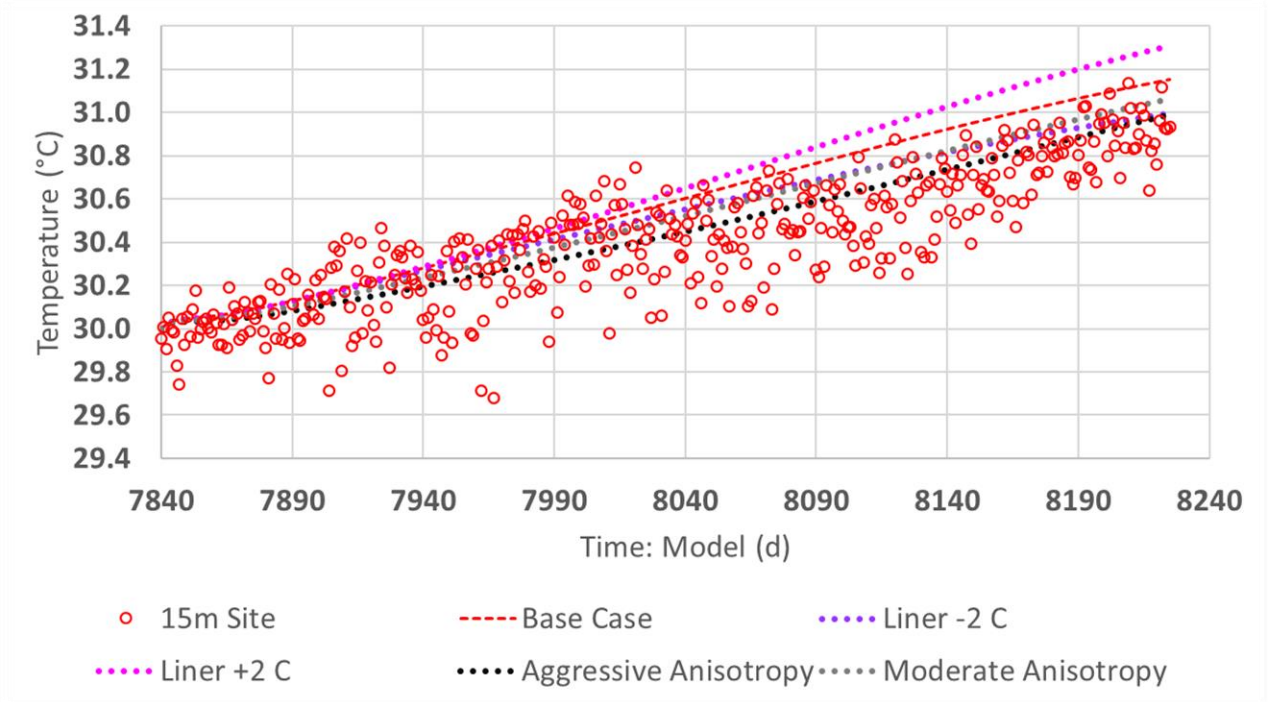

F) 15 m depth

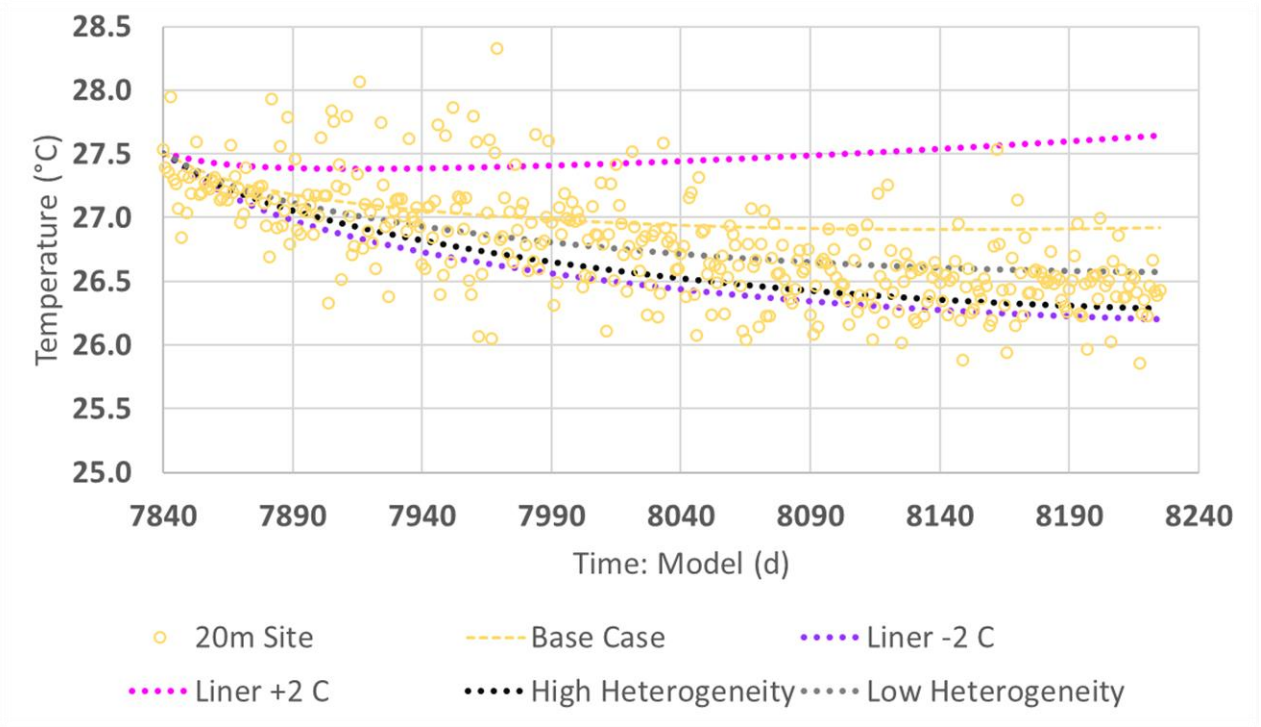

G) 20 m depth

Figure 4.11: BH18-01 transient site data and short-term model comparison at A) all depths; B) 1 m depth; C) 3 m depth; D) 5 m depth; E) 10 m depth; F) 15 m depth; G) 20 m depth

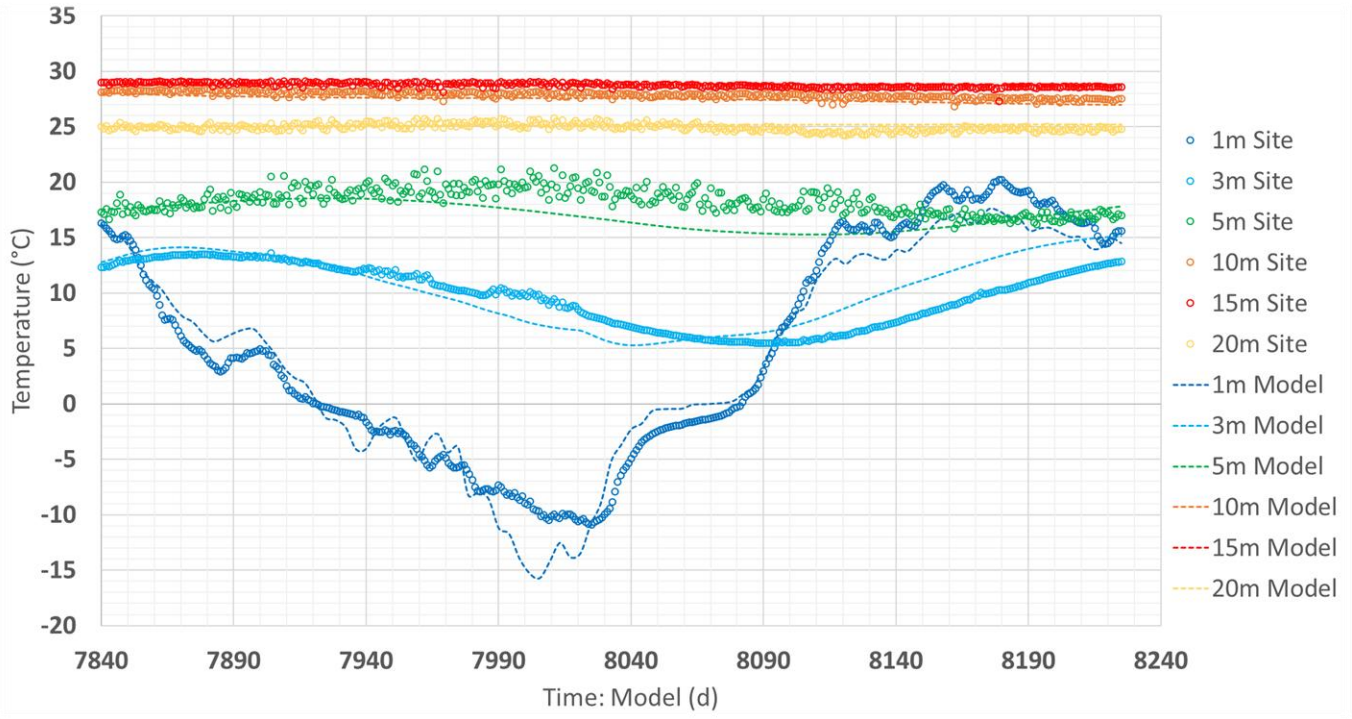

A) All depths

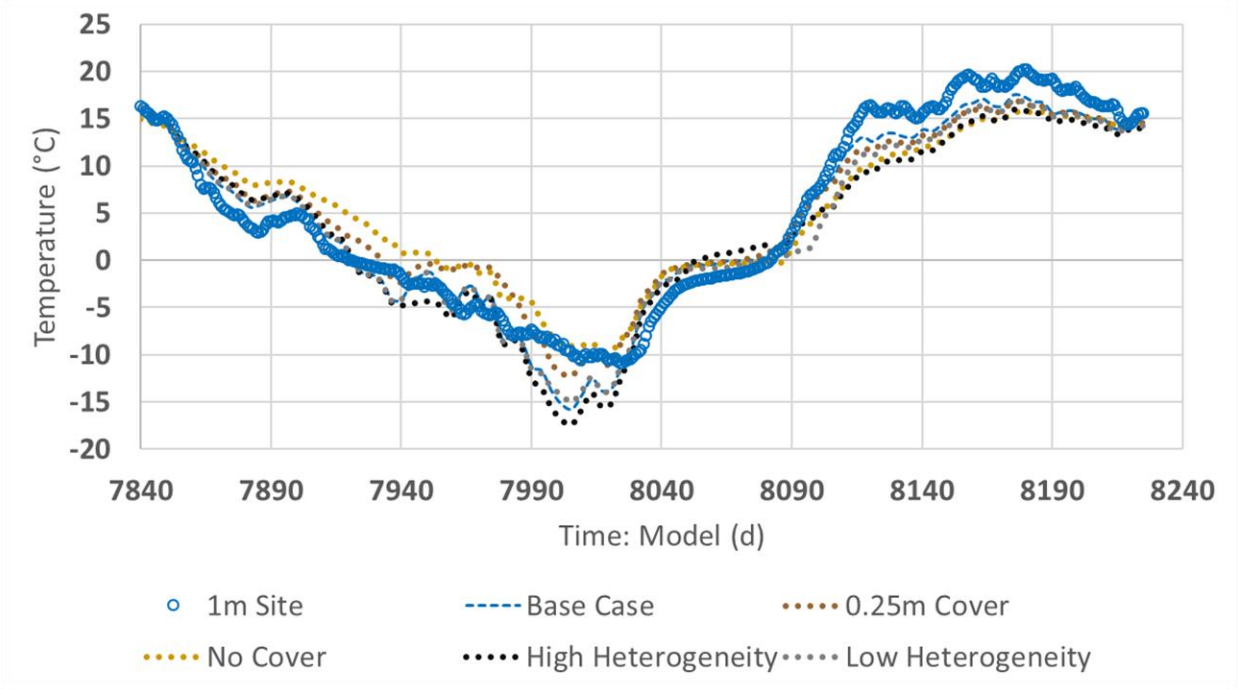

B) 1 m depth

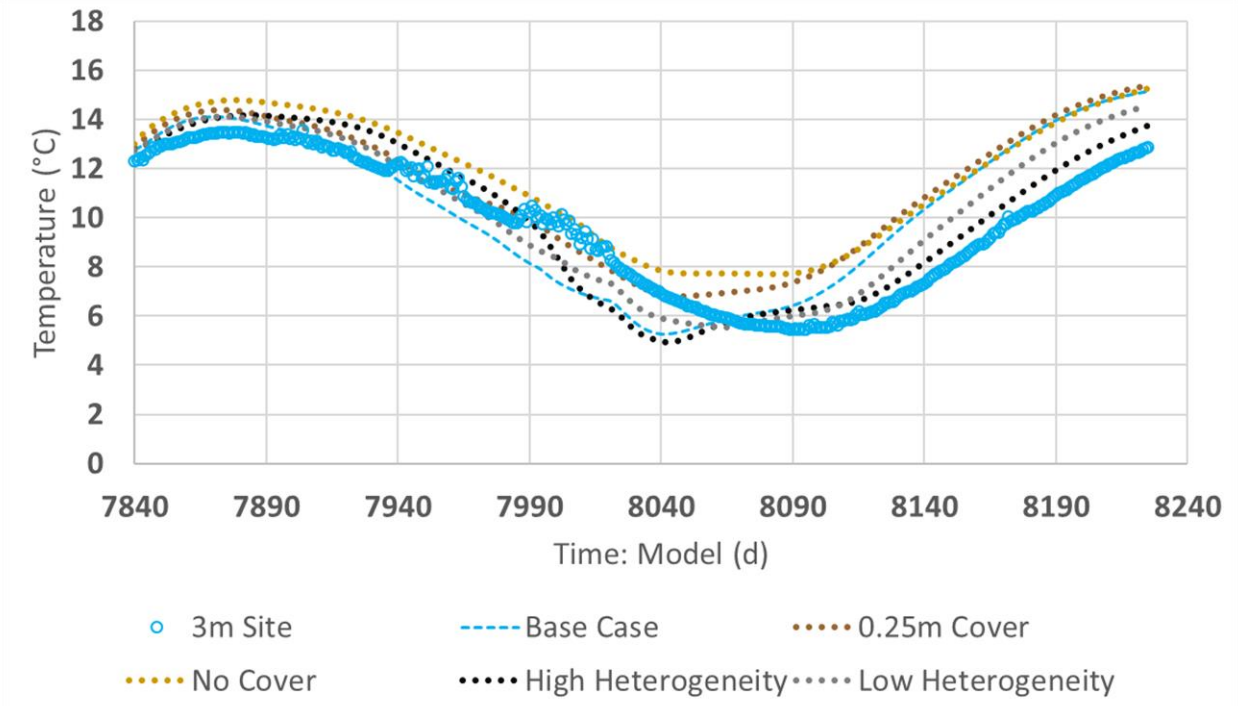

C) 3 m depth

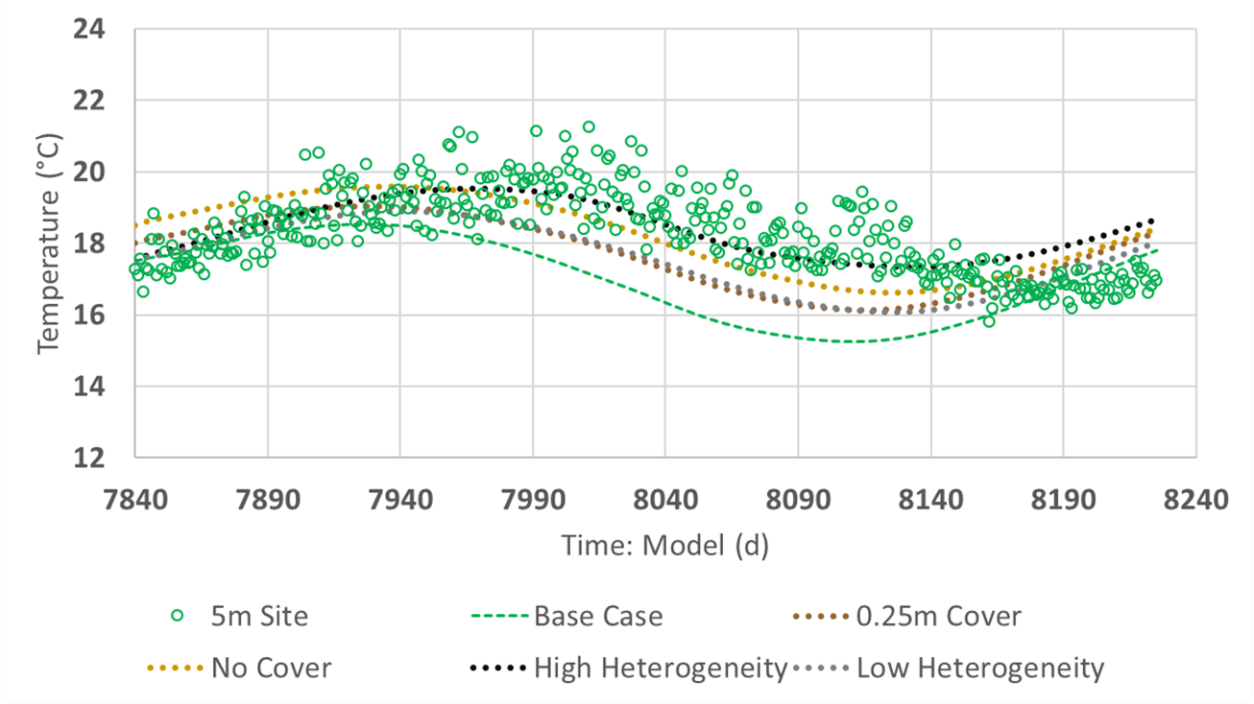

D) 5 m depth

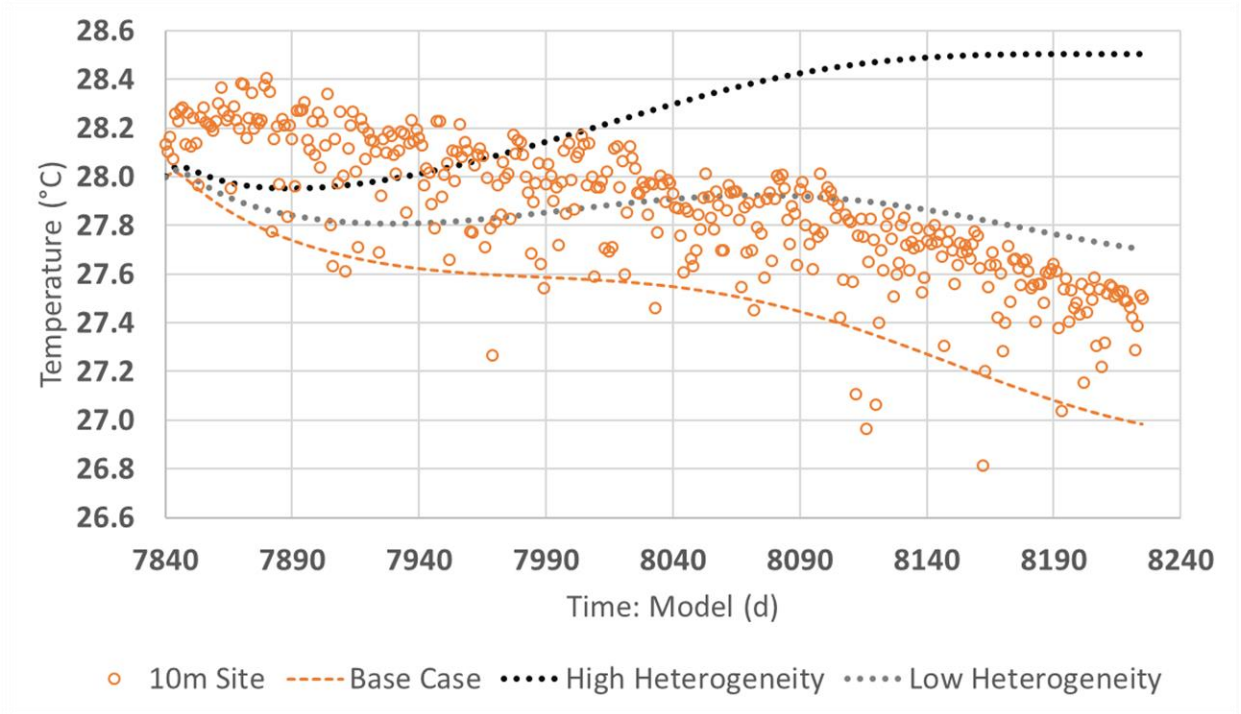

E) 10 m depth

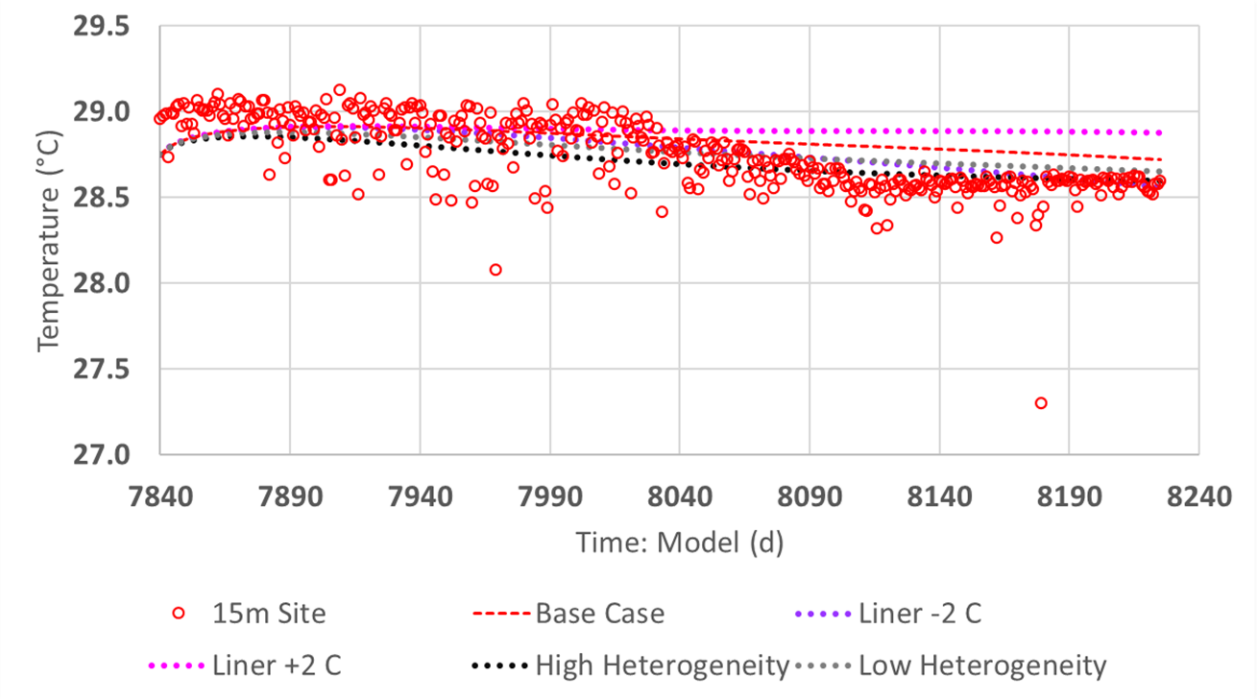

F) 15 m depth

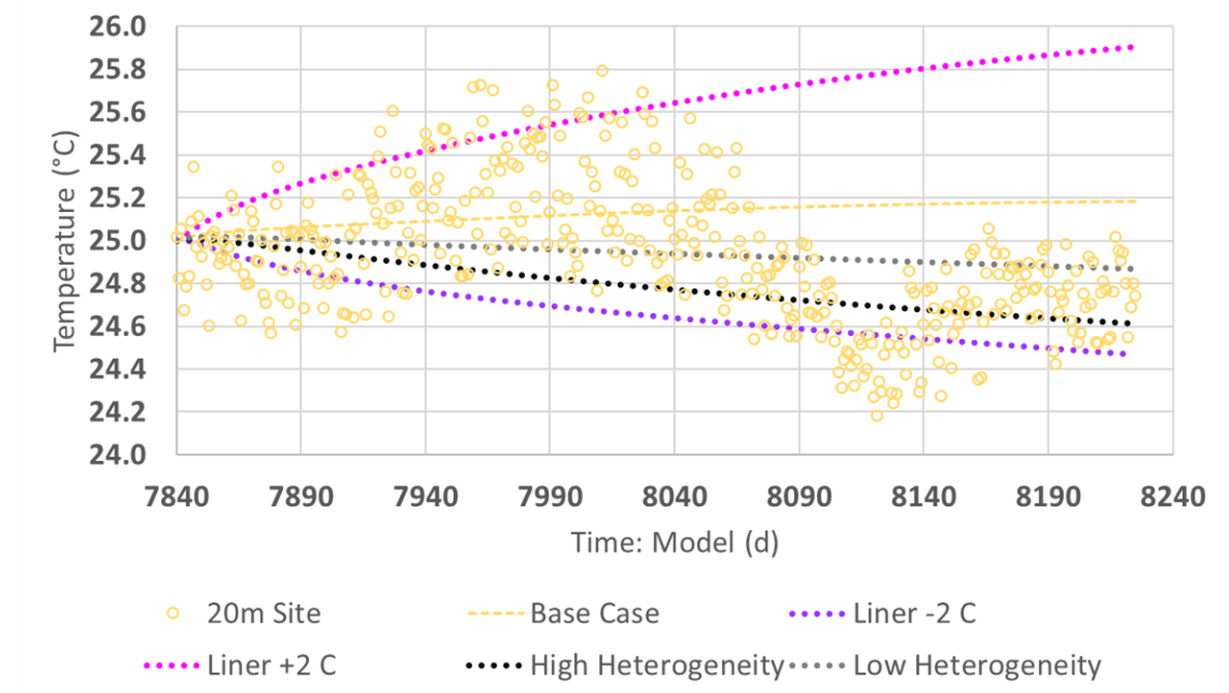

G) 20 m depth

From the transient data comparison in Figures 4.10 and 4.11, it was observed that model deviation from the measured temperature is greater at shallower depths. This is expected as temperatures at the deeper thermistors were more stable over the monitoring period. In the shallow MSW (1, 3,

and 5 m thermistors) the modelled temperatures may deviate from those measured during the monitoring period even if the final modelled temperatures are comparable to the actual. The deep thermistors (10, 15, and 20 m depths) experiencing more stable conditions produced temperature over smaller ranges that may be influenced by the ±0.4 °C error range determined for the instruments in the laboratory. This inherent error could contribute to the variability in temperature data observed at the smaller scales plotted in Figures 4.10 and 4.11 E through G and the trends are therefore considered more reliable than the magnitudes when comparing data to the results of the short-term model and sensitivity analysis.

The sensitivity to each model parameter analyzed differs depending on the location (borehole) and depth. Consistently, the increased liner temperature (+2 °C) produced observably worse model fitment to site data compared to the base case and other parameters in every case. The lower liner temperature (-2 °C) has observably better fitment to site data than the base case for each of the deep thermistors. The method used for extrapolating the liner temperature may have overestimated the temperature at that depth. The different liner thicknesses only affected the shallow 1, 3, and 5 m positions. Radiation adsorbing and emitting properties of the cover material is expected to be a significant factor affecting the shallow MSW temperatures, in combination with the cover thickness and thermal properties (Bonany et al., 2013; Megalla et al., 2016).

4.2.3 Future Model Predictions

The calibrated heat rates from Table 4.5 were used to calculate variable decay rates and BHP_{ULT} values for the future model to assess the different scenarios in which heat could be generated according to Equation 3.4 (first-order decay) and still equal the estimated present-day heat rate values. The calculated HR parameters for the three scenarios described in Section 3.4.4 are listed in Table 4.6. The base case BHP_{ULT} values for each borehole were the average of the high and low diffusivity long-term results (238 MJ/m^3 for BH18-01 and 148 MJ/m^3 for BH18-03). The base case decay rate was $1x10^{-4}$ d^{-1}.

Table 4.6: Future model waste heat generation scenarios

Borehole	**Waste Layer**	**Scenario 1 base case BHP variable *k*** (d^{-1})	**Scenario 2 variable BHP** (MJ/m^3) **base case *k***	**Scenario 3 variable BHP** (MJ/m^3) ***k* = $3x10^{-4}$ d^{-1}**
BH18-01	L1B	$4.4 x10^{-6}$	12	9
	L1T	$3.9 x10^{-6}$	12	6
	L2+L3B	$2.9 x10^{-5}$	71	34
	L3T	$5.6 x10^{-5}$	143	65
	L4	$7.9 x10^{-5}$	185	73
	L5	$6.9 x10^{-5}$	167	61
Thickness Weighted Average:		$3.9 x10^{-5}$	94	40
BH18-03	L1B	$1.4 x10^{-5}$	43	57
	L1T	$1.1 x10^{-5}$	44	59
	L2	$2.8 x10^{-5}$	52	64
	L3	$4.0 x10^{-5}$	102	103
	L4	$1.0 x10^{-4}$	148	137
	L5	$1.0 x10^{-4}$	148	127
	L6	$1.0 x10^{-4}$	148	66
Thickness Weighted Average:		$5.6 x10^{-5}$	98	88

Each scenario in Table 4.6 created a set of HR functions to be applied to the long-term and future model. Each HR scenario was modeled as homogeneous with either high, low, or average diffusivity MSW properties. The transient results until the beginning of the year 2030 were plotted as well as temperature profiles from September 1st, 2019. The transient results of the future model are included in Appendix 5. The year 2030 is arbitrary but represented a decade over which the variable decay heat rate functions could be modelled. The profiles are in Figures 4.12 and 4.13.

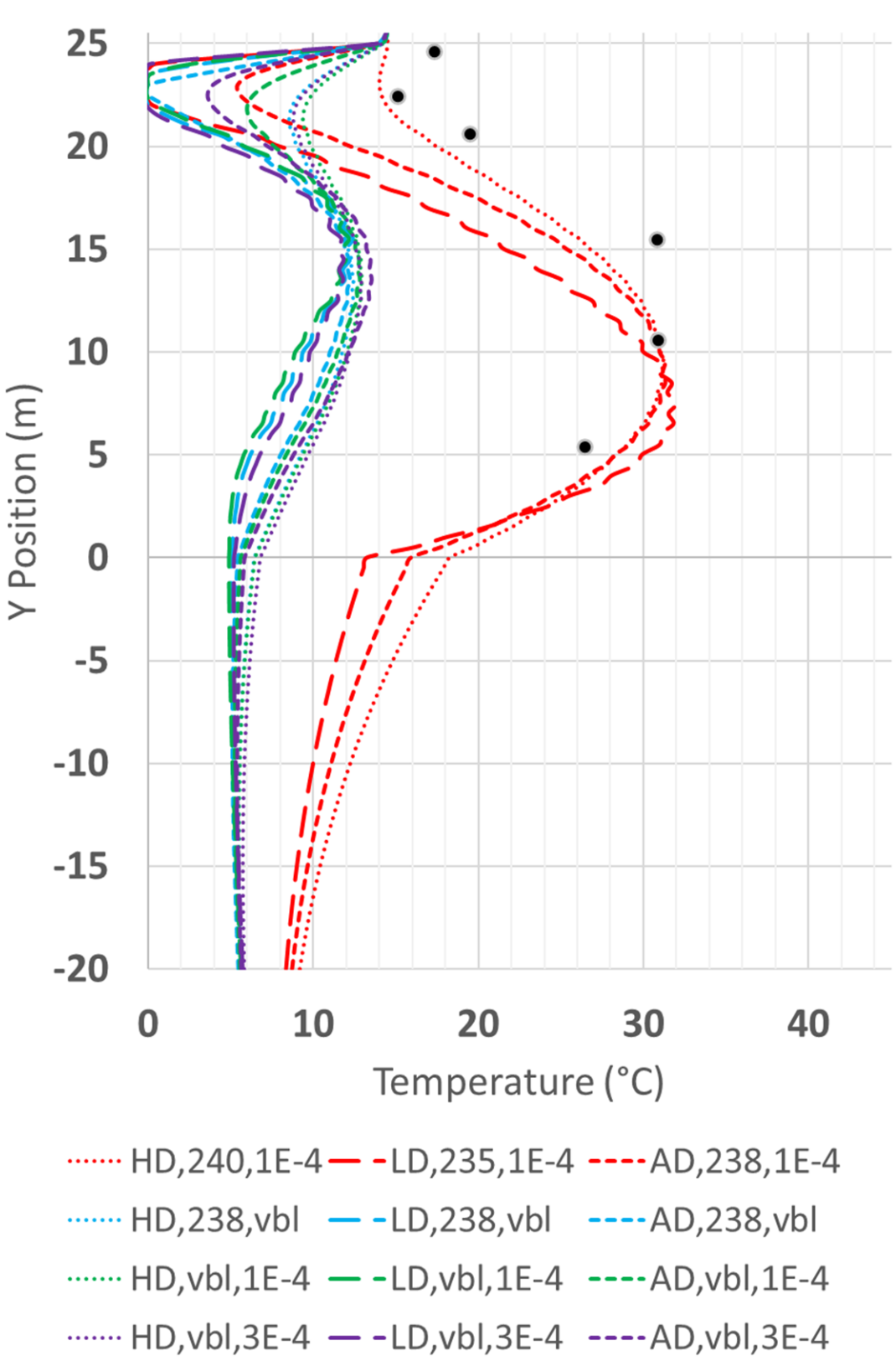

Figure 4.12: Results for different decay and heat potential scenarios in the format (Diffusivity Scenario, BHP_{ULT}, k) for BH18-01 as of 01-Sep-19; **Note:** *if parameter is "vbl" refer to Table 4.6 for layer-specific values*

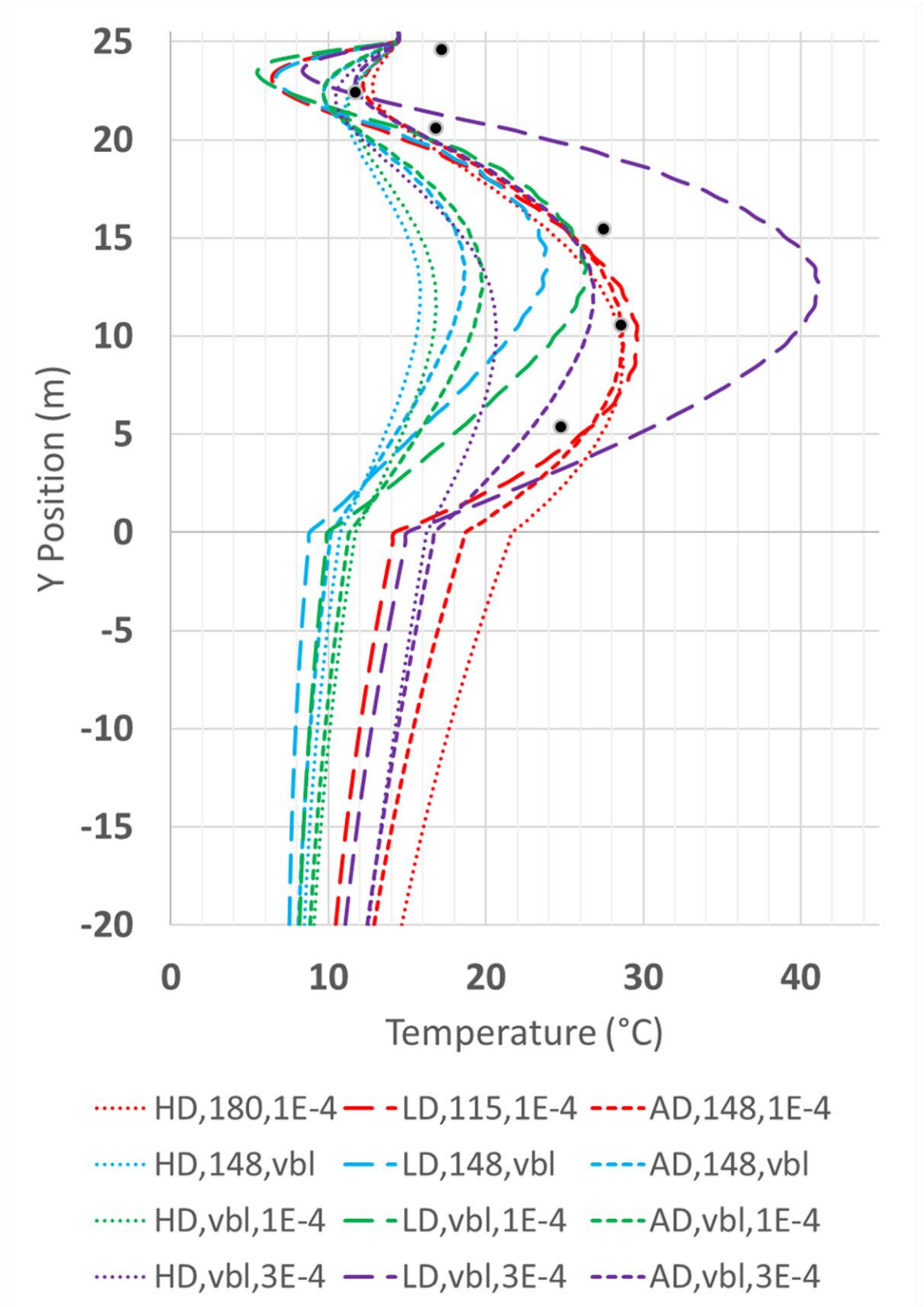

Figure 4.13: Results for different decay and heat potential scenarios in the format (Diffusivity Scenario, BHP_{ULT}, k) for BH18-03 as of 01-Sep-19; **Note:** *if parameter is "vbl" refer to Table 4.6 for layer-specific values*

From Figures 4.12 and 4.13, it was observed that almost all the decay scenarios significantly underestimated the waste temperature at depth at the end of the long-term model period. Only the low diffusivity waste and rapid decay, variable BHP_{ULT} scenario overpredicted the temperatures at mid-depth for BH18-03. The position of the maximum temperature is much shallower for the variable scenarios when compared to the base case of the long-term model. This suggests that variation in either BHP_{ULT} or k applied to 1 m thick waste layers may improve the fitment of the long-term model profile when considering the base case. The constant decay rates do not accurately replicate the variable temperature trends of the waste layers with depth following placement when considering the dependency of microorganism growth to stable, warm temperatures. The long-term model likely overestimated the average decay rate (and thus heat generation rate) in layers exposed to the atmosphere for extended periods of time and underestimated it in layers that maintain temperatures above 20 °C for extended periods. The layer-specific organic contents or BMP would have to be measured if variable heat potentials were to be explored, which would be most accurately evaluated from fresh MSW samples.

Transient 'future' model results are plotted in Appendix E for each thermistor position. The graphs demonstrate that the various combinations of limiting thermal diffusivities, variable heat potentials, and variable decay rates from Table 4.6 result in a broad range of predicted temperatures and trends in 2030 at each depth within the landfill and subgrade. The different scenarios provide insight into the relationship between MSW thermal properties, heat generation, and temperatures simulated by the 1D model over a longer period. This includes that the 1 m depth at both locations demonstrate very similar transient temperature trends regardless of the thermal properties or heat generation rates applied to the MSW material. This exemplifies the significance the transient temperature boundary has on shallow MSW temperatures in the model, and an insensitivity to both thermal properties and heat generation parameters at shallow depths even over long periods of time. Another observation is that the low diffusivity MSW consistently results in higher temperatures being predicted for the end of the future modelling period, when compared to the other diffusivity scenarios with the same heat generation parameters. This occurred at all depths below 1 m and above the liner elevation, which demonstrates both the greater temperature gain in lower diffusivity MSW as well as the reduced affect on subgrade temperatures, as it doesn't transmit as much energy when compared to higher diffusivity MSW.

4.2.4 Discussion of Conduction-Only Model and Significance to Geothermal Energy Potential

The 1D numerical model and derived transient heat generation function resulted in a reasonable prediction of heat potential for MSW based on temperatures measured in the core of the Northern Landfill. However, the conduction-only approach is limited in that forced convection and advection such as leachate and gas flux and diffusion are ignored in the heat transport analysis. A hydraulic and pneumatic model would have to be coupled with heat transport to quantify the amount of energy transported within and out of the landfill system as convective or advective components.

A method of determining if heat transport in the landfill is conduction-dominated may exist with the use of Peclet numbers, a ratio of convection to conduction, which has been applied to solute and heat transport within aquifers. The product of an average seepage velocity over a characteristic length is divided by thermal diffusivity, and the resulting magnitude can be indicative of the relative importance of the conductive and convective components (Domenico & Schwartz, 1998; Anderson, 2005). If the vertical seepage velocity of leachate within the MSW is estimated, measured, or modelled as part of future research, the need to include convection in heat transport models and analyses can be assessed by calculating a Peclet number. Similarly, a value can be calculated for heat transport within the subgrade, where seepage velocities are anticipated to be much lower than in the MSW. A more extensive review of the literature regarding Peclet numbers and heat transport at the landfill scale would have to be conducted to determine the exact implications of the resulting values.

The results of this research are the groundwork for evaluating geothermal energy extraction options at landfills and provides site-specific estimates of waste age and magnitudes of bulk MSW heat potential for the Northern Landfill. Provided the uncertainty that exists in a problem of this scale, the range of thermal properties (K_T, HC), enthalpies of reaction (ΔH), and peak/present-day heat generation rates assessed in this research are reasonable starting points for any future modelling or analyses to be performed using the derived heat generation function. The methods used for this research could be applied to predict temperatures in the core of new or future waste cells, however improvements could be made to improve the accuracy of the results. A comprehensive list of conclusions and recommendations is provided in the next Chapter.

5.0 Conclusion and Recommendations

A vertical 1D thermal model analyzing conduction within the Northern Landfill near Saskatoon, SK was created. The purpose of this model and related research was to assess the applicability and effectiveness of a first-order decay heat generation function at predicting temperatures and heat potential within the waste fill. The function was derived from the equation representing cumulative methane production of MSW in a laboratory setting (BMP). The heat generation and energy potential contained within buried MSW is an important mechanism to understand for assessing low-grade geothermal energy extraction or temperature optimization within landfills, especially in parts of Canada where cold and semi-arid climates can affect rates of microorganism activity.

The conduction-only modelling technique was optimal for reducing the number of required material parameters and for initial assessment of landfill temperature progression and heat generation, however no unique solution existed for either model. The resulting estimate of heat potential included energy introduced to the MSW by anaerobic digestion of cellulose as well as any other means such as incoming solar radiation, aerobic digestion, and oxidation reactions as examples. The first-order decay equation applied to the model was able to predict the measured landfill temperatures at mid-depth over the lifespan of two different waste cells. A sensitivity analysis of each model explored the affects of various parameters on modelled temperature outputs.

The literature relevant to anaerobic gas and heat generation in MSW, its material properties, and thermal numerical models created by various authors was reviewed in Chapter 2. The methods of measuring in-situ temperatures within completed cells at the Northern Landfill was described in Chapter 3. A reasonable estimate of the landfilling sequence and thus the age and thickness of layers at the instrumented locations was presented in Chapter 3 along with the derived heat generation function and boundary conditions applied to the numerical model. In Chapter 4, the modelled waste temperatures as they varied with different MSW thermal properties, decay rates, and energy potentials were graphed and compared to temperatures measured at the Northern Landfill. My recommendations for future work and improvements to the presented thermal model are listed in this Chapter.

5.1 Conclusions of First-Order Decay Thermal Model

The following are the conclusions and recommendations resulting from this research:

- A single decay rate, representing the average over the lifespan of the MSW, is inadequate for predicting the present-day heat generation rates and the effects that cold, dry climate has on microorganism activity responsible for anaerobic heat production.
    - Equation 3.4 requires modification to have the decay rate term (k) be a function of temperature and water content, bounded by threshold conditions that promote mesophilic microbial growth and reaches a maximum decay rate such as that measured in a BMP laboratory setting that is optimal for methanogenesis.
- It is recommended that a model capable of iterating k at each timestep and node based on the temperature of the surrounding elements be developed which would more accurately simulate the in-situ transient gas and heat generation over long periods of time.
    - This would more realistically model the slower growth and delayed anaerobic activity expected within frozen or cold, dry wastes placed in such climates.
    - It would have to be explored as to whether the cumulative energy of a curve such as this would eventually equate to the value of BHP_{ULT} applied to the equation.
- The estimated range of values for BHP_{ULT} in this thesis can be repeatedly improved upon and compared to the results of future models and the results of BMP tests being performed on the MSW samples from the Northern Landfill.
    - As the estimate of heat potential is improved, future models can be used to calibrate other unknown parameters such as the thermal properties of the MSW or the age of waste at depth.
    - Field or laboratory tests capable of measuring the thermal properties of the in-situ MSW would improve the estimated BHP_{ULT} range after calibrating the updated model.

5.2 Recommendations for Future Models and Predicting Heat Potential

In addition to the inclusion of a temperature and moisture-dependent decay rate in Equation 3.4 to calculate heat rates, the following items are recommended to improve heat transport models in a landfill environment:

- It is recommended that temperature instrumentation be installed between or within waste lifts as they are placed in new or young cells and a model created to continuously compare with the measured conditions.
    - This would eliminate the need to estimate waste age, placement temperatures, and lift thickness and provide valuable insight into the thawing timeframe of frozen MSW and initial rates of temperature increase and heat generation.
    - The data could be used to produce a refined numerical model for young and future cells which could be utilized to better assess the potential for geothermal energy extraction at the Northern Landfill or comparable sites.
    - It is recommended that operators interested in geothermal energy recovery at landfills document waste placement locations and lift thicknesses on a regular basis. The smaller the timeframe (daily documentation) the more accurate the inputs for modelling heat generation and transport. At a minimum, annual documentation of waste placement is recommended and would provide a similar scale of inputs as the model in this thesis while removing the error in the estimation techniques. This could be achieved through routine topographic surveys for example, however settlement in areas where new lifts were placed would still have to be predicted.
- A coupled thermal, mechanical, hydraulic, and pneumatic model should be constructed that simulates the other mechanisms known to influence heat transport and relevant material properties.
    - These mechanisms include leachate flow and gas migration (convection) and consolidation of the void space within the waste mass with time and degradation (primary and secondary consolidation).
- A 3D model of the landfill or cell geometry should be created because waste layers are finite in extent (10s of metres) and are placed at different rates, meaning the upper surface geometry and side slopes are transient in nature.
    - The landfill environment is not accurately represented by a 1D, 2D, or axisymmetric model if heat transport occurs in the direction of the side slopes or neighbouring waste layers placed at, or achieving, different temperatures and densities.

- It is recommended that future modelling incorporate radiation absorbing and emitting properties of the intermediate cover and MSW materials to more accurately simulate the energy budget in the shallow MSW.
    - An improved upper boundary surface would allow for short-term models to be used to narrow the range of potential thermal properties for the shallow MSW.

The 1D conduction-only model constructed in this thesis can evidently be improved by reducing the number of assumed inputs, applying a temperature and moisture-dependent decay rate to the anaerobic heat generation function, and by coupling heat transport with transient hydraulic and mechanical components. As well, a range of values for thermal conductivity, heat capacity, and enthalpy of reaction were used to estimate the heat potential, BMP, and organic content of the MSW. Specific measured values or a narrower range would further improve the model and prediction of BHP_{ULT}.

Though no unique solution exists, the methods outlined in this thesis can be applied and tailored to any landfill if temperatures within the core of the waste mass (>20 m from the side slopes) are of interest. As a starting point, selecting an average decay rate *k* for use in Equation 3.4 is a tool that can be used to account for conditions that slow or delay anaerobic digestion when modelling heat generation. The transient heat rate curves can be calculated using the BHP_{ULT} values in Table 4.3, bounded by the maximum and minimum magnitudes reported. The conduction-only approach was the simplest applicable method and temperatures with depth almost 22 years after the estimated initiation of landfilling were predicted with reasonable accuracy using a transient heat generation function derived from gas generation and enthalpy of methanogenesis theory.

LIST OF REFERENCES

Abu-hamdeh, Nidal H. 2003. “Thermal Properties of Soils as Affected by Density and Water Content.” *Biosystems Engineering* 86(1):97–102.

Anderson, M. 2005. "Heat as a Ground Water Tracer". Ground Water, 43(6), 951-968.

Bonany, James E., Paul J. Van Geel, H. Burak Gunay, and O. Burkan Isgor. 2013. “Heat Budget for a Waste Lift Placed under Freezing Conditions at a Landfill Operated in a Northern Climate.” *Waste Management* 33(5):1215–28.

Coccia, Charles J. R., Ranjiv Gupta, Jeremy Morris, and John S. McCartney. 2013. “Municipal Solid Waste Landfills as Geothermal Heat Sources.” *Renewable and Sustainable Energy Reviews* 19:463–74.

El-Fadel, M., A. N. Findikakis, and J. O. Leckie. 1996a. “Temperature Effects in Modeling Solid Waste Biodegradation.” *Environmental Technology (United Kingdom)* 17(9):915–35.

El-Fadel, M, A. N. Findikakis, and J. O. Leckie. 1996b. “Transport of Gas and Heat in Landfills I: Model Formulation.” *Waste Management & Research* 14:483–504.

El-Fadel, A. N., N. Findikakis, and J. O. Leckie. 1996c. “Numerical Modelling of Generation and Transport of Gas and Heat in Sanitary Landfills II. Model Application.” *Waste Management & Research* 14:537–51.

Emmi, Giuseppe, Angelo Zarrella, Anna Zuanetti, and Michele De Carli. 2016. “Use of Municipal Solid Waste Landfill as Heat Source of Heat Pump.” *Energy Procedia* 101(September):352–59.

Faitli, József, Tamás Magyar, Attila Erdélyi, and Attila Murányi. 2015. “Characterization of Thermal Properties of Municipal Solid Waste Landfills.” *Waste Management* 36.

Gregory R.G., and Browell D.M. 2011. “Recent developments in understanding of waste degradation rates and modelling landfill gas generation and recovery.” Proceedings Sardinia 2011, Thirteenth International Waste Management and Landfill Symposium, S. Margherita di Pula, Cagliari, Italy.

Grillo, Robert J. 2014. “Energy Recycling – Landfill Waste Heat Generation and Recovery.” *Current Sustainable/Renewable Energy Reports* 1(4):150–56.

Gunaseelan V.N. 2004. “Biochemical methane potential of fruits and vegetable solid waste feedstocks.” Biomass and Bioenergy, 26: pp. 389-399.

Hamdhan, Indra Noer and Barry G. Clarke. 2010. “Determination of Thermal Conductivity of Coarse and Fine Sand Soils.” *Proceedings World Geothermal Congress 2010* (April):25–29.

Hanson, J. L., T. B. Edil, and N. Yesiller. 2000. “Thermal Properties of High Water Content Materials.” *ASTM STP* 1374:137–51.

Hanson, James L., Wei-Lien Liu, and Nazli Yesiller. 2008. “Analytical and Numerical Methodology for Modeling Temperatures in Landfills.” *GeoCongress* 24–31.

Hanson, James L., Nazli Yesiller, and Nicolas K. Oettle. 2010. “Spatial and Temporal Temperature Distributions in Municipal Solid Waste Landfills.” *Journal of Environmental Engineering* 136(8):804–14.

Hanson, James L., Nazli Yeşiller, Michael T. Onnen, Wei Lien Liu, Nicolas K. Oettle, and Janelle A. Marinos. 2013. “Development of Numerical Model for Predicting Heat Generation and Temperatures in MSW Landfills.” *Waste Management* 33(10):1993–2000.

Hao, Zisu, Mei Sun, Joel Ducoste, and Morton Barlaz. 2017. “A Model to Describe Heat Generation and Accumulation at Municipal Solid Waste Landfills.” *Geotechnical Frontiers* 276:281–88.

Haug, M. D., D. J. L. Forgie, and S. L. Barbour. 1989. “Design of a Hydrodynamic Leachate Containment System.” *Canadian Journal of Civil Engineering* 16(5):615–26.

Ishimori, H., K. Endo, T. Ishigaki, H. Sakanakura, and M. Yamada. 2011. “Coupled Gas Flow and Thermal and Reactive Transport in Porous Media for Simulating Waste Stabilization Phenomena in Semi-Aerobic Landfill.” *Proceedings of the 2011 COMSOL Conference (13 - 15 October 2011)* 7.

Ivanova, Lyudmila K., David J. Richards, and David J. Smallman. 2008. “Assessment of the Anaerobic Biodegradation Potential of MSW.” *Proceedings of Institution of Civil Engineers: Waste and Resource Management* 161(4):167–80.

Jafari, Navid H. and Timothy D. Stark. 2016. “Slope and Settlement Movements of an MSW Landfill during Elevated Temperatures.” Pp. 275–84 in *Geotechnical Special Publication*. Vols. 2016-Janua.

Jafari, Navid H., Timothy D. Stark, and Todd Thalhamer. 2017. “Progression of Elevated Temperatures in Municipal Solid Waste Landfills.” *Journal of Geotechnical and Geoenvironmental Engineering* 143(8):1–16.

Khire, Milind V., Terry Johnson, and Richard Holt. 2020. “Geothermal Modeling of Elevated Temperature Landfills.” *GeoCongress 2020 GSP* 317:612–21.

Krause, Max J., Giles W. Chickering, Timothy G. Townsend, and Debra R. Reinhart. 2016. “Critical Review of the Methane Generation Potential of Municipal Solid Waste.” *Critical Reviews in Environmental Science and Technology* 46(13):1117–82.

Kutsyi, D. V. 2015a. “Numerical Modeling of Landfill Gas and Heat Transport in the Deformable MSW Landfill Body . Part 1 . Development of the Model.” *Thermal Engineering* 62(6):403–7.

Kutsyi, D. V. 2015b. “Numerical Modeling of Landfill Gas and Heat Transport in the Deformable MSW Landfill Body. Part 2. Verification and Application of the Model.” *Thermal Engineering* 62(7):495–502.

De La Cruz, Florentino B. and Morton A. Barlaz. 2010. “Estimation of Waste Component Specific Landfill Decay Rates Using Laboratory-Scale Decomposition Data Supporting Information (SI).” *Environmental Science and Technology* 44(12):4722–28.

Domenico, P.A., and F.W. Schwartz. 1998. "Physical and Chemical Hydrogeology", 2nd ed. New York: John Wiley & Sons Inc.

Macdonald, A. B. and E. Karl Sauer. 1970. “The Engineering Significance of Pleistocene Stratigraphy in the Saskatoon Area , Saskatchewan , Canada.” *Canadian Geotechnical Journal* 7(116).

Mathison, Kevin. 2015. “Alternative Methods for Determining the Biochemical Methane Potential of Municipal Solid Wastes.” University of Saskatchewan.

Megalla, Dina, Paul J. Van Geel, and James T. Doyle. 2016. “Simulating the Heat Budget for Waste as It Is Placed within a Landfill Operating in a Northern Climate.” *Waste Management* 55:108–17.

Nastev, Miroslav, Pierre Gelinas, Rene Therrien, and Rene Lefebvre. 2001. “Gas Production and Migration in Landfills and Geological Materials.” *Journal of Contaminant Hydrology* 52:187–211.

Owen W.F., Stuckey D.C., Healy J.B., Young L.Y., and McCarty P.L. 1979. “Bioassay for monitroing biochemical methane potential and anaerobic toxicity.” Water Research, 13: pp. 485-492.

Raposo F., Fernández-Cegrí V., De la Rubia M.A., Borja R., Béline F., Cavinato C., Demirer G., et al. 2011. “Biochemical methane potential (BMP) of solid organic substrates: Evaluation of anaerobic biodegradability using data from an international interlaboratory study.” Journal of Chemical Technology & Biotechnology, 86 (8): pp. 1088-1098.

Reddy, Krishna R., Girish Kumar, and Rajiv K. Giri. 2017. “Modeling Coupled Processes in Municipal Solid Waste Landfills: An Overview with Key Engineering Challenges.” *International Journal of Geosynthetics and Ground Engineering* 3(1):6.

Reinhart, Debra R., Robert Mackey, Sam Levin, Ryan Joslyn, and Amir Motlagh. 2017. “Field Investigation of an Elevated Temperature Florida Landfill.” *Geotechnical Frontiers* 276:298–301.

Rowe, R. K. 1998. “Geosynthetics and the minimization of contaminant migration through barrier systems beneath solid waste.” Proc., 6th Int. Conf. on Geosynthetics, R. K. Rowe, ed., Vol. I, IFAI, Atlanta, 27–102.

Rowe, R. Kerry, A. Hoor, and A. Pollard. 2010. “Numerical Examination of a Method for Reducing the Temperature of Municipal Solid Waste Landfill Liners.” *Journal of Environmental Engineering* 136(8):794–803.

Shi, Jianyong, Guohui Lei, Jingfeng Zhang, Yazhou Wei, Yu Ping Li, Zhenming Sun, and Yuchen Zhang. 2020. “A Unit-Cell Model for Thermal Regulation of Degradation of Organics in Solid Waste.” *Waste Management and Research* 1–9.

SNC Lavalin. 2020. "2019 Environmental Monitoring - Loraas Landfill". *Northern Landfill Annual Report.*

Yanful, Ernest K., Moir D. Haug, and Lionel C. Wong. 1990. “The Impact of Synthetic Leachate on the Hydraulic Conductivity of a Smectitic till Underlying a Landfill near Saskatoon, Saskatchewan.” *Canadian Geotechnical Journal* 27(4):507–19.

Yeşiller, Nazli, James L. Hanson, and Wei-Lien Liu. 2005. “Heat Generation in Municipal Solid Waste Landfills.” *Journal of Geotechnical and Geoenvironmental Engineering* 131(11):1330–44.

Yeşiller, Nazli, James L. Hanson, and Emma H. Yee. 2015a. “Waste Heat Generation: A Comprehensive Review.” *Waste Management* 42:166–79.

Yesiller, N., J. L. Hanson, K. B. Kopp, and E. H. Yee. 2015b. “Assessing Approaches for Extraction of Heat From MSW Landfills.” *Proceedings Sardinia International WM&LF Symposium* (15th).

Yeşiller, Nazli, James L. Hanson, and Kevin B. Kopp. 2016a. “Design and Installation of a Prototype Heat Extraction System at a Municipal Solid Waste Landfill.” *Geo-Chicago* 271:111–20.

Yeşiller, Nazli, James L. Hanson, Kevin B. Kopp, and Emma H. Yee. 2016b. “Heat Management Strategies for MSW Landfills.” *Waste Management* 56:246–54.

APPENDICES

Appendix A: Thermistor Array Calibration and Installation Data

BH18-01	Water Bath Reading			**Installed**
Thermistor	**5.0 C**	**25.0 C**	**45.0 C**	**Depth (m)**
sfc	4.76	24.72	44.69	
1m	4.94	24.82	44.69	0.91
3m	5.16	25.11	45.12	3.05
5m	5.06	25.11	45.18	4.88
10m	5.20	25.22	45.18	10.06
15m	4.98	24.84	44.76	14.94
20m	4.89	24.75	44.63	20.12
N: 5791896.322, E: 387053.942, Z: 530.354				

BH18-03	Water Bath Reading			**Installed**
Thermistor	**5.0 C**	**25.0 C**	**45.0 C**	**Depth (m)**
sfc	5.02	24.95	44.79	
1m	4.89	24.79	44.62	0.91
3m	4.99	25.01	45.12	3.05
5m	4.92	25.05	45.09	4.88
10m	5.11	25.16	45.28	10.06
15m	4.78	24.76	44.61	14.94
20m	4.81	24.68	44.52	20.12
N: 5791900.473, E: 387355.515, Z: 531.605				

BH19-02A	Water Bath Reading			**Installed**
Thermistor	**5.0 C**	**25.0 C**	**45.0 C**	**Depth (m)**
sfc	2.95	24.56	46.23	
0m	3.25	25.08	46.89	
1m	3.26	24.89	46.49	0.79
3m	3.62	25.16	46.72	2.79
5m	3.52	25.15	46.62	4.79
10m	3.4	25.15	46.82	9.79
15m	3.52	24.86	46.26	14.79
20m	3.07	24.58	46.08	19.79
24m	3.10	24.69	46.27	23.39
N: 5791910.789, E: 387211.844, Z: 530.848				

TH19-02	Water Bath Reading			**Installed**
Thermistor	**5.0 C**	**25.0 C**	**45.0 C**	**Depth (m)**
0m	3.50	25.15	46.89	
1m	3.35	25.08	46.72	0.36
3m	3.19	24.93	46.69	2.36
5m	3.39	25.08	46.79	4.36
10m	3.28	24.81	46.56	9.36
15m	3.16	24.65	46.18	14.36
20m	3.18	24.66	46.12	19.36
24m	3.14	24.69	46.26	23.86
N: 5791907.432, E: 387211.204, Z: 530.691				

TH19-04	Water Bath Reading			**Installed**
Thermistor	**5.0 C**	**25.0 C**	**35.0 C**	**Depth (m)**
1m	4.85	24.90	34.95	0.36
3m	4.98	25.01	35.08	2.36
5m	5.07	25.13	35.13	4.36
10m	5.02	25.09	35.13	9.36
15m	5.02	24.91	34.94	14.36
20m	4.91	24.76	34.78	19.36
24m	4.95	24.86	34.87	23.86
N: 5791946.514, E: 387178.609, Z: 530.456				

Linear correction for BH19-02A: $Y = 0.9258 * T + 1.9173$

Linear correction for TH19-02: $Y = 0.9247 * T + 2.0232$

Where Y is the actual temperature and T is the recorded temperature

Appendix B: Northern Landfill Contour Map and Cross Sections

Included in this appendix are the contour map and associated cross-sections reported to Loraas Disposal in 2015.

The table below lists the tier thicknesses and offsets for developing the 3D landfilling sequence model.

Tier	Thickness (m)	Top Elevation (m ASL)	Exterior Offset (m)	Interior Offset (m)
1	4	509	13.5	9
2	2	511	1	22.5
3	3	514	11	33.5
4	3	517	24.5	47
5	3	520	38	60.5
6	3	523	51.5	74
7	3	526	65	87.5
8	4	530	81	103.5

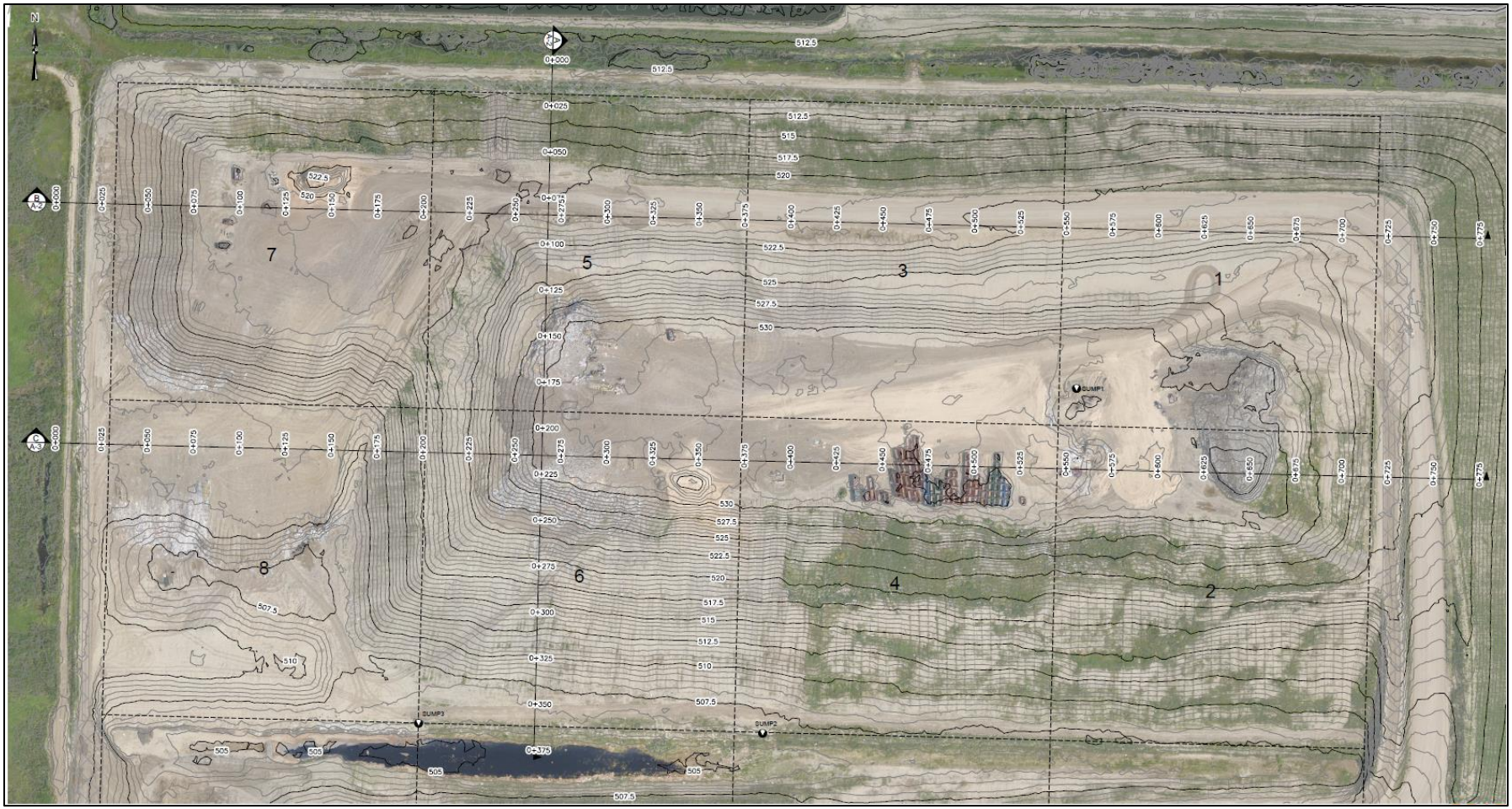
N
0+000
0+025
0+050
0+075
0+100
0+125
0+150
0+175
0+200
0+225
0+250
0+275
0+300
0+325
0+350
0+375
0+400
0+425
0+450
0+475
0+500
0+525
0+550
0+575
0+600
0+625
0+650
0+675
0+700
0+725
0+750
0+775
512.5
515
517.5
520
522.5
525
527.5
530
510
507.5
505
522.5
SUMP1
SUMP2
SUMP3
1
2
3
4
5
6
7
8

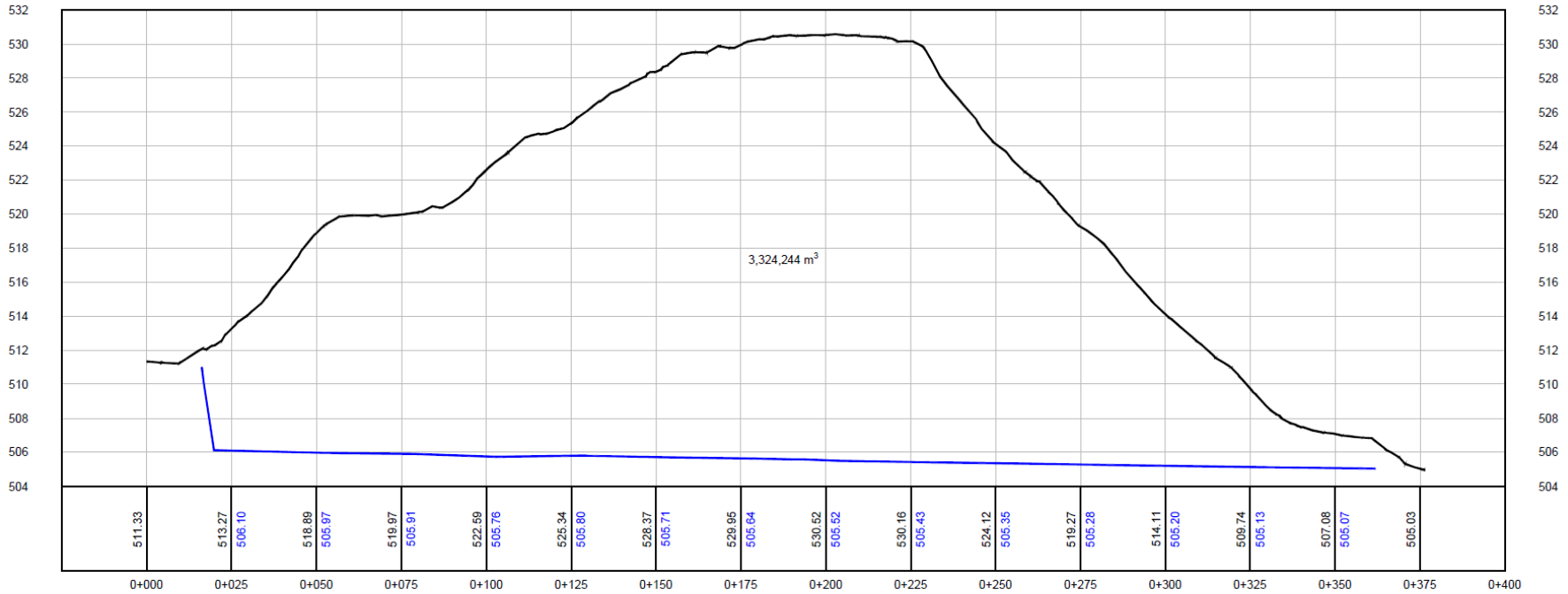

NORTH-SOUTH CROSS-SECTION
SCALE: H 1:1,000 V 1:200

A
A-1

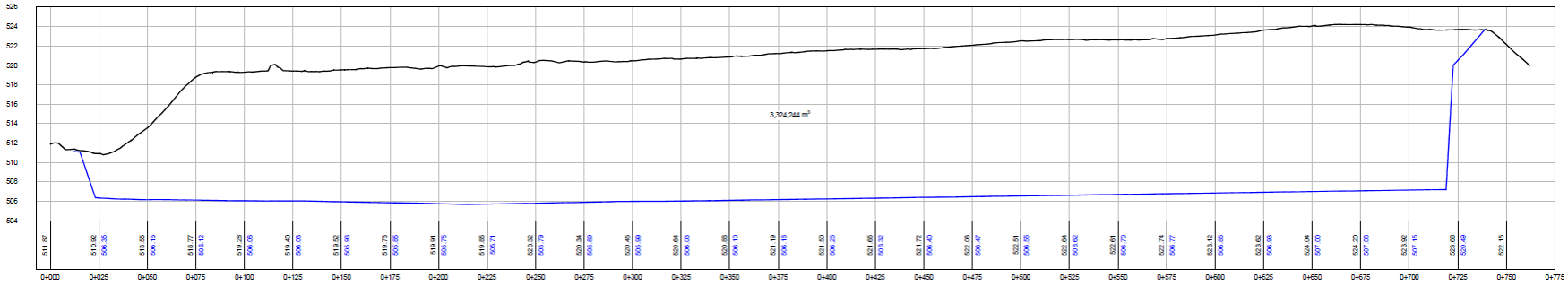

WEST-EAST CROSS-SECTION
SCALE: H 1:1,000 V 1:200
B
A-1

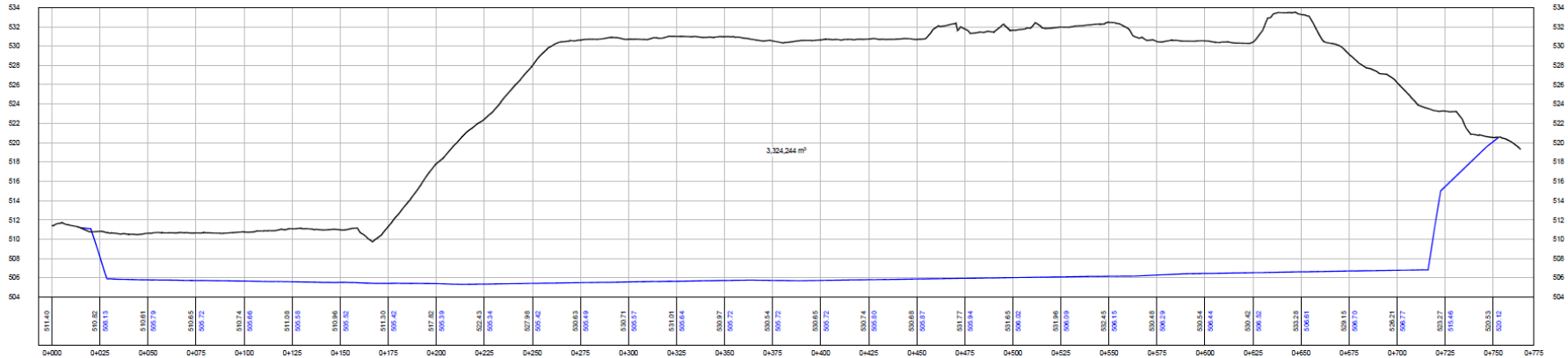

WEST-EAST CROSS-SECTION
SCALE: H 1:1,000 V 1:200
C
A-1

Appendix C: Recovered MSW Core Densities and Water Contents

BH18-01

Sample	Wet weight (kg)	Dry Weight (kg)	Length (m)	Dry Density (kg/m3)	VWC (m3/m3)
1A	13.90	12.38	3.05	1378	0.24
1B	17.93	14.74			
2A	9.53	7.94	3.05	791	0.15
2B	9.17	7.76			
3A	8.05	6.65	3.05	735	0.18
3B	9.97	7.96			
4A	6.57	4.75	3.05	1072	0.3
4B	20.50	16.43			
5A	9.60	8.69	3.05	1027	0.14
5B	3.80	3.08			
5C	9.83	8.69			
6A	12.96	10.61	3.05	1297	0.27
6B	5.86	5.14			
6C	12.18	9.96			
7A	14.75	12.59	3.05	1242	0.2
7B	7.23	6.24			
7C	3.56	3.16			
7D	3.09	2.82			
8A	3.85	2.57	3.05	976	0.29
8B	14.21	11.38			
8C	6.95	5.51			
9A	14.13	10.78	1.98	840	0.26
Sum:	217.62	176.31	26.38		
	Thickness-weighted average			**1048**	**0.22**

BH18-02

Sample	Wet weight (kg)	Dry Weight (kg)	Length (m)	Dry Density (kg/m3)	VWC (m3/m3)
1A	22.74	19.84	3.05	1489	0.20
1B	10.50	9.44			
2A	8.02	6.50	3.05	1093	0.23
2B	14.99	12.76			
2C	3.23	2.48			
3A	13.00	11.11	3.05	790	0.28
3B	8.19	4.58			
4A	12.87	10.76	3.05	1002	0.24
4B	12.54	9.06			
5A	11.57	7.14	3.05	1230	0.37
5B	14.34	11.57			
5C	6.73	5.69			
6A	5.90	4.52	1.52	448	0.14
7A	6.18	5.16	1.83	428	0.09
8A	10.37	7.15	2.74	941	0.41
8B	13.59	9.65			
9A	9.03	6.73	3.35	1237	0.51
9B	16.52	11.90			
9C	12.31	8.32			
Sum:	212.62	164.36	24.69		
	Thickness-weighted average			1024	0.29

BH18-03

Sample	Wet weight (kg)	Dry Weight (kg)	Length (m)	Dry Density (kg/m3)	VWC (m3/m3)
1A	12.07	10.21	3.05	1060	0.19
1B	12.60	10.73			
2A	17.38	14.31	3.05	1042	0.23
2B	5.52	4.56			
2C	2.24	1.88			
3A	17.97	15.12	3.05	1037	0.21
3B	7.07	5.81			
4A	11.92	11.27	1.83	1209	0.12
4B	4.17	3.37			
5A	19.79	17.69	2.74	1121	0.19
5B	3.56	2.26			
6A	3.63	2.5	3.05	529	0.19
6B	10.66	8.12			
7A	5.71	-	-	-	-
7B	1.25	0.87			
8A	8.20	7.63	2.44	480	0.04
9A	16.57	13.98	3.05	1002	0.23
9B	7.65	5.67			
Sum:	167.96	135.98	22.26		
	Thickness-weighted average			930	0.18

Dated Objects and Approximate Depths in Phase 1 Boreholes

Borehole	Sample	Position in core	Approximate Depth (m)	Date	Item
BH18-01	2B	N/A so mid	3.7	Mar 2016	coupon expiry
	3B	N/A so mid	6.7	2010	bag with copyright
	6A	mid	17.7	2009	trademark on food product
BH18-02	2C	mid	3.7	2011	coke bottle celebrating 125yr anniversary
	3B	top	6.1	2010	newspaper publish date
	3B	top	6.2	May 2011	newspaper publish date
	3A	bot	12.2	2009	chip bag with copyright

Appendix D: Groundwater Piezometer Data and Locations

Piezometer Information (SNC 2020 Report)				
Piezometer	**Location Description**	**Ground Elevation (mASL)**	**Screen Top (mBGS)**	**Screen Bot (mBGS)**
637579-01	W side of site, SW of Cell 15	511.1	3.4	4.9
637579-02	E side of site, SE of Cell 2	509.6	3.4	4.9
637580-01	S side of site, E of site shop/scale	509.4	3.9	5.4
MDH-00-01	NE corner of site	510.6	4	4.7
MDH-00-02	N side of site, NW corner of Cell 3	510.8	3.8	4.5
MDH-00-03	S side of site, SE of surface pond	509.3	4.5	5.2
PI 2011	N side of site, NE corner of Cell 3	510.8	6.1	7.0
TH 103	SW corner of site, by gate	509.4	29.8	33.3
TH 104	NW corner of site	511.4	27	33.5
TH 201	SW corner of site, by gate	509.3	18.4	19.5
TH 202	SW corner of site, by gate	509.4	18.4	19.5
TH 203	NW corner of site	510.9	6.9	9.4
TH 205	S side of site, SE of surface pond	509.3	3.1	10.7

far from landfill mound
moderate distance from lf
close to landfill mound

Piezometer Locations:

Subgrade simulation results demonstrating similarity in the subgrade temperature profile between the four seasons in 1996 and 2005. All available piezometer data is included on the plot for reference.

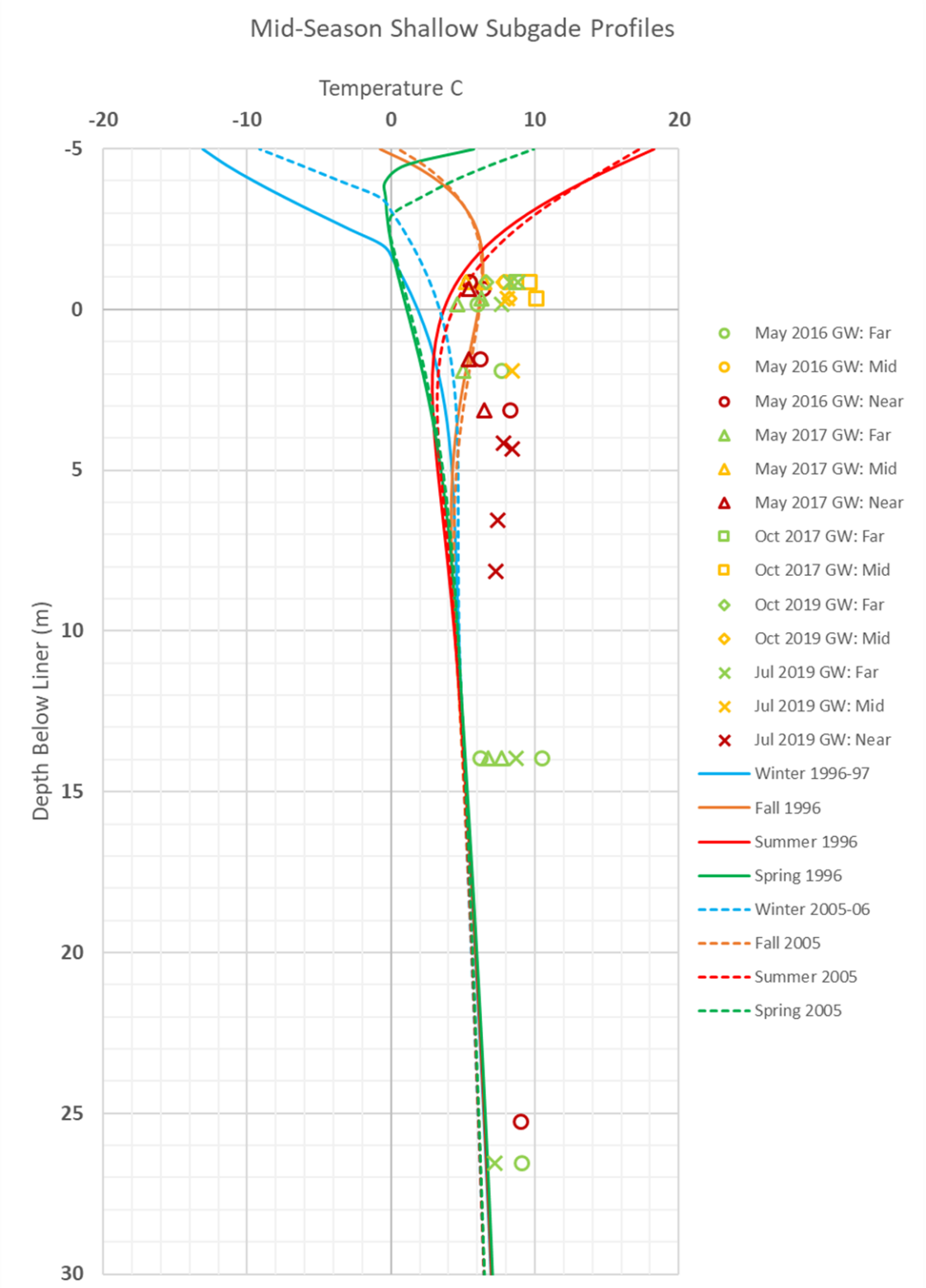

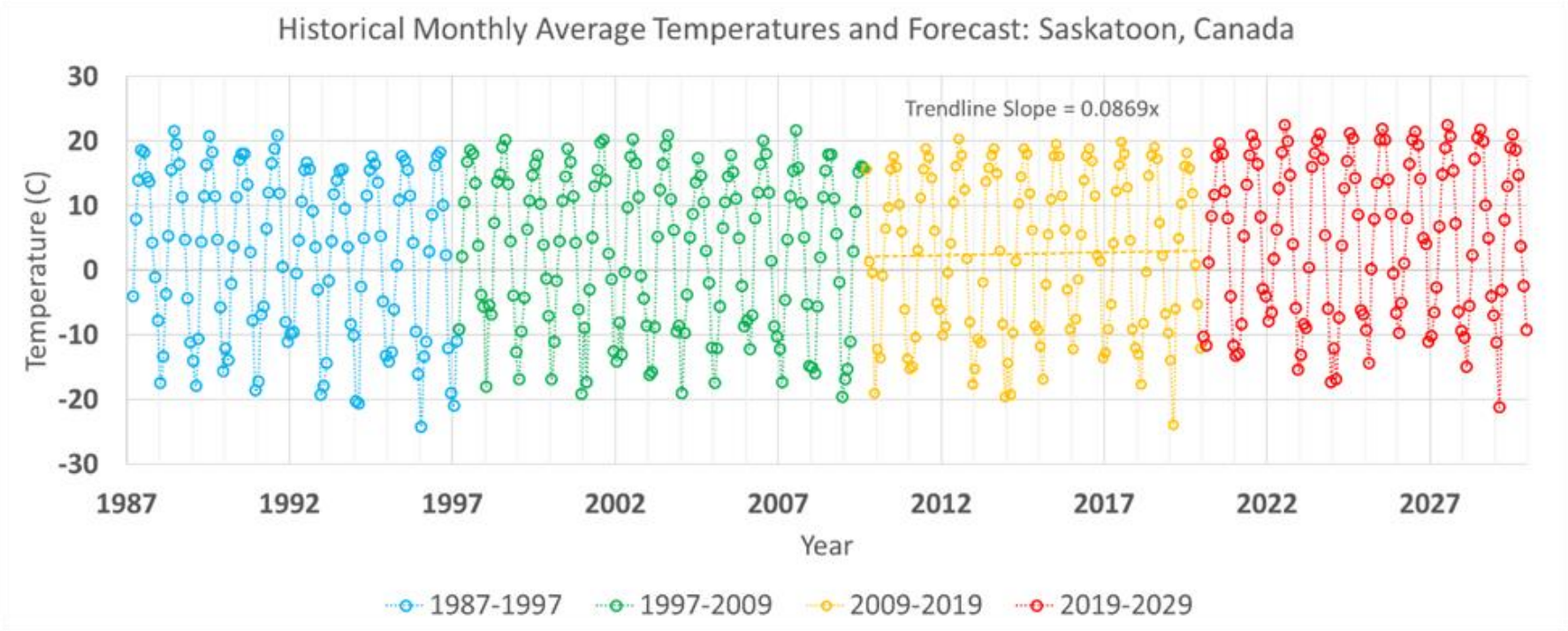
Historical Monthly Average Temperatures and Forecast: Saskatoon, Canada
Trendline Slope = 0.0869x
Temperature (C)
30
20
10
0
-10
-20
-30
1987
1992
1997
2002
2007
2012
2017
2022
2027
Year
1987-1997
1997-2009
2009-2019
2019-2029

Appendix E: Transient Results of the Future Model

Below are the transient results at the various thermistor depths for the future model. The vertical black line represents the time of the end of the long-term model (1st September, 2019) and the black circle is the monthly average temperature measured at the respective thermistor. Temperature profiles were plotted at the time of the black line for comparison to the original long-term model.

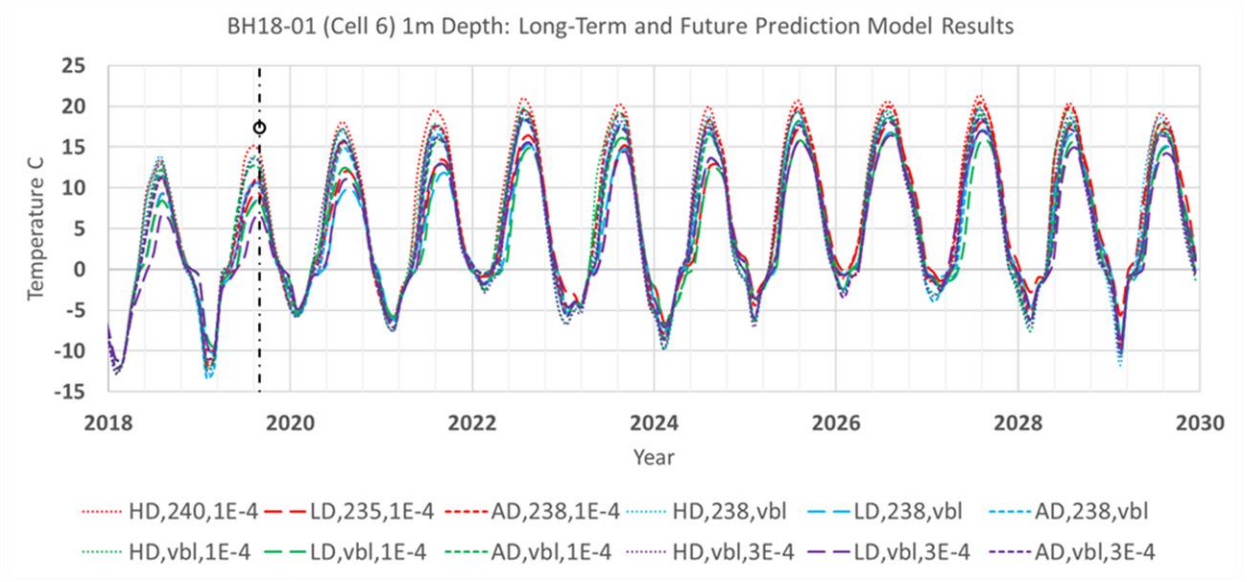

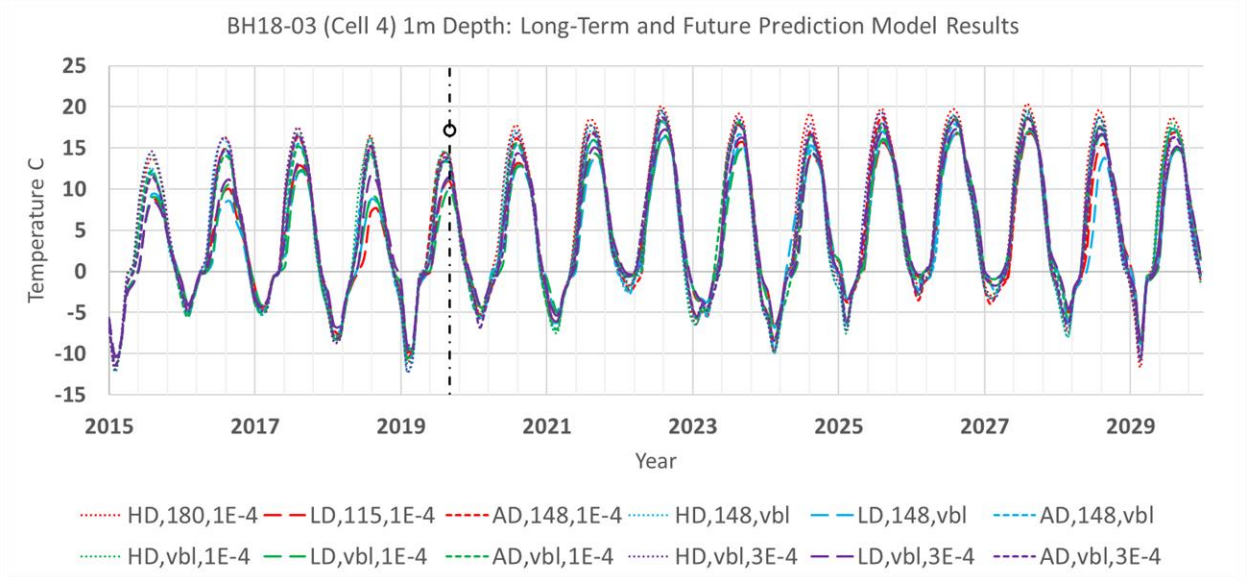

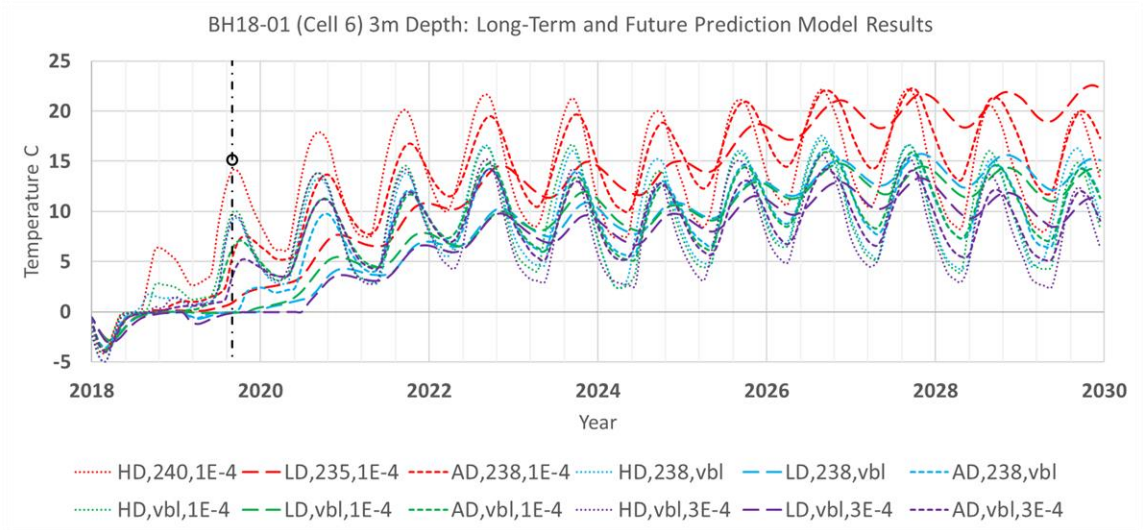
BH18-01 (Cell 6) 3m Depth: Long-Term and Future Prediction Model Results
Temperature C
25
20
15
10
5
0
-5
2018
2020
2022
2024
2026
2028
2030
Year
HD,240,1E-4
LD,235,1E-4
AD,238,1E-4
HD,238,vbl
LD,238,vbl
AD,238,vbl
HD,vbl,1E-4
LD,vbl,1E-4
AD,vbl,1E-4
HD,vbl,3E-4
LD,vbl,3E-4
AD,vbl,3E-4

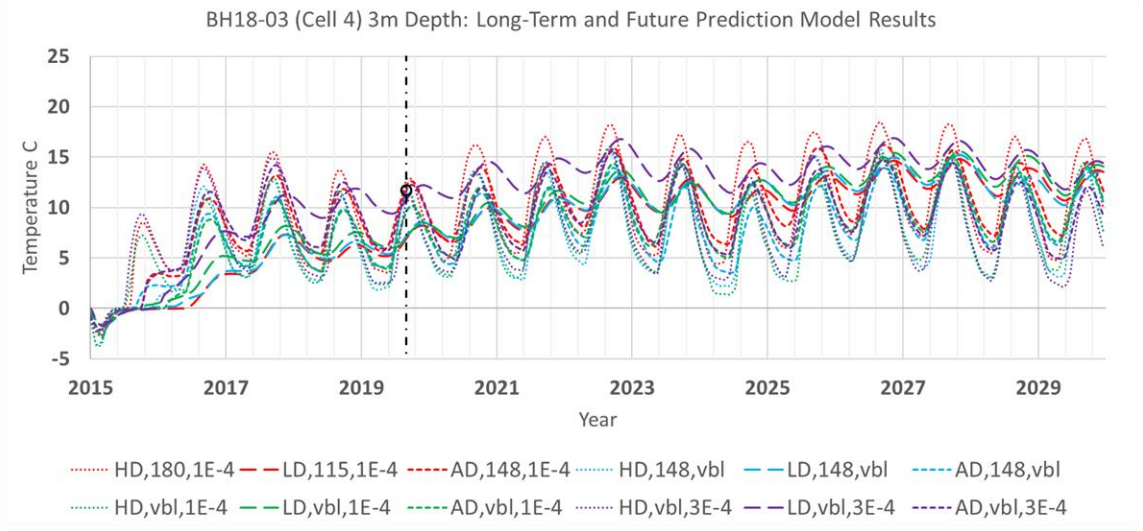
BH18-03 (Cell 4) 3m Depth: Long-Term and Future Prediction Model Results
Temperature C
25
20
15
10
5
0
-5
2015
2017
2019
2021
2023
2025
2027
2029
Year
HD,180,1E-4
LD,115,1E-4
AD,148,1E-4
HD,148,vbl
LD,148,vbl
AD,148,vbl
HD,vbl,1E-4
LD,vbl,1E-4
AD,vbl,1E-4
HD,vbl,3E-4
LD,vbl,3E-4
AD,vbl,3E-4

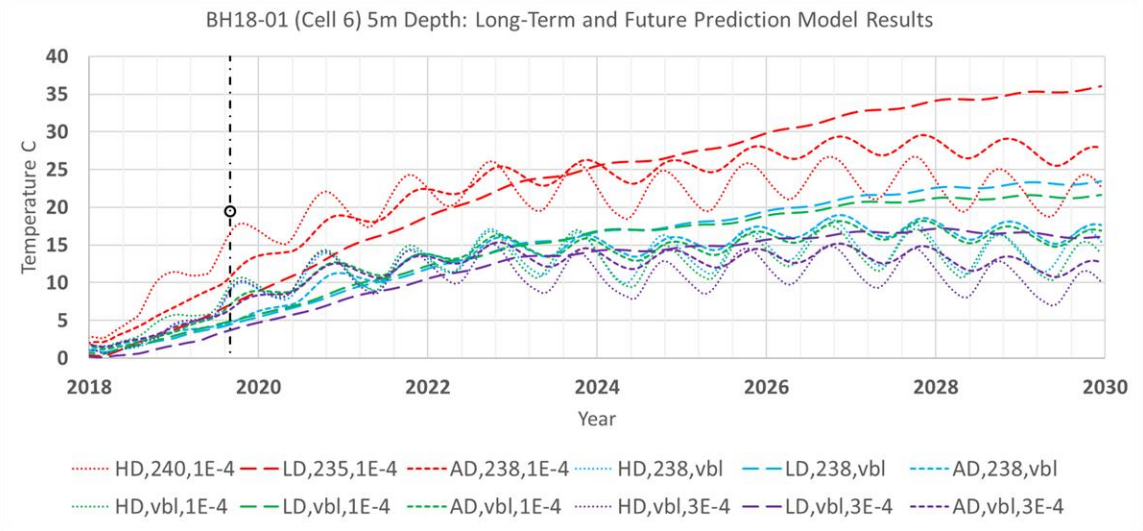
BH18-01 (Cell 6) 5m Depth: Long-Term and Future Prediction Model Results
Temperature C
40
35
30
25
20
15
10
5
0
2018
2020
2022
2024
2026
2028
2030
Year
HD,240,1E-4
LD,235,1E-4
AD,238,1E-4
HD,238,vbl
LD,238,vbl
AD,238,vbl
HD,vbl,1E-4
LD,vbl,1E-4
AD,vbl,1E-4
HD,vbl,3E-4
LD,vbl,3E-4
AD,vbl,3E-4

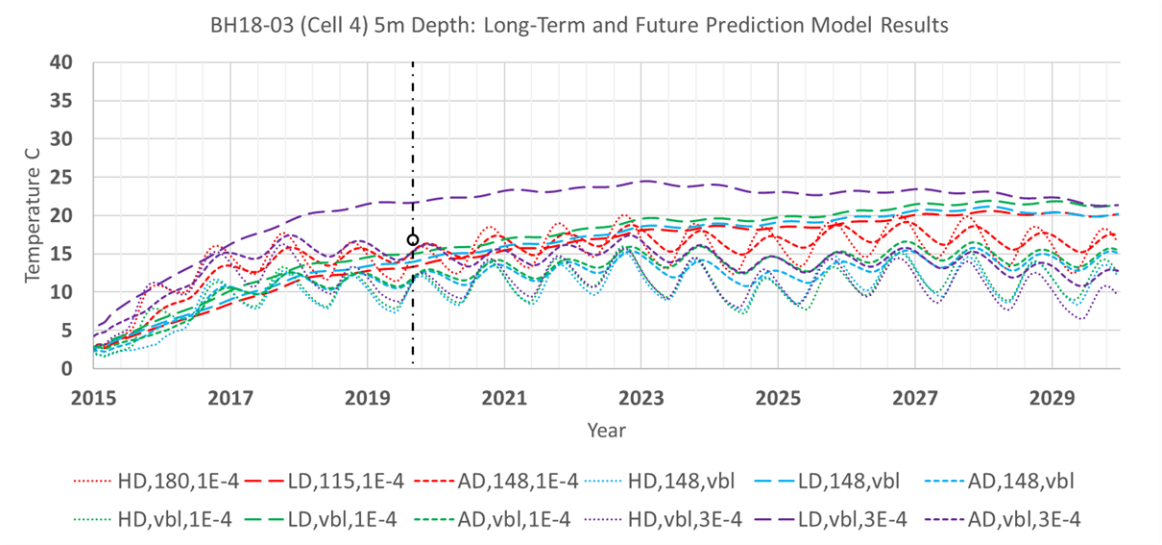
BH18-03 (Cell 4) 5m Depth: Long-Term and Future Prediction Model Results
Temperature C
Year
HD,180,1E-4
LD,115,1E-4
AD,148,1E-4
HD,148,vbl
LD,148,vbl
AD,148,vbl
HD,vbl,1E-4
LD,vbl,1E-4
AD,vbl,1E-4
HD,vbl,3E-4
LD,vbl,3E-4
AD,vbl,3E-4

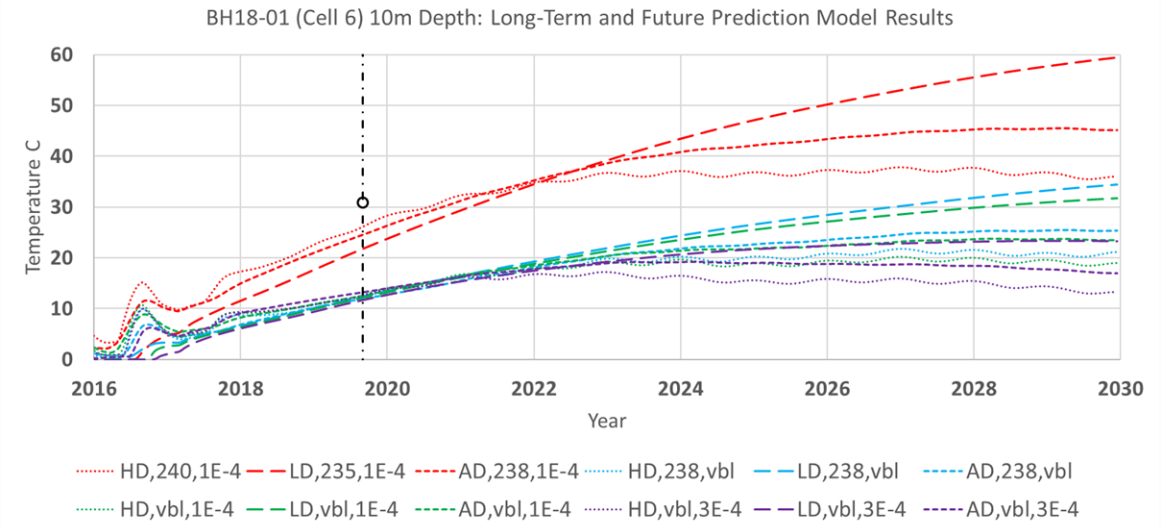
BH18-01 (Cell 6) 10m Depth: Long-Term and Future Prediction Model Results
Temperature C
Year
HD,240,1E-4
LD,235,1E-4
AD,238,1E-4
HD,238,vbl
LD,238,vbl
AD,238,vbl
HD,vbl,1E-4
LD,vbl,1E-4
AD,vbl,1E-4
HD,vbl,3E-4
LD,vbl,3E-4
AD,vbl,3E-4

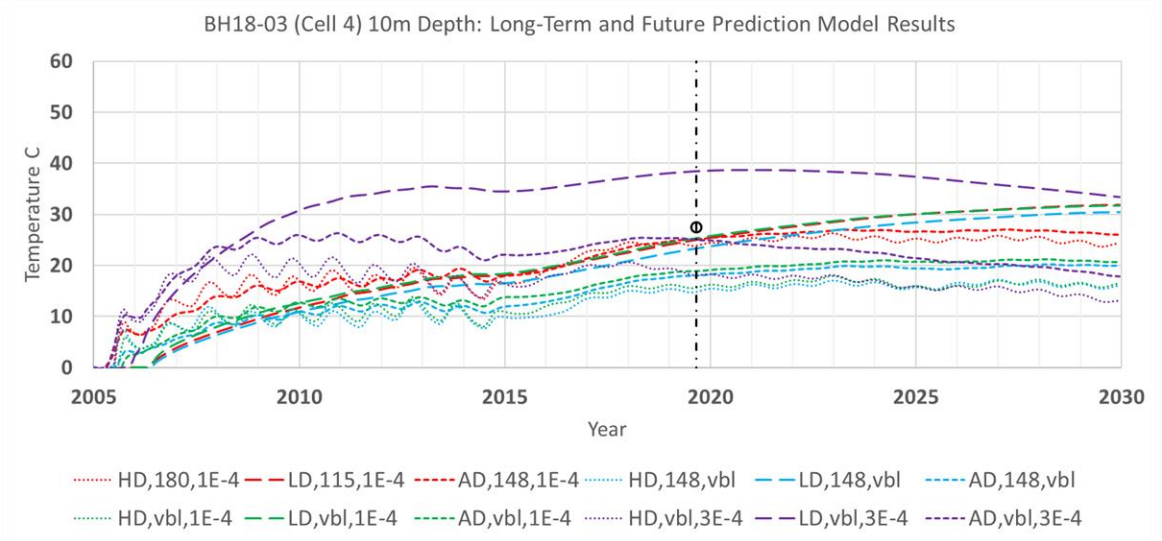
BH18-03 (Cell 4) 10m Depth: Long-Term and Future Prediction Model Results
Temperature C
Year
HD,180,1E-4
LD,115,1E-4
AD,148,1E-4
HD,148,vbl
LD,148,vbl
AD,148,vbl
HD,vbl,1E-4
LD,vbl,1E-4
AD,vbl,1E-4
HD,vbl,3E-4
LD,vbl,3E-4
AD,vbl,3E-4

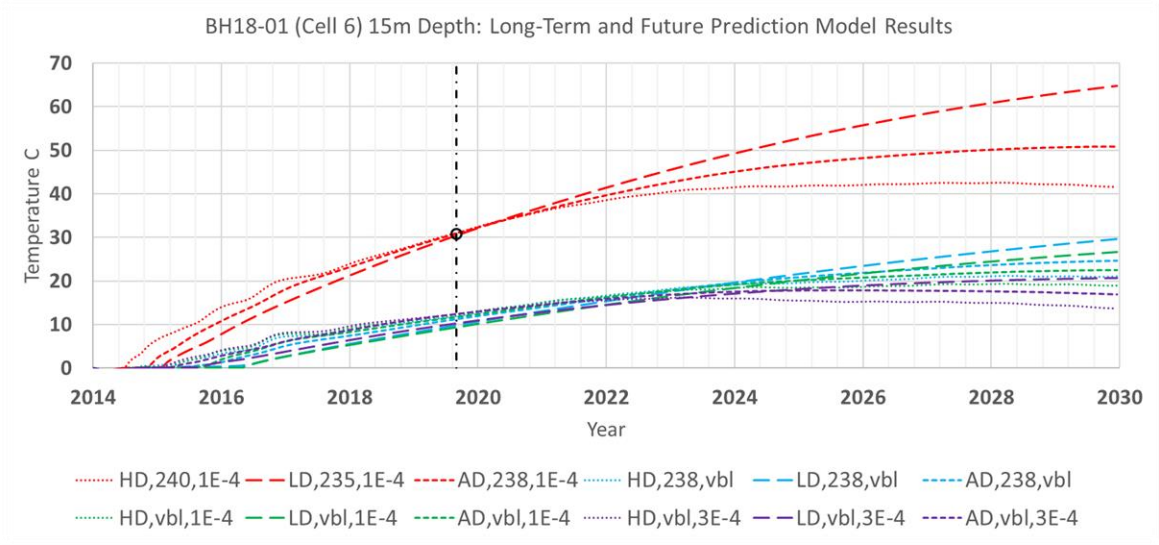
BH18-01 (Cell 6) 15m Depth: Long-Term and Future Prediction Model Results
Temperature C
Year
HD,240,1E-4
LD,235,1E-4
AD,238,1E-4
HD,238,vbl
LD,238,vbl
AD,238,vbl
HD,vbl,1E-4
LD,vbl,1E-4
AD,vbl,1E-4
HD,vbl,3E-4
LD,vbl,3E-4
AD,vbl,3E-4

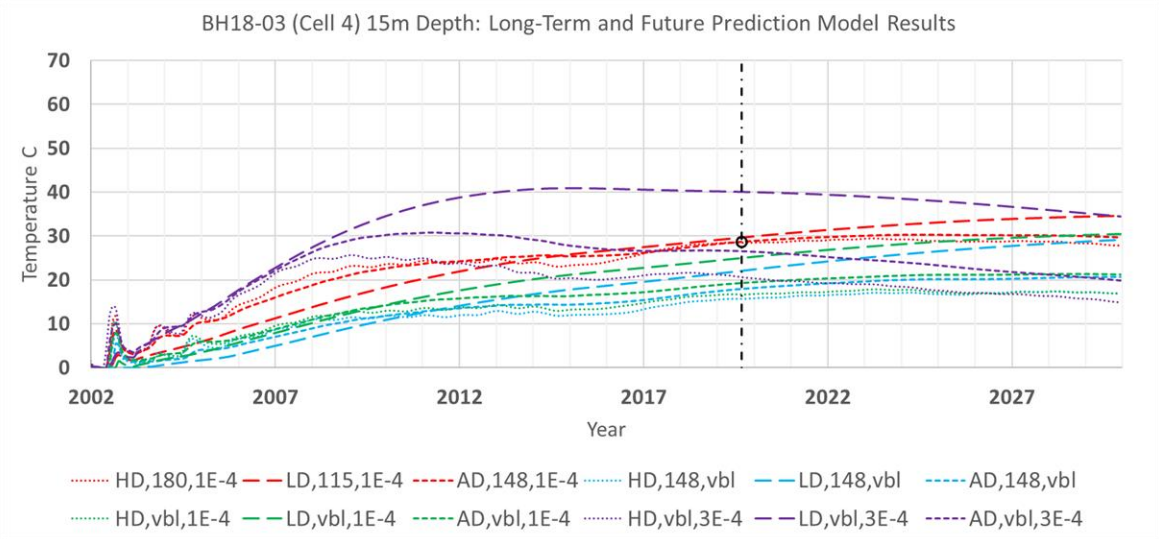
BH18-03 (Cell 4) 15m Depth: Long-Term and Future Prediction Model Results
Temperature C
Year
HD,180,1E-4
LD,115,1E-4
AD,148,1E-4
HD,148,vbl
LD,148,vbl
AD,148,vbl
HD,vbl,1E-4
LD,vbl,1E-4
AD,vbl,1E-4
HD,vbl,3E-4
LD,vbl,3E-4
AD,vbl,3E-4

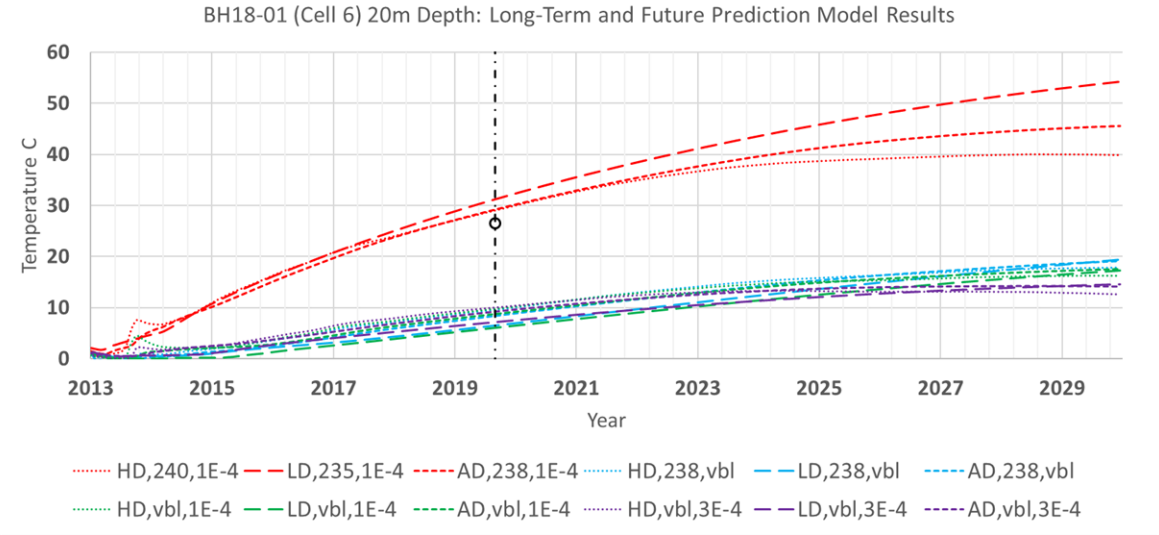
BH18-01 (Cell 6) 20m Depth: Long-Term and Future Prediction Model Results
Temperature C
Year
HD,240,1E-4
LD,235,1E-4
AD,238,1E-4
HD,238,vbl
LD,238,vbl
AD,238,vbl
HD,vbl,1E-4
LD,vbl,1E-4
AD,vbl,1E-4
HD,vbl,3E-4
LD,vbl,3E-4
AD,vbl,3E-4

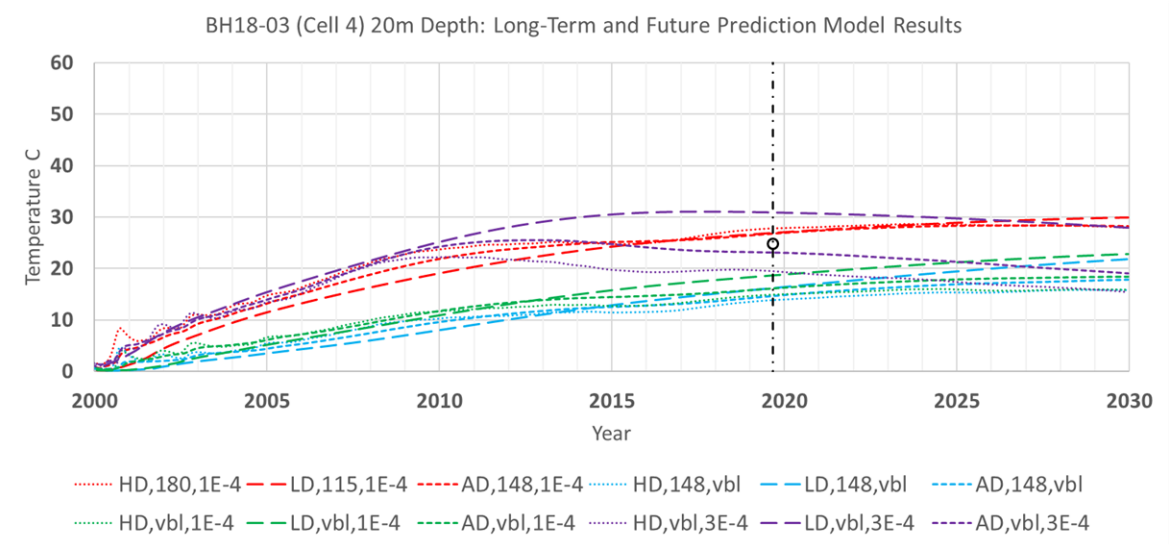
BH18-03 (Cell 4) 20m Depth: Long-Term and Future Prediction Model Results
Temperature C
60
50
40
30
20
10
0
2000
2005
2010
2015
2020
2025
2030
Year
HD,180,1E-4
LD,115,1E-4
AD,148,1E-4
HD,148,vbl
LD,148,vbl
AD,148,vbl
HD,vbl,1E-4
LD,vbl,1E-4
AD,vbl,1E-4
HD,vbl,3E-4
LD,vbl,3E-4
AD,vbl,3E-4

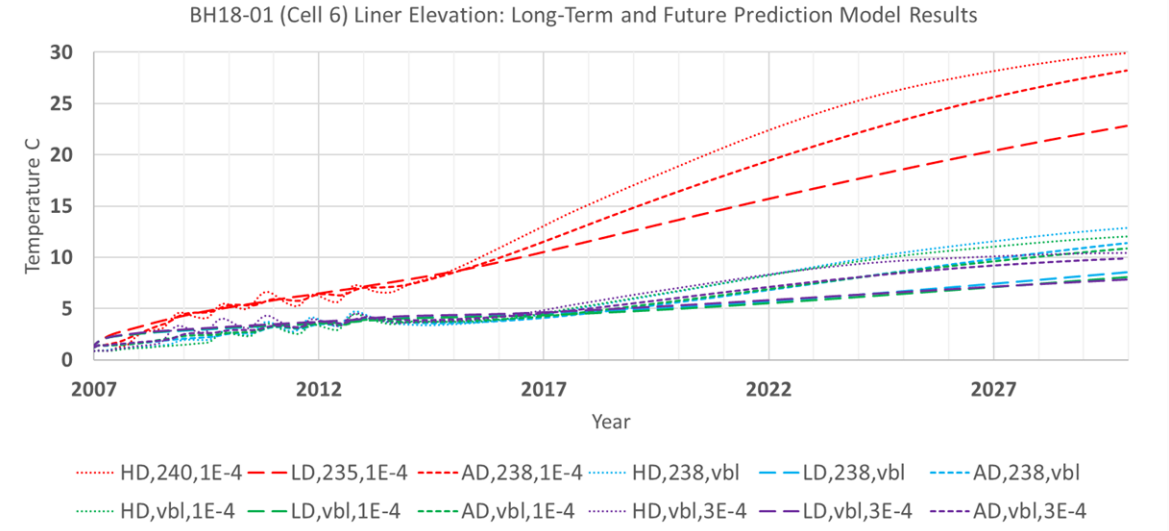
BH18-01 (Cell 6) Liner Elevation: Long-Term and Future Prediction Model Results
Temperature C
30
25
20
15
10
5
0
2007
2012
2017
2022
2027
Year
HD,240,1E-4
LD,235,1E-4
AD,238,1E-4
HD,238,vbl
LD,238,vbl
AD,238,vbl
HD,vbl,1E-4
LD,vbl,1E-4
AD,vbl,1E-4
HD,vbl,3E-4
LD,vbl,3E-4
AD,vbl,3E-4

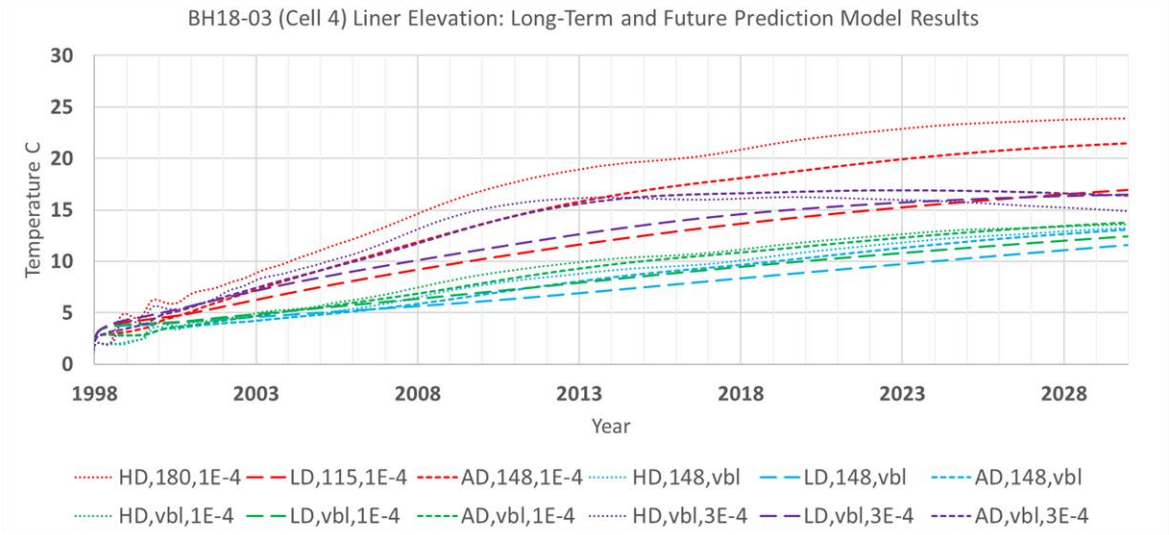
BH18-03 (Cell 4) Liner Elevation: Long-Term and Future Prediction Model Results
Temperature C
30
25
20
15
10
5
0
1998
2003
2008
2013
2018
2023
2028
Year
HD,180,1E-4
LD,115,1E-4
AD,148,1E-4
HD,148,vbl
LD,148,vbl
AD,148,vbl
HD,vbl,1E-4
LD,vbl,1E-4
AD,vbl,1E-4
HD,vbl,3E-4
LD,vbl,3E-4
AD,vbl,3E-4

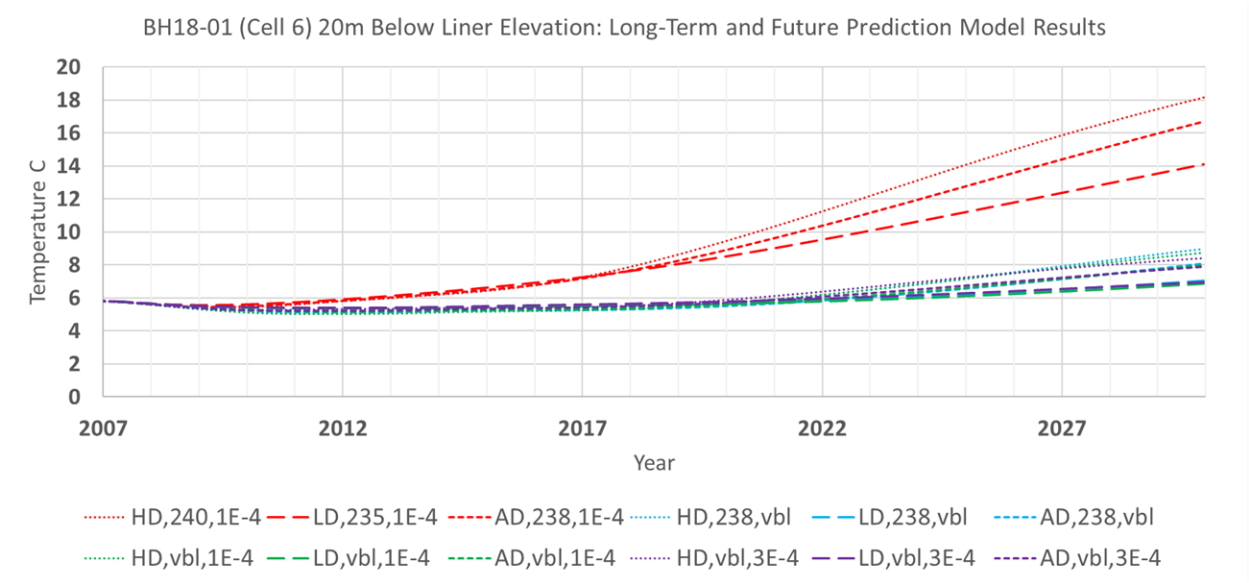
BH18-01 (Cell 6) 20m Below Liner Elevation: Long-Term and Future Prediction Model Results
Temperature C
20
18
16
14
12
10
8
6
4
2
0
2007
2012
2017
2022
2027
Year
HD,240,1E-4
LD,235,1E-4
AD,238,1E-4
HD,238,vbl
LD,238,vbl
AD,238,vbl
HD,vbl,1E-4
LD,vbl,1E-4
AD,vbl,1E-4
HD,vbl,3E-4
LD,vbl,3E-4
AD,vbl,3E-4

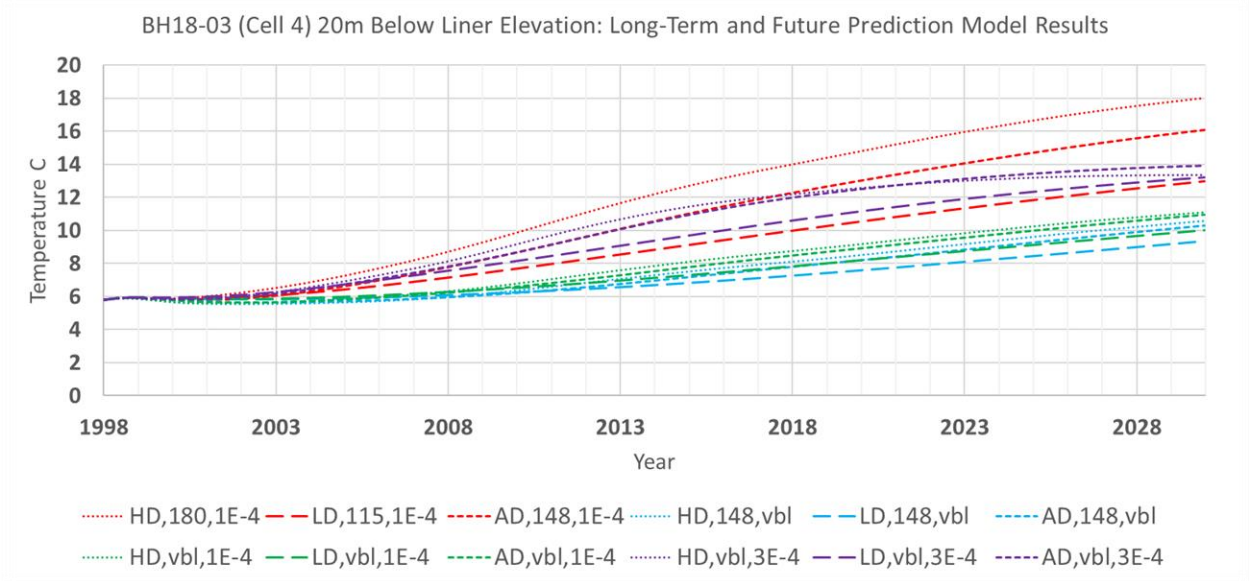
BH18-03 (Cell 4) 20m Below Liner Elevation: Long-Term and Future Prediction Model Results
Temperature C
20
18
16
14
12
10
8
6
4
2
0
1998
2003
2008
2013
2018
2023
2028
Year
HD,180,1E-4
LD,115,1E-4
AD,148,1E-4
HD,148,vbl
LD,148,vbl
AD,148,vbl
HD,vbl,1E-4
LD,vbl,1E-4
AD,vbl,1E-4
HD,vbl,3E-4
LD,vbl,3E-4
AD,vbl,3E-4